U.PORTO

PROGRAMA DOUTORAL EM BIOLOGIA BÁSICA E APLICADA

The changing brain in Alzheimer's disease: is the retina a mirror of disease onset and progression?

Samuel Duarte Chiquita

D
2019

Samuel Duarte Chiquita The changing brain in Alzheimer's disease: is the retina a mirror of disease onset and progression?

The changing brain in Alzheimer's disease: is the retina a mirror of disease onset and progression?

Samuel Duarte Chiquita

U.PORTO

D.ICBAS **2019**

SEDE ADMINISTRATIVA

INSTITUTO DE CIÊNCIAS BIOMÉDICAS ABEL SALAZAR
FACULDADE DE CIÊNCIAS
FACULDADE DE MEDICINA

U.PORTO

INSTITUTO DE CIÊNCIAS BIOMÉDICAS ABEL SALAZAR
UNIVERSIDADE DO PORTO

U.PORTO

FACULDADE DE CIÊNCIAS
UNIVERSIDADE DO PORTO

U.PORTO

FMUP FACULDADE DE MEDICINA
UNIVERSIDADE DO PORTO

The changing brain in Alzheimer's disease: is the retina a mirror of disease onset and progression?

Samuel Filipe Duarte Chiquita

Tese de doutoramento em Biologia Básica e Aplicada

2019

Samuel Filipe Duarte Chiquita

The changing brain in Alzheimer's disease: is the retina a mirror of disease onset and progression?

Tese de Candidatura ao grau de Doutor em Biologia Básica e Aplicada submetida ao Instituto de Ciências Biomédicas Abel Salazar da Universidade do Porto.

Orientador – António Francisco Rosa Gomes Ambrósio

Categoria – Investigador Principal com Agregação

Afiliação – Faculdade de Medicina da Universidade de Coimbra.

Orientador – Miguel de Sá e Sousa de Castelo-Branco

Categoria – Professor Associado com Agregação

Afiliação – Faculdade de Medicina da Universidade de Coimbra.

Coorientador – João Carlos Bettencourt de Medeiros Relvas

Categoria – Investigador Principal

Afiliação – Instituto de Investigação e Inovação em Saúde da Universidade do Porto.

Support: Portuguese Foundation for Science and Technology (SFRH/BD/52045/2012, PEst UID/NEU/04539/2013 and MEDPERSYST SAICTPAC/0010/2015), COMPETE-FEDER (POCI-01-0145-FEDER-007440 and POCI-01-0145-FEDER-016428), Santa Casa Mantero Belard Award 2015 (MB-1049-2015) and Centro 2020 Regional Operational Programme (CENTRO-01-0145-FEDER-000008: BrainHealth 2020 and CENTRO-01-0145-FEDER-000016: BIGDATIMAGE).

Host institution: IBILI-Institute for Biomedical Imaging and Life Sciences, Faculty of Medicine, University of Coimbra.

Abstract

It has been claimed that the retina can be used as a window to study brain disorders. However, concerning Alzheimer's disease (AD), there are missing links between changes occurring in the brain and retina. Thus, there is an urgent need to clarify whether the retina can indeed mirror changes occurring in the brain. We aim to understand when changes start appearing in the retina and brain, how changes progress and how they can be correlated. To fill in the gaps concerning these missing links between the retina and brain pathology in AD, we carried out a longitudinal and multimodal study using a triple transgenic mouse model of AD (3xTg-AD) and age matched wild type (WT) mice. Several parameters were evaluated in the same animals *in vivo* at 4, 8, 12 and 16 months of age both in the retina and brain.

Retinal structure was evaluated by optical coherence tomography (OCT), which allows performing segmentation of retinal layers and identifying affected layers. Retinal physiology was evaluated by electroretinography (ERG), which measures the electrical response of retinal cells. With pattern electroretinography (PERG) we assessed the function of retinal ganglion cells. Since the main feature of AD is memory loss, we also performed behavioral studies, namely the open field and novel object recognition tests. These studies were crucial to better correlate structural changes with functional alterations with implications in learning and memory. Changes in brain structure, perfusion and neurospectroscopy were evaluated with magnetic resonance imaging (MRI). Brain amyloid accumulation was assessed with ^{11}C-PIB positron emission tomography (PET) and neuroinflammatory status was evaluated with ^{11}C-PK11195, a marker of microglia activation.

OCT results show that there is a reduction of retinal thickness in 3xTg-AD mice when compared with WT animals at all time points. ERG recordings show a higher b-wave response at all time points in 3xTg-AD mice, while PERG did not show any statistically significant difference between 3xTg-AD and WT mice. Behavioral tests show that there is a memory impairment at all time points and an altered locomotor activity at 4, 8 and 16 months in 3xTg-AD mice. Brain structural analysis reveals substantial hippocampal and visual cortex grey matter volumes reduction at 4, 8, 12 and 16 months of age in 3xTg-AD mice. Neurospectroscopy results show that hippocampal taurine concentrations of 3xTg-AD animals are significantly decreased at 4, 8 and 16 months of age. PET evaluation does not show significant changes in amyloid accumulation and neuroinflammation, while blood brain barrier permeability is altered only at 16 months of age. Molecular characterization reveals an increase in amyloid β and hyperphosphorylated tau in the hippocampus of 3xTg-AD mice at 4, 8, 12 and 16 months of age.

In summary, results indicate that there are structural and functional changes in the retina of the 3xTg-AD, which are associated with behavioral and structural brain alterations. These

changes show that the retina is a mirror of AD progression creating the possibility to use the eye as a noninvasive model for early AD diagnosis. Therefore, the results obtained highlight the possibility to use the 3xTg-AD as a valuable tool for testing new potential treatments with impact in AD pathological hallmarks and particularly in taurine neuroprotector levels modulation.

Resumo

Foi proposto que a retina pode ser utilizada como uma janela para o estudo de doenças a nível cerebral. Contudo, no que diz respeito à doença de Alzheimer existe ainda alguma falta de evidência relativamente a possíveis ligações causais entre alterações existentes na retina e correspondentes mudanças a nível cerebral. Consequentemente existe uma necessidade premente de esclarecer se a retina pode de facto ser um espelho de alterações que ocorram a nível cerebral. O objetivo deste trabalho é determinar quando é que as alterações associadas à doença de Alzheimer começam a surgir na retina e no cérebro, como é que estas alterações progridem e como podem ser correlacionadas. Com vista a preencher as lacunas referentes a possíveis correlações entre a retina e o cérebro na patologia da doença de Alzheimer foi efetuado estudo longitudinal utilizando um modelo animal triplo transgénico e o correspondente controlo. Vários parâmetros foram avaliados nos mesmos animais *in vivo* aos 4, 8, 12 e 16 meses de idade quer na retina quer no cérebro.

A estrutura da retina foi avaliada por tomografia de coerência ótica, que permite segmentar as várias camadas da retina e determinar quais são as camadas afetadas. A fisiologia da retina foi avaliada através da técnica de eletroretinografia, que permite medir a atividade elétrica das células da retina. Com a eletroretinografia padrão avaliámos a função das células ganglionares da retina. Uma vez que a principal característica da doença de Alzheimer é a perda de memória, efetuámos estudos de comportamento animal, nomeadamente os testes do campo aberto e de reconhecimento do objeto novo. Estes estudos foram essenciais para melhor correlacionar mudanças a nível da estrutura com alterações a nível da função com implicações na aprendizagem e na memória. Com a imagiologia por ressonância magnética foram avaliadas alterações da estrutura, perfusão e neuroespectroscopia do cérebro. A acumulação de beta amiloide e neuroinflamação a nível cerebral foram avaliadas com a tomografia por emissão de positrões utilizando os radiofármacos ^{11}C-PIB e ^{11}C-PK11195, respetivamente.

Os resultados obtidos com a tomografia de coerência ótica demonstram que existe redução da espessura da retina dos animais do grupo transgénico quando comparados com os animais do grupo controlo em todas as idades avaliadas. As medidas de eletroretinografia permitem verificar que a resposta da onda b dos animais do grupo transgénico é maior em todas as idades avaliadas, por sua vez as medidas com a eletroretinografia padrão não demonstram qualquer diferença significativa entre o grupo dos animais controlo e o grupo dos animais transgénicos. Os testes de comportamento demonstram que existe défice na memória em todas as idades avaliadas e também na atividade locomotora aos 4, 8 e 16 meses de idade nos animais do grupo transgénico. A análise estrutural dos volumes de substância cinzenta no hipocampo e córtex visual revelam que estes se encontram reduzidos nos animais

transgénicos aos 4, 8, 12 e 16 meses de idade. Os resultados de neuroespectroscopia demonstram que os níveis de taurina no hipocampo se encontram reduzidos aos 4, 8 e 16 meses de idade. Com a tomografia por emissão de positrões não foi detetada diferença na acumulação de beta amiloide e neuroinflamação sendo que a permeabilidade da barreira hematoencefálica se encontrou alterada apenas aos 16 meses de idade. A caracterização molecular revelou que os níveis de beta amiloide e tau hiperfosforilada se encontram elevados aos 4, 8, 12 e 16 meses de idade. Sucintamente, os resultados obtidos indicam que há alterações na estrutura e função da retina do modelo animal triplo transgénico da doença de Alzheimer que estão associadas com alterações no comportamento e na estrutura do cérebro. Estas alterações podem ser encaradas como um espelho da progressão da doença de Alzheimer criando a possibilidade de utilizar o olho como um modelo não invasivo para o diagnóstico desta doença. Consequentemente os resultados obtidos evidenciam a possibilidade de utilizar este modelo animal da doença de Alzheimer no sentido de testar novos compostos com potencial impacto no tratamento das principais características patológicas da doença de Alzheimer e particularmente na modulação dos níveis de taurina.

Acknowledgements

I would like to acknowledge my supervisors, Dr. António Francisco Ambrósio and Dr. Miguel Castelo-Branco, for providing me the possibility to perform the research work of this doctoral thesis. In particular, a special thanks to the Retinal Dysfunction and Neuroinflammation Lab and to the group leader Dr. António Francisco Ambrósio for allowing me to be a member of his group. I also acknowledge Dr. João Relvas, for the co-supervision.

I would like to express my gratitude to the Graduate Program in Areas of Basic and Applied Biology (GABBA), for giving me the opportunity to perform my doctoral work. In particular, I would like to thank the directors of the GABBA Program, Dr. Alexandre do Carmo and Professor António Amorim, for allowing me to reach this point in my scientific path.

I also would like to thank God, my family and friends that have always believed in me. Finally, I would like to thank the Portuguese Foundation for Science and Technology for providing me with the financial support necessary to perform the doctoral work with the fellowship SFRH/BD/52045/2012 and the Santa Casa Mantero Belard Award 2015 for financing the project “The changing brain in Alzheimer’s disease: is the retina a reliable mirror of disease onset and progression?”.

Publications

The following original publications resulted from doctoral research work:

1. **Chiquita, S.**, M. Ribeiro, J. Castelhano, F. Oliveira, J. Sereno, M. Batista, A. Abrunhosa, A.C. Rodrigues-Neves, R. Carecho, F. Baptista, C. Gomes, P. I. Moreira, A. F. Ambrósio, M. Castelo-Branco (2019). “A longitudinal multimodal *in vivo* molecular imaging study of the 3xTg-AD mouse model shows progressive early hippocampal and taurine loss.” Human Molecular Genetics: ddz045.

2. Bernardes, R., G. Silva, **S. Chiquita**, P. Serranho and A. F. Ambrósio (2017). "Retinal Biomarkers of Alzheimer’s Disease: Insights from Transgenic Mouse Models." International Conference Image Analysis and Recognition: 541-550.

Contents

Abbreviations

Aβ	Amyloid β
AD	Alzheimer's disease
ADNI	Alzheimer's Disease Neuroimaging Initiative
ANOVA	Analysis of variance
ANCOVA	Analysis of covariance
APOE4	Apolipoprotein E4
APP	Amyloid β precursor protein
APP_{SWE}	Amyloid precursor protein-Swedish mutation
AUC	Area under the curve
BBB	Blood brain barrier
BBBi	Blood brain barrier perfusion index
B0	Static magnetic field
CSF	Cerebrospinal fluid
C57BL6/129S	Wild type mice strain
CRLB	Cramér-Rao lower bound
^{11}C-PIB	^{11}C Pittsburgh compound B
DCE	Dynamic contrast enhanced
DICOM	Digital imaging and communications in medicine
ERG	Electroretinogram/electroretinography
FDG	Fluorodeoxyglucose
FIDs	File identifiers
FLASH	Fast low angle shot
FOV	Field of view
FWE	Family-wise error rate
FWHM	Full width at half maximum
GABA	γ-aminobutyric acid
GCL	Ganglion cell layer
GM	Grey matter
GSK3	Glycogen synthase kinase 3
^{1}H-MRS	Proton magnetic resonance spectroscopy
INL	Inner nuclear layer
IPL	Inner plexiform layer
IS	Inner segments
LCModel	Linear combination of model spectra
MCI	Mild cognitive impairment

MMSE	Mini-Mental State Examination
MRI	Magnetic resonance imaging
NFT	Neurofibrillary tangle
NINCDS-ADRDA	National Institute of Neurological and Communicative Disorders and Stroke-Alzheimer's Disease and Related Disorders Association
OCT	Optical coherence tomography
ONH	Optic nerve head
ONL	Outer nuclear layer
OPL	Outer plexiform layer
OP	Oscillatory potentials
OS	Outer segments
OSEM	Ordered subset expectation maximization algorithm
PERG	Pattern electroretinogram/electroretinography
PET	Positron emission tomography
PRESS	Point resolved spectroscopy
PS1	Presenilin 1 protein
PS2	Presenilin 2 protein
P-tau	Phosphorylated tau
RARE	Rapid acquisition with relaxation enhancement
rCBF	Regional cerebral blood flow
RGCs	Retinal ganglion cells
RNFL	Retinal nerve fiber layer
ROI	Regions of interest
RPC	Resistive plate chambers
SD-OCT	Spectral domain optical coherence tomography
SEM	Standard error of the mean
SLD	Superluminescent diode
SLO	Scanning laser ophthalmoscopy
SPM	Statistical parametric mapping
TE	Time of echo
TR	Time of repetition
TSPO	Translocator protein
T-tau	Total tau
TTP	Time to peak
TUNEL	Terminal deoxynucleotidyl transferase dUTP nick end labeling
VAPOR	Variable power and optimized relaxation delays
VBM	Voxel based morphometry

V1	Primary visual cortex
V2, V3, V4, V5	Visual association areas
WM	White matter
WT	Wild type mice
3xTg-AD	Triple transgenic mouse model of Alzheimer's disease
5xFAD	Familial Alzheimer's disease mouse model with five mutations

Chapter 1 | Introduction

1.1. Retina and vision

The visual world is firstly processed through the retina, a highly organized neural extension of the brain. The retina is constituted by different cell types involved in processing the information from the visual scene (Figure 1), namely photoreceptors, horizontal, bipolar, amacrine and ganglion cells. When light reaches the retina cones and rods transduce the information from the visual scene and this information is transmitted through different types of bipolar cells, namely ON and OFF bipolar cells (Masland 2001). The information contained in these parallel channels is then conveyed to ganglion cells, the output cells of the retina being involved in the discrimination of distinct features from the visual scene (Roska and Meister 2014). Other important players are amacrine cells that are involved in sharing information with ganglion cells. Horizontal cells also play a role in the modulation of the signal that goes to the inner retina. The most prevalent cells observed in mammalian species, and this depends on each species, include rods and around three types of cones, two types of horizontal cells, twelve types of bipolar cells, thirty types of amacrine cells and more than thirty types of ganglion cells. These cell types form a mosaic arrangement that enables to tile the retina evenly. Therefore, the information of the visual scene is transmitted to the inner retina by approximately twelve distinct pathways that serve as input signals for amacrine and ganglion cells. Depending on the stratification level, distinct bipolar cells transmit distinct response signatures to the connected cells. Ganglion cells therefore transmit precise information resulting from the combination of these parallel channels that stratify at different levels of the inner plexiform layer (IPL) (Masland 2012, Baden, Berens et al. 2016).

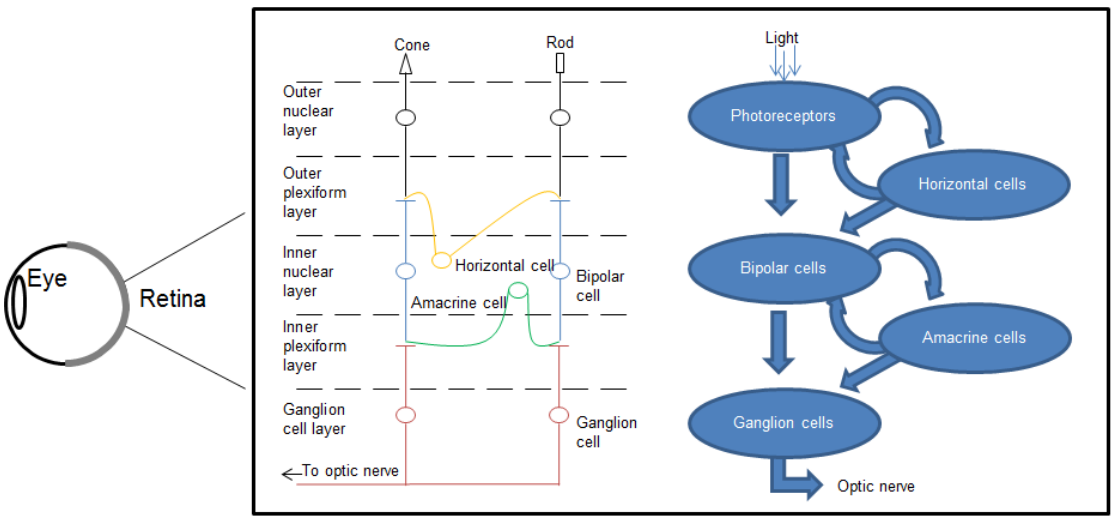

Figure 1 - Schematic overview of retinal layers and cell types. The retina is situated at the back of the eye and is constituted by distinct cell types.

The axons of retinal ganglion cells bundle together to form the optic nerve that contains fibers conveying visual features. In humans retina axonal projections synapse in several regions of the brain, such as the lateral geniculate body, superior colliculi, pretectal nuclei, and the suprachiasmatic nucleus (Marieb and Hoehn 2007). Several studies have been performed in different systems in order to try to understand how these features are encoded in different species. Moreover, the computations performed in order to extract specific information such as the "bug perceiver" described by Lettvin and colleagues is still an area of intensive research (Lettvin, Maturana et al. 1959). More recently mice have started to be used in vision research due to the available genetic tools that enable to study neural circuits of vision. Mouse retina is similar to primate retina in the peripheral region which makes it an interesting model for low acuity vision research (Huberman and Niell 2011). The retina can be viewed as a parallel image processor made of a multitude of small computational devices. Neural circuits of the retina are constituted by various cell types that separate the incoming visual information in different channels. Visual information is processed by retinal neural circuits and several computations are performed extracting distinct features from the visual scene. Several feature detectors have been identified in distinct ganglion cell types, namely center-surround, direction selective, object motion sensitive, looming detectors and Y (nonlinear summation) versus X cells (linear summation). Moreover, retinal neurons can respond to bright stimuli (ON cell), dark stimuli (OFF cell) or to both stimuli (ON-OFF cell). The conjugation of these features creates a variety of response patterns making possible to encode the information of the visual scene into a comprehensible signal that is transmitted to the brain through the optic nerve. The detection of dim light, texture motion, differential object motion or approaching motion are specific retinal computations implemented by dedicated microcircuits (Gollisch and Meister 2010).

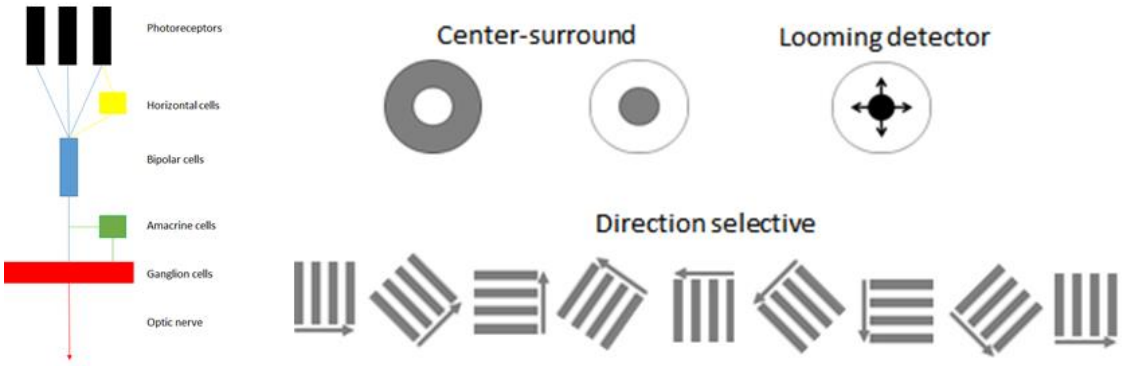

Figure 2 - Schematic representation of the interactions among distinct retinal cells. These interactions create microcircuits in which specific computations are performed originating several visual features that are transmitted to the brain through the optic nerve.

The signals generated in the retina are sent to the brain where the cortex performs a combination of the input signals into a meaningful perception of the visual world (Masland and Martin 2007). Cells with distinct structures encode distinct functional retinal outputs. In order to determine which cell types correspond to a given function anatomical studies and multielectrode array recordings play a fundamental role since they enable to match structure with function at a cell population level. Moreover, the concerted activity of ganglion cells may serve as a way to encode spatial information of the visual scene (Masland 1996).

1.2. Brain, vision and memory

The axons of retinal ganglion cells bundle together to form the optic nerve that after crossing the optic chiasma forms the optic tracts. These tracts transmit visual information to several relay stations in the brain, such as the lateral geniculate nucleus and the superior colliculus. Thalamic axonal projections are sent to the primary visual cortex, also designated as striate cortex, which together with visual association areas enable us to perceive the visual world. Two visual pathways of information are important in the definition of visual memory. These streams are involved in the discrimination of objects in the visual scene – what stream – and in the determination of objects spatial location – where stream. While the ventral stream is more involved in the discrimination of objects and faces the dorsal stream is more involved in determining the spatial location of objects and in visually guided behavior due to its projections to the frontal cortex. Other models of vision have been proposed in which the hierarchy of brain areas for visual perception is not the one proposed in the two visual streams model. Nevertheless, the two pathways model continues to be the view currently accepted. The information of the visual field is integrated in the primary visual cortex (V1) and transmitted to the visual association areas (V2, V3, V4, V5) being conveyed to two pathways of visual information processing that are used to recognize objects and determine its spatial location. Visual information originating from the occipital lobe is conveyed through two parallel pathways, the ventral pathway transmits information to the temporal lobe and the dorsal pathway connects with the parietal lobe (Marieb and Hoehn 2007, de Haan and Cowey 2011, Bachatene, Bharmauria et al. 2012). The information that comes from sensory inputs can be stored and used when necessary. Several regions in the brain are involved in the formation of memories, such as the medial temporal lobe that integrates information from what and where streams. This information is conveyed to the hippocampus where memories relating objects in a given context are expressed. In the case of visual processing, storage and retrieval the visual cortex, hippocampus and prefrontal cortex assume particular importance. The two visual streams associated with object recognition and spatial location also interact with the prefrontal cortex that has an active role in visual memory representation. This means that the

communication between the hippocampus and prefrontal cortex plays an essential role in memory representation. While the hippocampus is a structure involved in memory formation and retrieval, the prefrontal cortex acts by choosing which memories to retrieve in a given circumstance. Therefore, there is a crosstalk between these two structures in which the prefrontal cortex controls the retrieval of information from the hippocampus due to trigger signals coming from the hippocampus itself. Moreover, the communication between the prefrontal cortex and the hippocampus provides a mechanism to accommodate new information in previously acquired memories (Nadel and Hardt 2011, Haxby, Clark et al. 2012, Preston and Eichenbaum 2013).

1.3. Alzheimer's disease

Alzheimer's disease (AD) is a neurodegenerative disease characterized by memory deficits associated with progressive deterioration of cognitive and executive functions. This neurodegenerative disorder was first reported by Alois Alzheimer in 1907 based on a patient with several clinical features, including memory loss, disorientation and an atrophic brain (Alzheimer 1907, Stelzmann, Norman Schnitzlein et al. 1995). AD is the most common form of dementia. According to the World Health Organization in 2010 there were about 35.6 million people with dementia in the world and this number is predicted to reach 115.4 million by 2050 (Organization 2012). The World Alzheimer Report 2015 states that in 2015 there were 46.8 million people with dementia and that this value will increase to 131.5 million by 2050 (Prince, Wimo et al. 2015). In Portugal the number of people with dementia in 2013 was estimated to be 160287 and from those between 80144 and 112201 patients suffer from AD (Santana, Farinha et al. 2015). Aging leads to a deterioration of memory and in AD patients this decline can be particularly evident. Episodic memory impairment seems to be one of the most important memory deficits in AD, a memory depicting the ability of one individual to remember a particular recent event in his life. The hippocampus, a brain region involved in episodic memory, is particularly affected in AD and structural alterations have been observed in patients suffering from this disease. Both the medial temporal lobes and frontal lobes exhibit dysfunctions underlying AD impairments. Therefore, AD patients have some difficulty to remember recent events. Besides episodic memory deficits AD patients also experience semantic memory impairments and visual problems. In AD there seems to be an impairment of acetylcholine inputs that are important in the storage and access to information. Consequently, acetylcholinesterase inhibitors have been prescribed in order to mitigate AD memory impairment. Memantine has also been used for patients with moderate to severe AD that enables to refrain abnormal neuronal activity. Several lifestyle factors can also influence AD onset, such as physical activity and cognitive reserve. AD can appear due to genetic

determinants associated with amyloid precursor and presenilin proteins that arises due to familial genes with a role in AD. Nevertheless, the most common form is sporadic AD in which the apolipoprotein E4 (APOE4) gene can increase the risk for AD. Both amyloid β (Aβ), APOE4, presenilins and tau have a role in AD pathogenesis. Mutations in tau can cause frontotemporal dementia but in AD tau acts as a key player by mediating the effects in AD pathogenesis due to Aβ and APOE4. In order to be able to deliver effective treatments to AD patients before a severe impairment has occurred the current effort of AD research field is trying to find earlier biomarkers for AD diagnosis. In particular, transgenic mouse models are important tools in preclinical research since they enable to test the potential of new treatments before being translated into humans (Purves, Augustine et al. 2001, Marieb and Hoehn 2007, Gold and Budson 2008, Ballard 2011, Huang and Mucke 2012, Jahn 2013).

1.3.1. Alzheimer's disease biomarkers

The two major proteinopathies in AD are associated with Aβ and tau. The formation of Aβ plaques and tau neurofibrillary tangles leads to synaptic dysfunction and neuronal cell loss (Götz and Ittner 2008). Synaptic dysfunction is present at the beginning of AD onset and according to the amyloid hypothesis is associated with an increase in Aβ levels. Mutations in the amyloid β precursor protein (APP), presenilin 1 (PS1) and presenilin 2 (PS2) genes that lead to increased Aβ levels strongly support the amyloid cascade hypothesis. Moreover, according to this hypothesis tau hyperphosphorylation and neurofibrillary tangle formation is initiated due to Aβ (Figure 3).

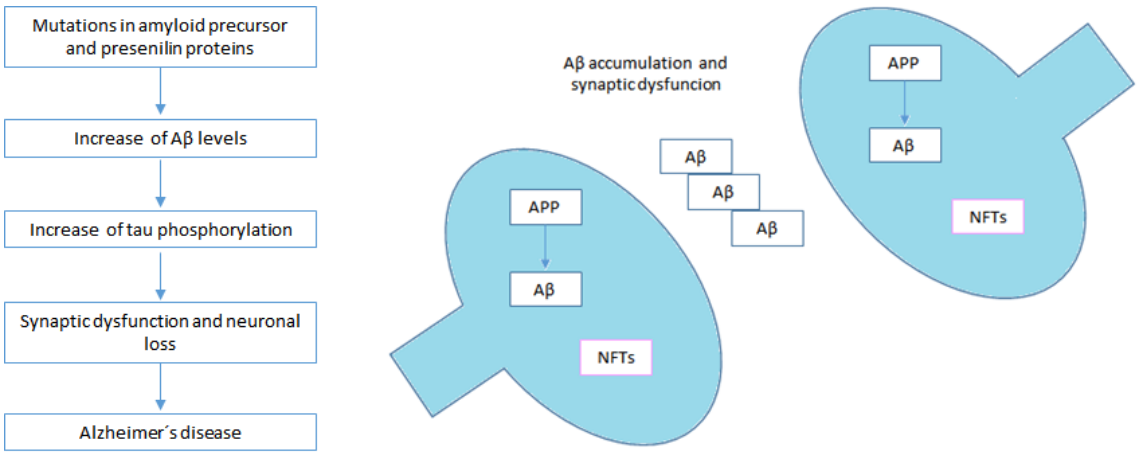

Figure 3 – Hypothetic model of Alzheimer's disease onset and progression in which amyloid β and tau represent the major hallmarks of this neurodegenerative disease. Aβ accumulation associated with tau hyperphosphorylation leads to neuronal dysfunction. Hyperphosphorylated tau accumulation leads to neurofibrillary tangle (NFT) formation.

Early onset AD is associated with mutations in APP, presenilin 1 and 2 while mutations in the tau gene lead to frontotemporal dementia. Other hypotheses have been proposed with impact in late onset AD, such as the dual pathway hypothesis that expresses the possibility to have an elevation in Aβ and tau hyperphosphorylation in two distinct pathways. The factors that increase the risk to have late onset AD include APOE4 gene that is supposed to reduce Aβ clearance, glycogen synthase kinase 3 (GSK3) that phosphorylates tau and retromer sorting pathway that acts by regulating Aβ levels (Hardy and Selkoe 2002, Selkoe 2002, Small and Duff 2008, Ballard 2011).

However, in AD it is still difficult to establish a link between a biomarker and the appearance of symptoms (Sperling, Aisen et al. 2011). Jack and colleagues proposed an approach for early stages AD diagnosis based on several biomarkers including measures of Aβ and neurodegeneration assessed by cerebrospinal fluid (CSF) $A\beta_{42}$, positron emission tomography (PET) amyloid imaging, CSF total tau (t-tau) and phosphorylated tau (p-tau), fluorodeoxyglucose (FDG) PET and magnetic resonance imaging (MRI) (Jack, Knopman et al. 2013). Neuroimaging provides the possibility to image potential alterations associated with AD onset and progression *in vivo*, enabling the detection of alterations in structure and function by MRI or PET. For instance, the Alzheimer's Disease Neuroimaging Initiative (ADNI) is a longitudinal study implemented to reach a consensus of biomarkers for early AD detection. This initiative has developed methods for clinical tests that include MRI, PET and CSF biomarkers (Weiner, Aisen et al. 2010, Weiner, Veitch et al. 2015). However, some of the techniques available are expensive and invasive. Moreover, in order to have a definitive assessment of AD it is needed to identify Aβ plaques and neurofibrillary tangles *postmortem* (Sutphen, Fagan et al. 2014). With the aim of having better and earlier treatments for AD patients it is also necessary to have a better and earlier diagnosis. There is an urgent need to identify new specific and sensitive biomarkers that can reliably help diagnosing early AD onset (Frost, Martins et al. 2010). Visual alterations have been observed in AD patients, and those alterations can be associated with molecular, structural and functional changes. The eye enables to perform noninvasive, inexpensive and *in vivo* tests. In particular, optical coherence tomography (OCT) stands as an appealing technique for imaging the retina. OCT measurements have shown that there is a thinning of the retina in AD patients (Chang, Lowe et al. 2014, Tzekov and Mullan 2014, Hart, Koronyo et al. 2016, Javaid, Brenton et al. 2016). With the aim of using the retina as an alternative tool for the diagnosis of early AD it will be important to be able to distinguish the retinal pathology associated to AD from the retinal pathology of other retinal diseases (Sivak 2013). Ultimately, the combination of structural and functional changes either in the retina or other brain regions may be used as a biomarker for early AD onset diagnosis. Moreover, it is important to understand how changes occurring in the eye might be correlated with changes occurring in the brain (Figure 4).

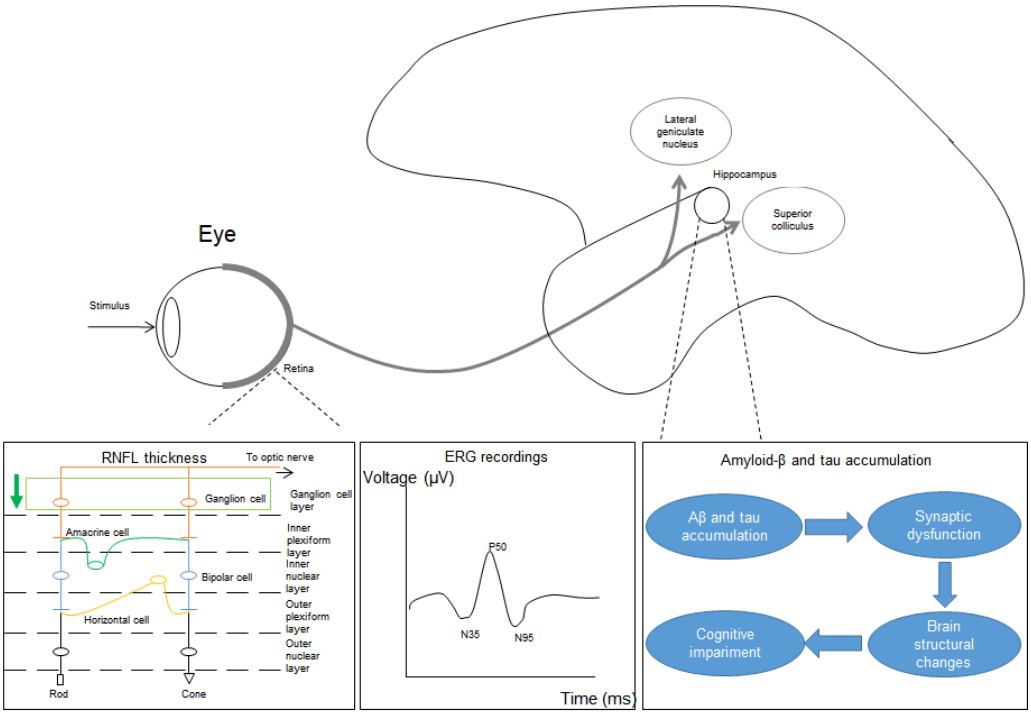

Figure 4 - The eye as a tool to study Alzheimer's disease. Retinal changes often precede central nervous system alterations and can be assessed by optical coherence tomography, electrophysiology and Aβ levels. Abbreviations: RNFL, retinal nerve fiber layer; ERG, electroretinogram.

1.3.2. Structural and functional retinal changes in Alzheimer's disease patients

The use of the eye as a tool to study central nervous system disorders has emerged as a promising path to follow (London, Benhar et al. 2013). Several layers form the wall of the eye. The retina, which is an extension of the brain (Krantic and Torriglia 2014), is the innermost layer, and is constituted by photoreceptors, horizontal, bipolar, amacrine and ganglion cells, which form a neuronal network responsible for processing information from the visual world (Marieb and Hoehn 2007, Masland 2012). Ganglion cell axons bundle together to form the optic nerve that projects to several regions of the brain, such as the superior colliculus and the lateral geniculate nucleus. Other targets of retinal ganglion cells include the pretectum, suprachiasmatic nucleus of the hypothalamus, nucleus of the optic tract and dorsal terminal nucleus, medial and lateral terminal nuclei (Purves, Augustine et al. 2001, Dhande and Huberman 2014). Retinal imaging and electrophysiology can be used to evaluate structural and functional abnormalities in the retina, a more accessible structure for a potential early AD detection. With this goal, several investigations have been performed in AD patients.

More than three decades ago, visual abnormalities have been described in patients with AD (Hinton, Sadun et al. 1986, Sadun, Borchert et al. 1987). Subsequent studies reported ganglion

cell loss in AD patients (Blanks, Schmidt et al. 1996, Blanks, Torigoe et al. 1996) as well as the reduction of retinal thickness in AD patients (Paquet, Boissonnot et al. 2007, Lu, Li et al. 2010, Kesler, Vakhapova et al. 2011, Kirbas, Turkyilmaz et al. 2013, Liu, Zhang et al. 2015, Thomson, Yeo et al. 2015). A meta-analysis that analyzed retinal nerve fiber layer (RNFL) assessed with OCT in patients with dementia demonstrated that there is a significant reduction in the RNFL in those patients (Thomson, Yeo et al. 2015). In fact, these changes in RNFL have been observed in several human studies (Paquet, Boissonnot et al. 2007, Lu, Li et al. 2010, Kesler, Vakhapova et al. 2011, Kirbas, Turkyilmaz et al. 2013, Liu, Zhang et al. 2015, Thomson, Yeo et al. 2015). It is also important to highlight a clinical trial (NCT01555827) that has already been completed that assessed the RNFL thickness in AD patients in which a reduction in the RFNL thickness has been observed (Méndez-Gómez, Rougier et al. 2017). AD patients also have optic nerve injury (Sadun and Bassi 1990, Danesh-Meyer, Birch et al. 2006). It has been claimed that RNFL thickness can be evaluated in order to foresee the cognitive status of AD patients (Shi, Zhu et al. 2016). However, others report that there are no differences in nerve fiber layer or ganglion cell-inner plexiform layer thickness between mild cognitive impairment or AD patients and control groups (Cronin-Golomb, Rizzo et al. 1991, Justino, Kergoat et al. 2001, Kergoat, Kergoat et al. 2001, Lad, Mukherjee et al. 2018).

Besides structural alterations, other studies also show functional retinal changes in AD patients detected via electrophysiology namely in the pattern electroretinogram (PERG) thus implying that there is retinal ganglion cell impairment (Trick, Barris et al. 1989, Parisi, Restuccia et al. 2001). Retinal ganglion cell dysfunction has been detected in patients with senile dementia of the Alzheimer type using PERG recordings (Trick, Barris et al. 1989). Moreover, a reduction in RNFL thickness evaluated with OCT has been correlated with retinal dysfunction assessed by PERG recordings in AD patients (Parisi, Restuccia et al. 2001). Several studies report not only abnormal PERG but also abnormal visual evoked potentials in AD patients (Katz, Rimmer et al. 1989, Nesher and Trick 1991, Krasodomska, Lubiński et al. 2010, Sartucci, Borghetti et al. 2010). However, reports of normal retinal function in AD patients have also been published (Strenn, Dal-Bianco et al. 1991, Prager, Schweitzer et al. 1993, Justino, Kergoat et al. 2001). Studies with PERG recordings in humans show contradictory results in which some claim that there are no alterations while others claim that there are alterations (T Reed, Behar-Cohen et al. 2017). This body of evidence clearly shows that there are contradictory results regarding the alterations in retinal physiology. This might be due to the size of the cohort studied, the sample selection criteria or the results analysis performed. However, since there are many studies reporting structural and physiological alterations in the retina, it is likely that the majority of AD patients have indeed visual alterations.

Fluorescence lifetime imaging ophthalmoscopy shows changes in the fluorescence of retinal endogenous fluorophores in AD patients (Jentsch, Schweitzer et al. 2015) and a fluorescent

signature of Aβ ligand has also been reported (Kerbage, Sadowsky et al. 2013). In particular, curcumin enabled to label and detect Aβ plaques in *postmortem* human retinas from AD patients (Koronyo-Hamaoui, Koronyo et al. 2011). Other studies support the existence of retinal hemodynamic abnormalities and microvascular network alterations (Berisha, Feke et al. 2007, Cheung, Ong et al. 2014). Retinal ganglion cell loss accompanied by glial alterations have been reported in AD patients (Blanks, Schmidt et al. 1996, Blanks, Torigoe et al. 1996). Moreover, both retrograde and anterograde degeneration may exist in AD brain progressing towards areas involved in the detection of the visual scene and in visual perception, namely the retina and the visual cortex. In fact, after retinal ganglion cell axonal damage there is retrograde and anterograde impairment (Kanamori, Catrinescu et al. 2012). OCT might play a pivotal importance in noninvasive and low cost early diagnosis of AD. Retinal imaging might provide the possibility of establishing new biomarkers at low cost and noninvasively, in opposition to the expensive tests performed with PET and MRI imaging, which are available only at some places.

Table 1 - Structural and functional alterations in the retina of AD patients.

Hallmark	Finding	References
Retinal thickness	Reduction of RNFL	(Paquet, Boissonnot et al. 2007, Lu, Li et al. 2010, Kesler, Vakhapova et al. 2011, Kirbas, Turkyilmaz et al. 2013, Laguna, Barallobre et al. 2013, Liu, Zhang et al. 2015, Thomson, Yeo et al. 2015); NCT01555827
Retinal cell loss	Retinal neuronal loss Optic nerve degeneration	(Hinton, Sadun et al. 1986, Blanks, Schmidt et al. 1996, Blanks, Torigoe et al. 1996, Danesh-Meyer, Birch et al. 2006)
Retinal function	Abnormal pattern electroretinograms	(Katz, Rimmer et al. 1989, Trick, Barris et al. 1989, Nesher and Trick 1991, Parisi, Restuccia et al. 2001, Krasodomska, Lubiński et al. 2010, Sartucci, Borghetti et al. 2010)
	Normal retinal function	(Strenn, Dal-Bianco et al. 1991, Prager, Schweitzer et al. 1993, Justino, Kergoat et al. 2001)

1.3.3. Structural and functional retinal changes in Alzheimer's disease murine models

Several studies have been performed to assess the structure and function of the retina in animal models of AD. However, there are just a few studies that analyzed the alterations in both the retina and brain in the same animals. Indeed, the potential links between the changes occurring in the retina and brain in AD still need to be further explored.

Various transgenic mouse models of AD have been described in the literature. These include models with mutations in the human genes encoding for amyloid precursor protein, presenilin, tau and apolipoprotein E. These models try to resemble the pathological features seen in human AD onset and progression. Models of familial AD combining the genes for the two major proteinopathies seen in AD have been generated and the effects in behavior, electrophysiology and histopathology have been assessed. Nevertheless, there is no perfect animal model. Since the majority of genetically engineered mouse models rely on genes for early familial AD, they only partially mimic the features of human AD (a comprehensive list of AD transgenic mouse models is available at: https://www.alzforum.org/research-models/alzheimers-disease). Moreover, since the animal models generated use genes mainly associated with familial AD care must be taken when trying to apply the conclusions obtained from these models to sporadic AD (Elder, Gama Sosa et al. 2010, Hall and Roberson 2012, Amram and Frenkel 2016).

These animal models allow assessing both the retina and other brain structures in the early and late stages of the disease. Moreover, the data obtained from animal models of AD might help identifying molecular targets or biomarkers that might then lead to clinical applications in humans (Götz and Ittner 2008). In double transgenic mice of AD (APP/PS1) alterations in APP expression, Aβ deposition and apoptotic cells were detected in the retina, namely in the retinal ganglion cell layer (GCL) and inner nuclear layer (INL) (Ning, Cui et al. 2008, Dutescu, Li et al. 2009, Chiu, Chan et al. 2012). Tau accumulation was studied *in vivo* using scanning laser ophthalmoscopy (SLO) by imaging mice expressing human mutant P301S tau. This study revealed the progression of hyperphosphorylated tau in the GCL (Schön, Hoffmann et al. 2012). The effect of P301L tau mutation was also investigated and a decrease in the INL thickness was observed (Ho, Leung et al. 2015). In the amyloid precursor protein-Swedish mutation (APP_{SWE}) mice (Tg2576), retinal ganglion cell dendritic integrity was reduced, indicating that the changes in the inner plexiform layer (IPL) might be considered as a potential early biomarker of neuronal dysfunction/degeneration (Williams, Thirgood et al. 2013). Moreover, Aβ vaccinations were administered in Tg2576 mice and the retinal thickness reduction due to cell loss previously observed in Tg2576 mice was attenuated (Liu, Rasool et al. 2009). Noninvasive retinal *in vivo* imaging of Aβ plaques was also performed in $APP_{SWE}/PS1_{\Delta E9}$ transgenic mice. This opens the possibility of developing new imaging

strategies for the early diagnosis of AD (Koronyo-Hamaoui, Koronyo et al. 2011). In TgCRND8 mice ($APP_{SWE/IND}$) RNFL/GCL thickness reduction, Aβ and p-tau deposition were detected in the retina (Buccarello, Sclip et al. 2017). Furthermore, alterations in the electroretinogram (ERG) were detected in several mouse models of AD (Perez, Lumayag et al. 2009, Ioshimoto, Nagy et al. 2012, Antes, Ezra-Elia et al. 2013, Liu, Cao et al. 2015, Gupta, Chitranshi et al. 2016, Millar, Webber et al. 2016, Joly, Lamoureux et al. 2017, Pernet, Rodriguez et al. 2018). The apolipoprotein E4 allele is associated with a higher risk to develop AD and APOE4 mice showed a reduction both in the a-wave and b-wave amplitudes in dark adapted animals (Antes, Ezra-Elia et al. 2013). Abnormal scotopic b-wave implicit time and decreased a-wave amplitude were reported in a triple transgenic mouse model of AD ($PS1_{M146V}$, APP_{SWE} and tau_{P301L}) (Ioshimoto, Nagy et al. 2012). Double transgenic mice (APP_{SWE}/ $PS1_{\Delta E9}$) exhibited higher photopic b-wave amplitude at 10.5 to 11 months and at 13 months of age than the controls. This means that cone response was more preserved than in controls (Joly, Lamoureux et al. 2017). In the same transgenic mouse model, it was detected Aβ deposition in the retina and a reduction of the scotopic a-wave and b-wave amplitudes, in comparison with wild type animals (Perez, Lumayag et al. 2009). Gupta and colleagues also found Aβ accumulation in the retina and scotopic threshold response alterations in a double transgenic mouse model (APP/PS1). Moreover, a thinning of the IPL and a decrease in ganglion cell density and optic nerve axon density were observed (Gupta, Chitranshi et al. 2016). In order to understand the role of Aβ in the function of retinal cells, Aβ subretinal injections were performed and alterations in the scotopic ERG were detected (Liu, Cao et al. 2015). In a transgenic mouse model that expresses five mutations of familial AD (5xFAD), Aβ was present in the retina and there was a disturbance in the intraocular pressure, but the alterations in PERG amplitude were not significant (Millar, Webber et al. 2016). A study with a transgenic mouse model of human tau showed that the cone driven b-wave ERG response was higher than in tau knockout mice (Pernet, Rodriguez et al. 2018).

As mentioned above, there are only a few studies that assess the pathophysiology of AD in animal models simultaneously in the retina and brain, trying to establish possible correlations between the retina and brain. The P301S tau transgenic mouse presented functional changes in the retina. PERG recordings demonstrated that retinal ganglion cell activity was smaller in P301S mice than in controls. Injection of brain extracts of P301S mice in the superior colliculus of the same mice enhanced tau pathology in several visual system areas and affected the PERG response (Mazzaro, Barini et al. 2016). Electroretinograms and visual evoked potential responses were recorded in APP_{SWE}/ $PS1_{\Delta E9}$ mice and only small functional changes in dark adapted ERG latency were detected in the retina (Leinonen, Lipponen et al. 2016). On the other hand, other study with APP/PS1 mice showed alterations in scotopic ERG, visual evoked potential and photopic negative responses meaning that besides the existence of functional

retinal changes there were also alterations in cortical response (Shimazawa, Inokuchi et al. 2008). Furthermore, in APP/ PS1 mice retinas PERG amplitude was reduced and flash visual evoked potential latency was delayed (Gao, Chen et al. 2015). In 5xFAD mice, Aβ was detected in the retina, hippocampus and cortex and it was detected an impairment in the scotopic threshold response and also a thinning in retinal nerve fiber layer (Lim, He et al. 2016). In summary, studies using different mouse models of AD allow to identify structural and functional alterations in the retina likely related with the pathophysiology of AD. These models can be useful to test therapeutic agents and evaluate their potential for further translation into humans.

Table 2 - Structural and functional alterations in the retina of AD animal models.

Hallmark	Finding	Animal model	Age	Reference
Retinal thickness	Reduction of the IPL thickness	APP/PS1$_{\Delta E9}$	13 to 16 months	(Gupta, Chitranshi et al. 2016)
	Reduction of retinal thickness	Tg2576 (APP$_{SWE}$)	14 months	(Liu, Rasool et al. 2009)
	Reduction of the INL thickness	P301L	10 and 30 months	(Ho, Leung et al. 2015)
	Reduction of RNFL/GCL thickness	TgCRND8 mice (APP$_{SWE/IND}$)	4 to 8 months	(Buccarello, Sclip et al. 2017)
Retinal function	Reduction in the scotopic a-wave and b-wave amplitudes	APOE4	4 months	(Antes, Ezra-Elia et al. 2013)
	Higher photopic b-wave amplitude	APP$_{swe}$/PS1$_{\Delta E9}$	3 to 13 months	(Joly, Lamoureux et al. 2017)
	Reduction in the scotopic a-wave and b-wave amplitudes	APP$_{swe}$/PS1$_{\Delta E9}$	12 to 21 months	(Perez, Lumayag et al. 2009)
	Abnormal scotopic b-wave implicit time and decreased a-wave amplitude	3xTg-AD	2 to 12 months	(Ioshimoto, Nagy et al. 2012)
	Retina Aβ injection induces reduction in scotopic ERG	C57BL/6	5 months	(Liu, Cao et al. 2015)
	Changes in PERG amplitude are not significant	5xFAD	14 to 24 weeks	(Millar, Webber et al. 2016)

Table 3 - Structural and functional alterations in the retina and brain of AD animal models.

Hallmark	Finding	Animal model	Age	Reference
Structural and functional alterations in the retina and brain	Reduced PERG amplitude and increased visual evoked potential latency	$APP_{swe}/PS1_{\Delta E9}$	13 months	(Gao, Chen et al. 2015)
	Minor changes in ERG response and no changes in visual evoked potential responses	$APP_{swe}/PS1_{\Delta E9}$	13 months	(Leinonen, Lipponen et al. 2016)
	Reduction of PERG amplitude and increased latency	P301S	1 to 5 months	(Mazzaro, Barini et al. 2016)
	Scotopic ERG a-wave and visual evoked potentials latencies were increased. Photopic negative response was reduced	APP/PS1	11 to 24 months	(Shimazawa, Inokuchi et al. 2008)
	Scotopic threshold response and RNFL thickness were reduced. Aβ was detected in the eye and brain	5xFAD	6 and 17 months	(Lim, He et al. 2016)

1.3.4. Triple transgenic mouse model of Alzheimer's disease

The animal model used in this research work was a triple transgenic mouse model (3xTg-AD) with $PS1_{M146V}$, APP_{SWE} and tau_{P301L} transgenes which enables to study AD features of Aβ plaques accumulation and tau neurofibrillary tangles deposition (Figure 5).

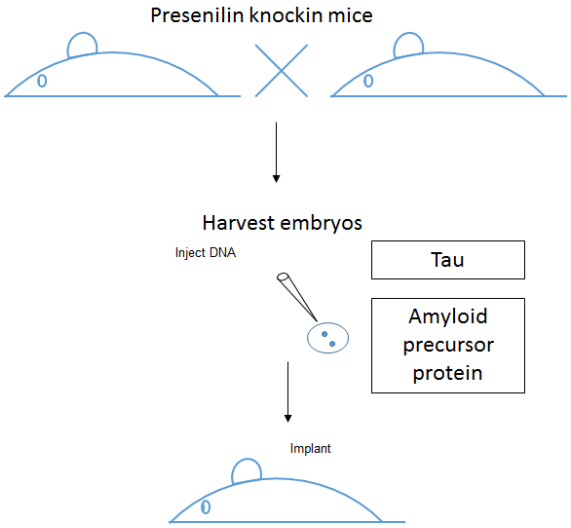

Figure 5 - Triple transgenic mouse model generation from presenilin knockin embryos injected with two transgenes encoding for human amyloid precursor protein and tau.

In this model both the hippocampus and cerebral cortex contain high levels of Aβ and tau proteins. Moreover, synaptic dysfunction in the hippocampus was detected by electrophysiological recordings. In fact, synaptic transmission deficits were observed before plaque and tangle accumulation, an important finding because synaptic dysfunction is associated with cognitive changes in AD. This synaptic dysfunction is due to Aβ species located inside the neurons. While in this mouse model Aβ deposits firstly appear in the cortex and after in the hippocampus, tau neurofibrillary tangles have a progression from the hippocampus to the cortex. Aβ deposits before tau, in accordance with the amyloid cascade hypothesis. Moreover, astrogliosis was observed in the brain of 3xTg-AD mice concomitant with the place of Aβ deposition (Oddo, Caccamo et al. 2003, Oddo, Caccamo et al. 2003). Rodriguez and colleagues showed that microglia also plays a role in AD and microglial activation was observed in the 3xTg-AD model. In addition, the density of resting microglia in the hippocampus of 3xTg-AD increased before microglial activation in the vicinity of Aβ plaques (Rodriguez, Witton et al. 2010). Taking these findings into account the 3xTg-AD model can be considered a promising tool for testing new potential therapeutics with impact in the pathophysiological processes mimicked by this model.

1.4. Objectives

It has been claimed that the retina can be used as a window to study brain disorders (London, Benhar et al. 2013). However, concerning AD, there are missing links between changes occurring in the brain and retina. Thus, there is an urgent need to clarify whether the retina can indeed mirror or be a window to see changes occurring in the brain. In this work we aimed to understand which changes occur in the retina and brain, when those changes start appearing and how changes in the retina and brain progress and can be correlated.

To fill in the gaps concerning the missing links between the retina and brain pathology in AD, we carried out a longitudinal study using 3xTg-AD (Oddo, Caccamo et al. 2003) and age matched wild type mice (C57BL6/129S). We evaluated, *in vivo*, several parameters in the same animals, at the same time points (4, 8, 12 and 16 months of age) in the retina and brain. Since the main feature of AD is memory loss, we performed behavioral studies, namely the novel object recognition and open field tests that allow to assess changes in recognition memory and locomotor activity, respectively. With positron emission tomography hippocampal Aβ accumulation and neuroinflammatory processes were assessed. Magnetic resonance imaging enabled to evaluate hippocampal and visual cortex grey matter volumes, blood brain barrier permeability and taurine concentration. By Western blotting Aβ and hyperphosphorylated tau protein levels were determined. Retinal structure was evaluated by optical coherence tomography, which allows performing segmentation of retinal layers and identifying affected layers. Retinal physiology was evaluated by electroretinography, which measures the electrical responses of retinal cells. With pattern electroretinography we assessed the function of retinal ganglion cells. Altogether, these studies were crucial to better correlate retinal structural and functional changes with alterations occurring in the brain.

Chapter 2 | Results

This chapter includes the results, methodology and discussion of the manuscript published in Human Molecular Genetics and the manuscript under preparation for submission.

1 - A longitudinal multimodal *in vivo* molecular imaging study of the 3xTg-AD mouse model shows progressive early hippocampal and taurine loss

This article was published in Human Molecular Genetics. Behavioral tests show that there is a memory impairment at all time points and an altered locomotor activity at 4, 8 and 16 months in 3xTg-AD mice. Brain structural analysis reveals substantial hippocampal grey matter volume reduction at 4, 8, 12 and 16 months of age in 3xTg-AD mice. Neurospectroscopy results show that hippocampal taurine concentrations of 3xTg-AD animals are significantly decreased at 4, 8 and 16 months of age. PET evaluation does not show significant changes in amyloid accumulation and neuroinflammation, while blood brain barrier permeability is altered only at 16 months of age. Molecular characterization reveals an increase in amyloid β and hyperphosphorylated tau in the hippocampus of 3xTg-AD mice at 4, 8, 12 and 16 months of age.

2 - Retinal thinning of inner sub-layers is associated with cortical atrophy in a mouse model of Alzheimer's disease: a longitudinal *in vivo* study

This article is currently under preparation for submission. OCT results show that there is a reduction of retinal thickness in 3xTg-AD mice when compared with WT animals at all time points. ERG recordings show an increased b-wave response at all time points, while PERG did not show any statistically significant difference between 3xTg-AD and WT mice. Brain structural analysis reveals substantial visual cortex grey matter volume reduction at 4, 8, 12 and 16 months of age in 3xTg-AD mice. Correlations between retinal structure, function and visual cortex grey matter show that retinal thickness changes and physiological responses are correlated with visual cortex grey matter volume.

1. A longitudinal multimodal *in vivo* molecular imaging study of the 3xTg-AD mouse model shows progressive early hippocampal and taurine loss

*Samuel Chiquita[1,2], *Mário Ribeiro[2,3,4], João Castelhano[2,3,4], Francisco Oliveira[2,3,4], José Sereno[2,3,4], Antero Abrunhosa[2,3,4], Ana Catarina Rodrigues-Neves[1,2], Rafael Carecho[1,2], Filipa Baptista[1,2], Catarina Gomes[1,2], Paula I. Moreira[2,5,6], ‡António Francisco Ambrósio[1,2], ‡Miguel Castelo-Branco[2,3,4]

[1]Coimbra Institute for Clinical and Biomedical Research (iCBR), Faculty of Medicine, University of Coimbra, 3000-548 Coimbra, Portugal; [2]CNC.IBILI Consortium, University of Coimbra, 3000-504 Coimbra, Portugal; [3]Coimbra Institute for Biomedical Imaging and Translational Research (CIBIT), University of Coimbra, 3000-548 Coimbra, Portugal; [4]Institute for Nuclear Sciences Applied to Health (ICNAS), University of Coimbra, 3000-548 Coimbra, Portugal; [5]Center for Neuroscience and Cell Biology (CNC), University of Coimbra, 3004-517 Coimbra, Portugal; [6]Institute of Physiology, Faculty of Medicine, University of Coimbra, 3004-517 Coimbra, Portugal

* These authors contributed equally to this work

‡ These authors contributed equally to this work, as senior authors

Corresponding Authors:

Dr. Miguel Castelo-Branco

Associate Professor, Principal Investigator

Coimbra Institute for Biomedical Imaging and Translational Research (CIBIT)

Institute for Nuclear Sciences Applied to Health (ICNAS), Faculty of Medicine

University of Coimbra, 3000-548 Coimbra, Portugal

Email: mcbranco@fmed.uc.pt, Phone: +351239488514

Dr. António Francisco Ambrósio

Principal Investigator

Coimbra Institute for Clinical and Biomedical Research (iCBR), Faculty of Medicine

University of Coimbra, 3000-548 Coimbra, Portugal

Email: afambrosio@fmed.uc.pt, Phone: +351239480093

1.1. Abstract

The understanding of the natural history of Alzheimer's disease (AD) and temporal trajectories of *in vivo* molecular mechanisms requires longitudinal approaches. A behavioral and multimodal imaging study was performed at 4, 8, 12 and 16 months of age in a triple transgenic mouse model of Alzheimer's disease (3xTg-AD). Behavioral assessment included the open field and novel object recognition tests to evaluate exploratory locomotor activity and object recognition memory. Molecular characterization evaluated hippocampal levels of amyloid β (Aβ) and hyperphosphorylated tau. Magnetic resonance imaging (MRI) included assessment of hippocampal structural integrity, blood brain barrier (BBB) permeability and neurospectroscopy to determine the concentration of taurine which is related to endogenous neuroprotection. Longitudinal brain amyloid accumulation was assessed using ^{11}C-PIB positron emission tomography (PET) and putative neuroinflammation was investigated using ^{11}C-PK11195, a marker of microglia activation. We found altered locomotor activity at 4, 8 and 16 months and recognition memory impairment at all time points. Substantial early reduction of hippocampal volume started at month 4 and progressed over 8, 12 and 16 months. Hippocampal taurine levels were significantly decreased at 4, 8 and 16 months. No differences were found for amyloid and inflammatory status with PET and BBB was disrupted only at month 16. In summary, 3xTg-AD mice have recognition memory and exploratory activity impairments as well as early hippocampal structural loss, increased Aβ and hyperphosphorylated tau levels and decreased levels of taurine. This study shows that the 3xTg-AD animal model mimics pathological and neurobehavioral features of AD, with early onset recognition memory loss and MRI documented hippocampal damage. The early onset profile suggests temporal windows and opportunities for therapeutic intervention, targeting endogenous neuroprotectors such as taurine.

Keywords: Alzheimer's disease, 3xTg-AD, hippocampus, memory, biomarkers, taurine.

Graphical abstract

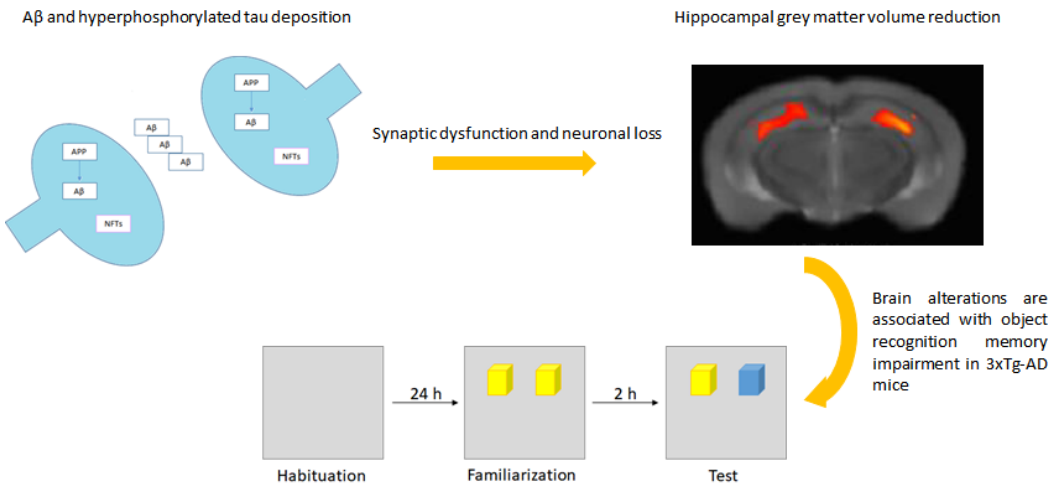

Main points

- Early recognition memory impairments and alterations in hippocampal structure are key features in 3xTg-AD mice.
- Taurine levels in the hippocampus are significantly reduced in 3xTg-AD mice since early time points, which may compromise endogenous neuroprotection.

1.2. Introduction

Alzheimer's disease (AD) is a neurodegenerative disease characterized by memory deficits associated with progressive deterioration of cognitive and executive functions. Episodic memory impairment is one of the most important memory deficits in AD. The hippocampus, which is involved in episodic memory, is particularly affected and structural alterations have been observed in AD patients (Ballard 2011, Jahn 2013). Moreover, behavioral assessment of cognitive function is pivotal to determine the impact of AD progression.

The need to identify mechanisms of disease and new diagnostic and therapeutic tools for AD has led to the development of several transgenic mouse models to mimic AD pathophysiology (Janus and Westaway 2001, Wong, Cai et al. 2002, Harper 2010, Hall and Roberson 2012). Since most genetically engineered mouse models rely on genes for early onset familial AD these models only partially mimic the features of human AD. However, one expects that these animal models share biological characteristics of human AD, such as brain amyloid plaques and neurofibrillary tangles, as well as the pattern of behavioral deficits observed in the human disease (Bryan, Lee et al. 2009). In this study we used the 3xTg-AD mouse model, a model of early onset AD, which has mutant genes for amyloid precursor protein, presenilin and tau.

Concerning the molecular characteristics of this model it has been reported that the extracellular Aβ deposits become apparent in 6 months old mice in the cerebral cortex (Oddo, Caccamo et al. 2003). These authors also described that Aβ oligomers begin to accumulate between 2 and 6 months of age, with continued age dependent increase observed between 12 and 20 months. Concerning the human disease, it is also known that amyloid pathology starts very early on, several decades before clinical symptoms become apparent (Gordon, Blazey et al. 2018).

In order to understand disease mechanisms and test therapeutic interventions it is very important to track the natural history of the disease in a longitudinal way in the same animals. This requires the use of noninvasive techniques that allow to study molecular mechanisms *in vivo*. In this multimodal molecular imaging longitudinal study we have used 4 months old 3xTg-AD mice as the starting point because at this age they do not present Aβ plaques despite the presence of increased intraneuronal soluble Aβ levels that correlate with the earliest cognitive impairment (Oddo, Caccamo et al. 2003, Billings, Oddo et al. 2005). We decided to uniquely combine PET and MRI methods longitudinally to best evaluate the natural history of the pathology, from the points of view of amyloid load, microglia activation, presence of endogenous neuroprotectors (specifically taurine) and structural integrity in key brain structures.

Concerning amyloid binding, we chose ^{11}C Pittsburgh compound B (^{11}C-PIB) because its binding in PET correlates with Aβ load and can be related with impaired metabolism, as

measured by ^{18}F-Fluordesoxiglucose imaging (PET-FDG), as our own human data corroborates (Oliveira, Moreira et al. 2018). We also aimed to test the face value of ^{11}C-PIB binding to Aβ deposits in this transgenic mouse model as compared to MR imaging. This is because it is believed that binding of that radiopharmaceutical in the brain is highly dependent on the AD model and the structure of Aβ plaques. For example, binding of ^{11}C-PIB to Aβ-rich cortical regions was shown to occur in APP23 mice but in contrast no increases in binding were observed in aged Tg2576 or APPswe-PS1dE9 mice *in vivo* although extensive Aβ deposition as assessed by immunohistochemistry was shown in APPswe-PS1dE9 mice (Snellman, López-Picón et al. 2013). Voxel based analysis of *in vivo* Aβ PET imaging studies in mouse models of AD is feasible and allows studying the PIB retention patterns in whole brain maps as further shown in a recent study of the APP/PS1 double transgenic mouse model of AD (von Reutern, Grünecker et al. 2013).

The combined use of imaging techniques is very scarce in this model, although one can identify studies using isolated modalities. A notable exception is the combined PET/MRI study focusing on amyloid load and perfusion of Maier and colleagues (Maier, Wehrl et al. 2014) in two amyloid precursor protein (APP) transgenic mouse models (APP23 and APP/PS1). This study showed that in the presence of cerebral amyloid angiopathy, Aβ deposition is accompanied by a decline of regional blood flow (rCBF). PET-FDG does not assess amyloid load, and has been used to probe the effects of therapeutic interventions in 3xTg-AD (Baek, Ye et al. 2016, Ye, Chung et al. 2016, Ye, Chung et al. 2016).

The demonstration that PET imaging can quantitatively map amyloid accumulation in living amyloid precursor protein transgenic mice was performed by Maeda and colleagues (Maeda, Ji et al. 2007). They showed that *in vivo* imaging of amyloid-β plaque burden is feasible in mouse models of AD as a valuable translational research tool, and even longitudinally to monitor treatment effects. They also showed repeated measures in relatively old APP23 animals. A study with the APP/PS1 model allowed for multi-method cross-validations for the PET results using *ex vivo* and *in vitro* methodologies, such as regional brain biodistribution, multi-label digital autoradiography, protein quantification with ELISA, fluorescence microscopy, semi-automated histological quantification and radioligand binding assays (Manook, Yousefi et al. 2012).

Concerning MRI studies coupled with behavior, a recent study (Kong, Devenyi et al. 2018) suggested that early neuroanatomic changes seem to precede major memory deficits, which further justifies studies in a preclinical stage. Several behavioral tests performed with 3xTg-AD mice have previously shown that this model has both cognitive and non-cognitive deficits (Billings, Oddo et al. 2005, Gimenez-Llort, Blazquez et al. 2007, Pietropaolo, Feldon et al. 2008, Romberg, Mattson et al. 2011, Davis, Easton et al. 2013, Orta-Salazar, Feria-Velasco et al. 2013, Stevens and Brown 2015, Stover, Campbell et al. 2015). Memory deficits are a

hallmark of AD, as well as underlying hippocampal damage, and behavioral tasks in combination with methods to assess regional neural loss are therefore critical (Clarka and Squirea 2013, Snigdha, Milgram et al. 2013, Puzzo, Lee et al. 2014). In order to understand the natural history of core manifestations of human AD in a 3xTg-AD mouse model we performed a behavioral, molecular and multimodal imaging study. Importantly, hippocampal damage and potential underlying mechanisms were evaluated with voxel based morphometry, neurospectroscopy, molecular imaging of amyloid deposition (^{11}C-PIB PET) and neuroinflammation (^{11}C-PK11195) as well as molecular analysis and behavioral testing. Concerning MR spectroscopy we focused on taurine, given its role in preventing β-amyloid neurotoxicity (Louzada, Lima et al. 2004).

Moreover a recent *in vitro* study (Aytan, Choi et al. 2016) testing whether fingolimod modulates neuroinflammatory markers in the 5xFAD mouse model of AD used high-resolution magic angle spinning magnetic resonance spectroscopy (an MRS technique for *in vitro* samples). The authors found that fingolimod soluble plus insoluble Aβ measured by ELISA and that taurine levels, measured using that MRS technique, showed a very strong inverse correlation with GFAP levels and ELISA measurements of Aβ, but not with activated microglia levels. The notion that taurine inversely relates with amyloid load further motivated our MRS study of taurine as a potential biomarker of impaired neuroprotection and disease progression.

Ultimately, we aimed to understand temporal patterns of disease progression, their molecular underpinnings and the amount of biological homology with the human disease. Finally, we aimed to identify the best structural and/or molecular imaging biomarkers that best predict the course of the disease.

1.3. Materials and methods

1.3.1. Animals

Experiments were performed in 3xTg-AD mice harboring three human mutant genes: presenilin 1 ($PS1_{M146V}$), amyloid precursor protein (APP_{SWE}) and tau (Tau_{P301L}), and in age matched wild type animals (WT: C57BL6/129S background). Male 3xTg-AD mice and WT mice were used to evaluate *in vivo* structural, molecular imaging, neurospectroscopic and behavioral changes at 4, 8, 12 and 16 months of age. WT mice used in this study have the same genetic background of the presenilin knockin embryos used to generate the 3xTg-AD mouse model, but instead of expressing mutant presenilin 1 gene they express the endogenous WT mouse presenilin 1 gene (Oddo, Caccamo et al. 2003). The animals were maintained at 22 ± 1 ºC, 68% relative humidity, on a 12 h light/12 h dark cycle, with access to water and food *ad libitum*. In order to assess age related changes the animals were tagged. All procedures involving animals were approved by the Animal Welfare Committee of the

Coimbra Institute for Clinical and Biomedical Research (iCBR), Faculty of Medicine, University of Coimbra. The animal experimentation was conducted in accordance with the European Community directive guidelines for the use of animals in laboratory (2010/63/EU), transposed into the Portuguese law in 2013 (Decreto-Lei 113/2013) and was in agreement with the Association for Research in Vision and Ophthalmology (ARVO) statement for animal use.

1.3.2. Behavioral experiments

Mice behavior (WT, n=21; 3xTg-AD, n=23) was evaluated using the open field and novel object recognition tests, to assess changes in locomotor activity and memory performance. The behavioral tests were performed by the same researcher, who remained outside the view of each mouse while performing the test, only interfering in the test to replace the animals and clean the arenas between consecutive tests. The tests were video recorded and analyzed with Observador (http://en.pharmacology.med.uoa.gr/) and ANY-Maze software (version 4.99 m, http://www.anymaze.co.uk/). Tests were performed at 4, 8, 12 and 16 months of age in 3xTg-AD and age matched WT animals.

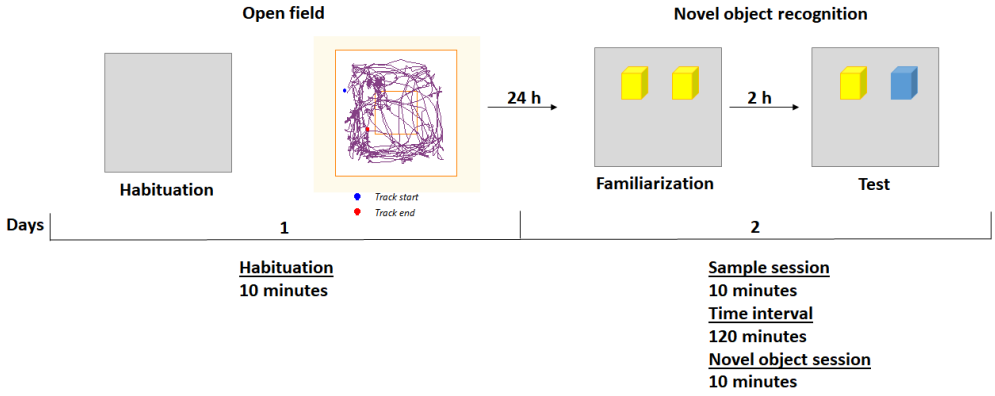

Figure 6 – Behavioral tests consisting of open field and novel object recognition tests used for assessing locomotor activity status and memory performance.

On the first day, the animals were placed in an open field maze during 10 min to allow their adaptation to the new environment and locomotor activity was analyzed during this period. The parameters evaluated were the distance traveled and the speed. The performance of the animals was analyzed using the behavioral scoring program ANY-maze.

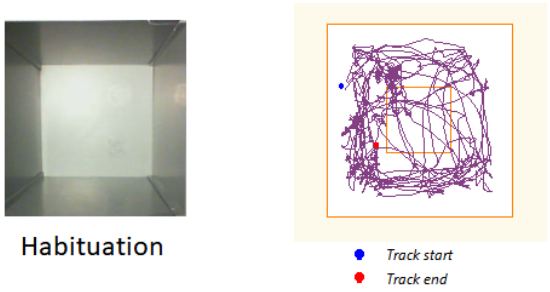

Figure 7 – The open field maze was used to evaluate locomotor activity in WT and 3xTg-AD. Schematic representation of traveled path of a mouse with the track start and track end depicted.

Habituation to the open field arena was performed to reduce possible anxiety like behavior due to placing in a novel environment. On the second day, the animals were placed in an open field apparatus with two identical objects and after a time interval one of the objects was kept in the arena (familiar object), while the other was replaced by a new one, approximately with the same size and texture, but different in shape (novel object). The novel object recognition test was performed in order to assess mice recognition memory. This test consisted of two 10 min sessions: the first with two identical objects (sample session) and the second (test session, 2 h after sample session) with two dissimilar objects (a familiar and a novel one). Exploration of objects was considered when animals were facing the objects with the nose up to 2 cm away from the object. The time exploring each object and the number of explorations were recorded. The performance of the animals was analyzed using the behavioral scoring program Observador.

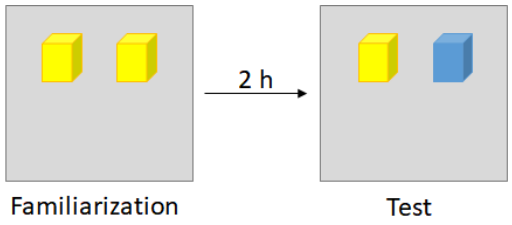

Figure 8 – Novel object recognition test consisted of two 10 min sessions: the first with two similar objects (familiarization) and the second with a novel object (test). The interval between sessions was 2 h. In the first session, each animal was exposed to two similar objects. Then, in the second session, one object was replaced by a new one.

1.3.3. Western blot

Hippocampus from 3xTg-AD (n=5) and WT (n=6) mice were dissected in ice-cold Hank's balanced salt solution (HBSS: 137 mM NaCl, 5.4 mM KCl, 0.45 mM KH_2PO_4, 0.34 mM NaHPO, 4 mM, $NaHCO_3$, 5 mM glucose, pH 7.4), frozen in liquid nitrogen and stored at -80°C. All

samples were lysed in cell lysis buffer (Cell Signaling Technology, Danvers, Massachusetts, USA) supplemented with complete mini ethylenediaminetetraacetic acid (EDTA)-free protease inhibitor cocktail tablets (Roche, Basel, Switzerland), PhosSTOP phosphatase inhibitor tables (Roche), 0.1 mM phenylmethylsulfonyl fluoride (PMSF; Roche) and 2 mM of dithiothreitol (DTT; Fisher, Hampton, New Hampshire, USA). After homogenization, samples were frozen and thawed three times. Then, the samples were centrifuged at 16,100xg during 10 min at 4°C and the supernatant was collected. After protein quantification by BCA method (Pierce Biotechnology, Waltham, Massachusetts, USA), samples were denatured by adding 6x concentrated sample buffer (0.5 M Tris, 30% glycerol, 10% sodium dodecyl sulfate (SDS), 0.6 M DTT, 0.012% bromophenol blue) and heated for 5 min at 95°C. Samples were separated in SDS-polyacrylamide gel electrophoresis (SDS-PAGE) and transferred onto PVDF membranes (Millipore, Burlington, Massachusetts, USA). The membranes were blocked with 5% BSA and were then incubated with the antibodies indicated in Table 4. Immunoreactive bands were visualized using Enhanced Chemi-Fluorescence system (ECF; GE Healthcare, Chicago, Illinois, USA) on an imaging system (Thyphoon FLA 9000, GE Healthcare), or with Enhanced Chemiluminescence system (ECL; Bio-Rad, Hercules, California, USA) on Image Quant LAS 500 (GE Healthcare). Digital quantification of band intensity was performed using Quantity One software (Bio-Rad). The membranes were then reprobed and tested for β-actin immunoreactivity to prove that similar amounts of protein were applied in the gels. Data were obtained by calculating the ratio between each target protein and β-actin, and expressed as percentage of wild type (control).

Table 4 - List of primary and secondary antibodies used in Western blotting.

Primary Antibody	**Host**	**Dilution**	**Protein (µg)**	**Supplier**
Anti-Amyloid-β (D54D2)	Rabbit	1:1,000	20	Cell Signaling Technology
Anti-p-tau $^{(ser396)}$	Rabbit	1:1,000	10	Santa Cruz Biotechnology
Anti-β-Actin	Mouse	1:5,000	20/10	Sigma-Aldrich
Secondary antibody				
HRP* Anti-Rabbit		1:10,000	-	Bio-Rad
AP** Anti-Mouse		1:10,000	-	Sigma-Aldrich

*HRP - Horseradish peroxidase, **AP - alkaline phosphatase

1.3.4. Magnetic resonance imaging acquisitions

MRI experiments were performed in a BioSpec 9.4T scanner with a standard cross coil setup using a volume coil for excitation (with 86/112 mm of inner/outer diameter, respectively) and quadrature mouse surface coil for signal detection (Bruker Biospin, Ettlingen, Germany). Mice (WT: n=6; 3xTg-AD: n=7) were kept anesthetized by isoflurane (1.5%) with 100% O_2 and body temperature and respiration monitoring (SA Instruments SA, Stony Brook, NY, USA).
For structural analysis, T2-weighted images were acquired in coronal planes using a rapid acquisition with relaxation enhancement (RARE) sequence with the following parameters: TR=3800 ms; TE=33 ms; 10 averages; pixel size of 0.078 mm x 0.078 mm and slice thickness of 0.5 mm without spacing between slices (total head volume: 256 pixels x 256 pixels x 34 slices). Brain permeability was assessed after injection of Gadovist® (0.1 mmol/kg) using the dynamic contrast enhanced (DCE) magnetic resonance imaging technique. The following parameters were used in 2D DCE-FLASH: TE/TR = 2.5/251.446 ms, flip angle = 70º, FOV= 20 x 20 mm, matrix= 156 x 85, slice thickness 0.5 mm, number of slices= 18, number of repetitions= 40. For localized ^{1}H-MRS, data were collected in a volume of interest placed on the hippocampus. B0 map was acquired before spectroscopy and shims were optimized through a mapshim voxel. A point resolved spectroscopy (PRESS) sequence was used in combination with outer volume suppression and variable power and optimized relaxation delays (VAPOR) water suppression with parameters as follows: TR= 2500 ms, TE=16.225 ms, number of averages=720, three flip angles=90º, 142º and 142º, bandwidth=5000 Hz, number of acquired points=2048 yielding a spectral resolution of 1.22 Hz/point and voxel size of 2.1x1.3x1.3 mm. For each animal, an unsuppressed water signal (TE=16.225 ms, TR=2500 ms, 16 averages and none water suppression) was acquired immediately before acquiring the water suppressed spectrum.

1.3.4.1. Voxel based morphometry

Voxel based morphometry (VBM) was performed using the statistical parametric mapping software (SPM, Welcome Department of Cognitive Neurology, London, UK), the SPMMouse toolbox (Sawiak, Wood et al. 2013) and a homemade script involving the following steps: a) T2-weighted images were corrected for the magnetic field inhomogeneity generated by the surface coil: this was done using intensity curves from T2-weighted images obtained for an homogeneous phantom and acquired with the same coil and system configuration; b) the rigid body was aligned by registering (affine transformation) the images to the template space; c) tissue segmentation was carried out by means of the grey matter (GM), white matter (WM) and cerebrospinal fluid (CSF) tissue probability maps as provided in the toolbox; d) GM images were non-linearly normalized to the template space and were modulated to correct for volume

changes that may have occurred during normalization; e) The obtained images were smoothed by applying a 0.5 mm FWHM Gaussian kernel. All steps were done using the default settings of the toolbox.

1.3.4.2. Volumetry

For volumetry, after correction of magnetic field inhomogeneity (as described for VBM), images were segmented using the ITK-SNAP software based on manual delineation of the hippocampus (-1.06 to -4.16 Bregma) performed by a user blind for the two groups. The atlas from Franklyn and Paxinos was used as reference (Paxinos and Franklin 2004). The hippocampal volume was then obtained by multiplying the number of voxels by the voxel size, as provided by the software.

1.3.4.3. Dynamic contrast enhanced imaging

Dynamic contrast enhanced imaging (DCE) depicts the wash in, plateau and wash out contrast kinetics of the tissue. DCE data were processed as follows: a) images were rescaled, filtered (excluding voxels outside the brain) and corrected for movement; b) regions of interest (ROI) were drawn for each animal in a semi-automatic procedure, using MRICron (2015) and custom made Matlab functions. Previously reported in house Matlab functions were used for further analysis and extraction of perfusion measurements (Rodrigues, Matafome et al. 2017); c) the perfusion curve (accumulation of contrast agent) was extracted per ROI and animal, and normalized to the baseline (time window before injection); d) from these curves, the time to peak (TTP; time delay between injection and perfusion peak), the peak amplitude (maximum perfusion value, representing the vascular volume) and the area under the curve (AUC) were calculated. Note that the AUC parameter is the overall accumulation of contrast agent in the ROI. Additionally, the blood brain barrier perfusion index (BBBi) was calculated as follows: the residual enhancement at the last ten dynamic acquisition time-points/frames included the contribution from the contrast agent that had leaked into the interstitial space, and this parameter, normalized to the vascular volume measured as the peak amplitude of the perfusion curve, was used as a BBBi (Wang, Golob et al. 2006, Lipsø 2016).

1.3.4.4. ^{1}H-MRS

^{1}H-MRS spectra were saved as FIDs, corrected for the frequency drift and for residual eddy current effects using the reference water signal. Data were analysed using the LCModel package (Provencher 1993), which calculates the best fit to the acquired spectrum as a linear combination of a model based on a set of brain metabolites. The Cramér-Rao lower bounds (CRLB) criterion was used as a measure of the reliability of the fitting and set to 21%. Representative spectra are given in Figure 17. Metabolite concentration was calculated as we

have previously described (Petrella, Castelhano et al. 2018, Ribeiro, Castelhano et al. 2018). For statistical analysis, we were particularly interested in taurine, and therefore its concentration in relation to the water signal was determined.

1.3.5. Positron emission tomography acquisitions

For *in vivo* assessment of cerebral Aβ plaque deposition by means of ^{11}C Pittsburgh compound B (^{11}C-PIB) and microglia activation (^{11}C-PK11195) mice were submitted to PET imaging in a high-resolution small animal PET-RPC scanner prototype developed by LIP-Coimbra, in collaboration with the Institute of Nuclear Sciences Applied to Health (ICNAS), University of Coimbra. PET scans were performed, starting at 8 months of age, using the prototype which is based on resistive plate chambers (PET-RPC) (Martins, Blanco et al. 2014). Animals were kept anesthetized and monitored, as for MRI acquisitions, and scanned after the injection of ^{11}C-PIB and PK11195 during 60 min, respectively. ^{11}C-PiB had a mean activity of 12.44 ± 2.11 µCi/g. These radiopharmaceuticals bind with high affinity to the Aβ plaques in the brain. PK11195, which is a marker of the translocator protein (TSPO), indexing microglia activation, had a mean activity of 12.66 ± 2.26 µCi/g. To facilitate the co-registration of PET and MRI images during pre-processing, and thus allowing the segmentation of regions of interest, three fiducial markers were positioned on the animal platform.

1.3.5.1. PET data processing

PET images were reconstructed using the OSEM algorithm with a voxel volume of 0.125 mm^3 (0.5 x 0.5 x 0.5 mm) using the data acquired between 20 and 60 min after injection. After reconstruction, a correction to the field of view was carried out and images were saved as DICOM. 3D Slicer software was then used to manually co-register PET and MRI images using the fiducial markers as reference. Manual segmentation of the hippocampus was then performed, using ITK-SNAP, and the mean counts per mm^3, normalised to the activity injected per gram and corrected for the system sensitivity, were computed. For statistical analyses the ratio between the uptake in the hippocampus and cerebellum was used.

1.3.6. Statistical analysis

The normality of the data was assessed with Shapiro-Wilk and D´Agostino and Pearson omnibus normality tests. Statistical analysis of molecular and behavioral data was performed with GraphPad Prism Version 6 (GraphPad Software, San Diego, CA, USA) using parametric Student´s t-test or nonparametric Mann-Whitney test. Longitudinal and between groups analyses of the hippocampal volumes, taurine concentrations, blood brain barrier permeability parameters and the uptakes of ^{11}C-PIB and PK11195 were carried out using SPSS 22.0 (SPSS

Inc., Chicago, IL, USA) with an ANOVA repeated measures (mixed-effect) followed by pairwise comparisons employing Bonferroni corrections. A regression analysis was also performed to fit the volumetric data to a linear model and assess the effect of aging and rate of volumetric reduction. Intercepts (β0) and slopes (β1) were compared using GraphPad Prism Version 6. During VBM, to analyze differences in GM volumes between groups, at each time point a Student's t-test was performed at the voxel level. Voxels with GM values less than 0.2 were not included. Results were, firstly, obtained as whole brain statistical maps. After that, the analysis was repeated on the region of interest and corrected for multiple comparisons using FWE ($P<0.05$). Differences were localized using the atlas from Franklyn and Paxinos (Paxinos and Franklin 2004). Data were considered to be significant at *$P<0.05$, **$P<0.01$, ***$P<0.001$. All data are reported as mean ± SEM.

1.4. Results

1.4.1. Behavioral impairment patterns in 3xTg-AD mice

The open field test evaluates the spontaneous activity of mice when exploring an environment. Several parameters can be measured as a way to determine locomotor function, namely distance and speed (Figure 9). WT mice had a better locomotor activity performance than 3xTg-AD mice at 4, 8 and 16 months, as can be seen by evaluating the overall distance traveled or the speed in the open field arena (Figure 9). Motor deficits were detected at 4 months and these deficits persisted until older ages. However, at 12 months of age no significant differences were detected both in distance traveled and speed between WT and 3xTg-AD mice (Distance $_{\text{WT at 4 months}}$=7.02 ± 0.39 m; Distance $_{\text{3xTg-AD at 4 months}}$=5.09 ± 0.49 m; Distance $_{\text{WT at 16 months}}$=3.86 ± 0.30 m; Distance $_{\text{3xTg-AD at 16 months}}$=2.54 ± 0.24 m). Novel object recognition memory measures show that there was an impairment in object recognition memory in 3xTg-AD mice at all time points (Figure 10A). WT animals spent more time exploring the novel object than the familiar object at all time points and this difference was statistically significant at 4, 8 and 16 months of age (Figure 10B). Moreover, at 4 and 16 months there was a statistically significant difference in the number of explorations of the novel object between groups (Figure 11A). At 12 and 16 months WT mice significantly explored more times the novel object than the familiar one. At 4 and 8 months of age WT mice explored more times the novel object than the familiar object, but this difference was not statistically significant (Figure 11B). In addition, 3xTg-AD animals did not show a statistically significant difference in the exploration time (Figure 10C) and number of explorations (Figure 11C) of the familiar and novel objects at all time points. Regarding the total exploration time, WT mice spent more time exploring both objects than transgenic mice at 4, 12 and 16 months of age. At 8 months WT mice spent more time exploring both objects than 3xTg-AD mice, but this difference was not significant (Figure

12A). Also, WT mice spent more time exploring the novel object than 3xTg-AD mice at all time points (Figure 12B).

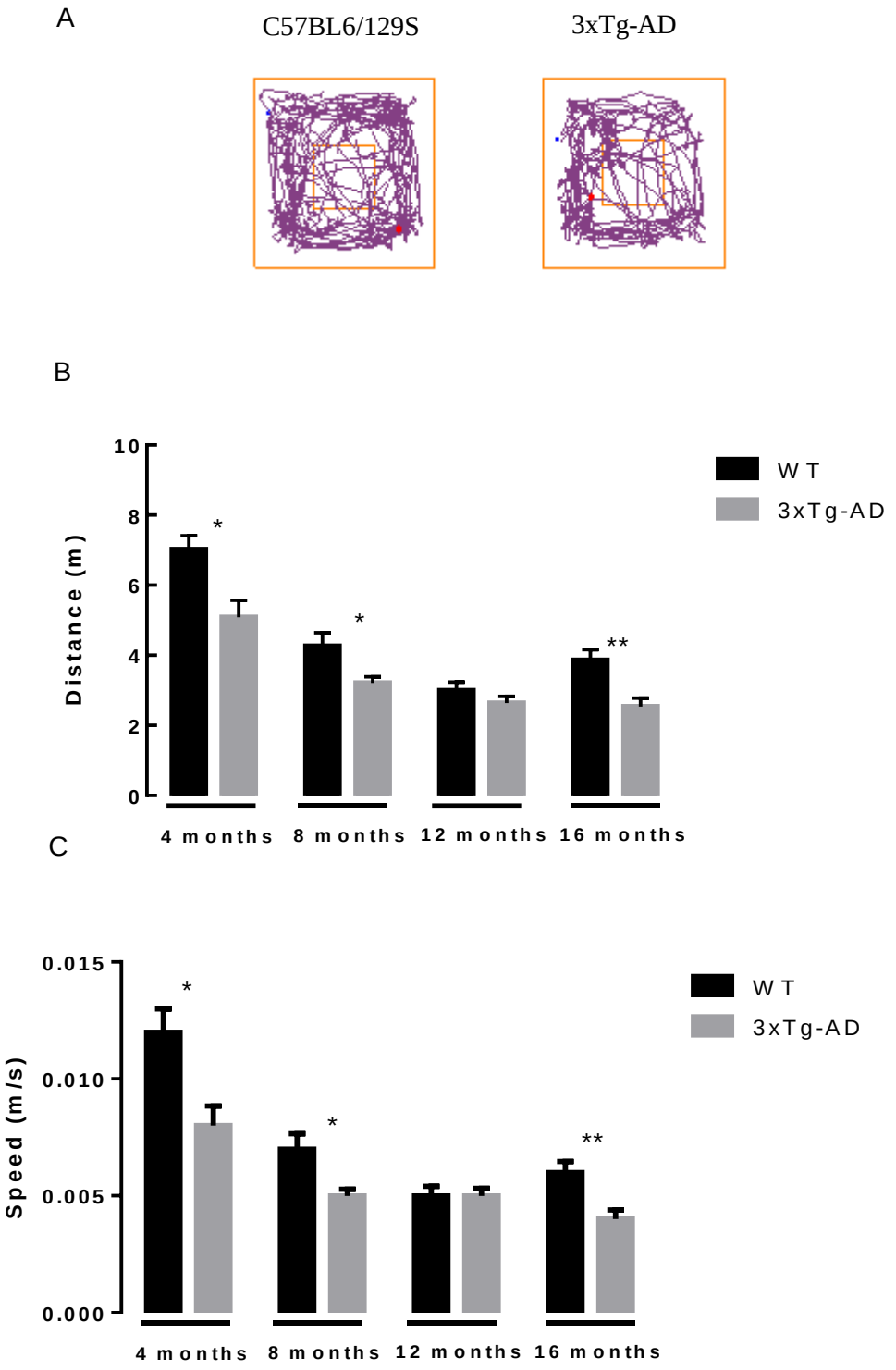

Figure 9 – (A) Representative trace images of WT and 3xTg-AD mice in the open field. Locomotor activity of WT and 3xTg-AD animals was evaluated by measuring the (B) distance traveled (m) and (C) speed (m/s) at different time points (4, 8, 12 and 16 months of age). Results are presented as mean ± SEM and were analyzed with the Student´s t-test; *P<0.05

and **P<0.01 ($n_{WT\ at\ 4\ months}$=21, $n_{WT\ at\ 8\ months}$=20, $n_{WT\ at\ 12\ months}$=17, $n_{WT\ at\ 16\ months}$=17, $n_{3xTg\text{-}AD\ at\ 4\ months}$=20, $n_{3xTg\text{-}AD\ at\ 8\ months}$=23, $n_{3xTg\text{-}AD\ at\ 12\ months}$=22, $n_{3xTg\text{-}AD\ at\ 16\ months}$=22).

B

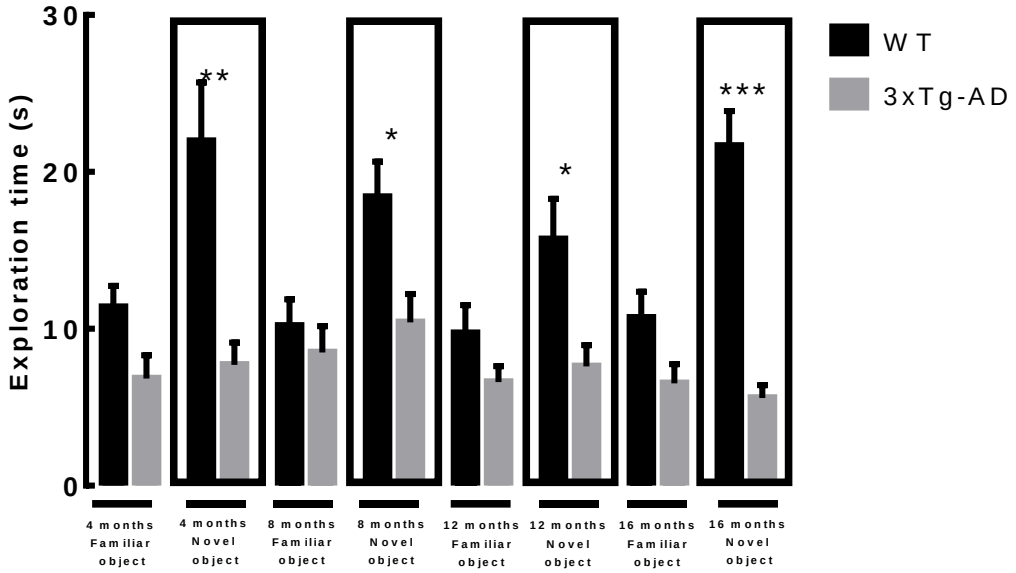

C

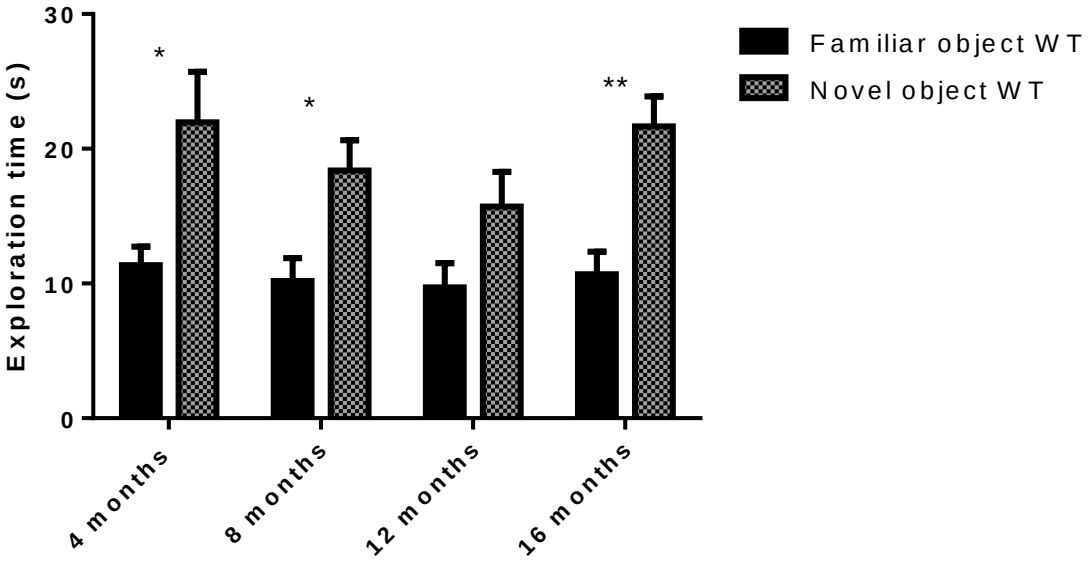

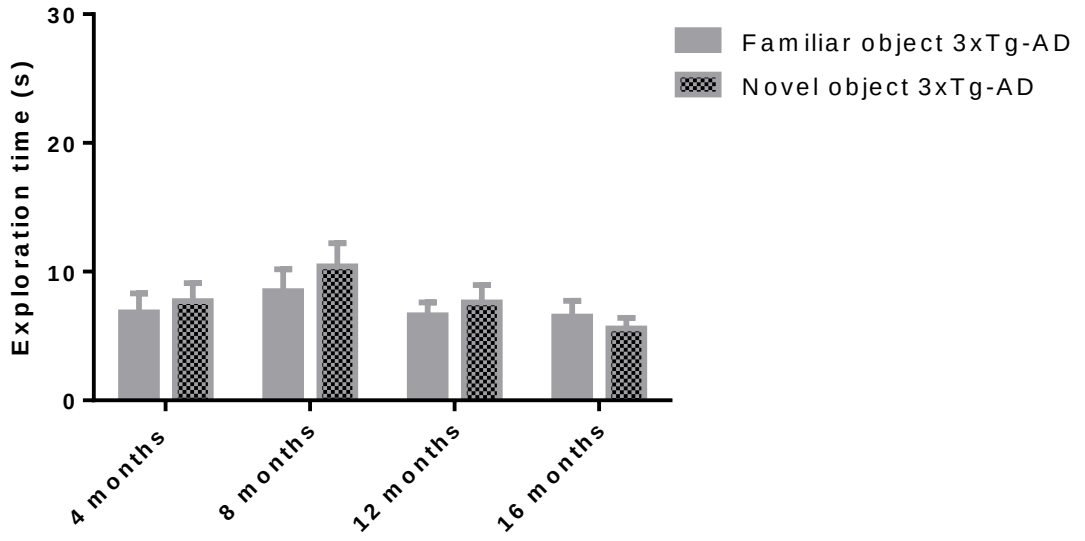

Figure 10 – Exploration time of WT and 3xTg-AD mice in the novel object recognition test at different time points (4, 8, 12 and 16 months of age). (A) Exploration time of both groups is compared; (B) Exploration time of WT in familiar and novel object; (C) Exploration time of 3xTg-AD in familiar and novel object. Results are presented as mean ± SEM and were analyzed with the Student´s t-test; *P<0.05, **P<0.01 and ***P<0.001 ($n_{WT\ at\ 4\ months}$=21, $n_{WT\ at\ 8\ months}$=20, $n_{WT\ at\ 12\ months}$=17, $n_{WT\ at\ 16\ months}$=17, $n_{3xTg\text{-}AD\ at\ 4\ months}$=20, $n_{3xTg\text{-}AD\ at\ 8\ months}$=23, $n_{3xTg\text{-}AD\ at\ 12\ months}$=22, $n_{3xTg\text{-}AD\ at\ 16\ months}$=22).

A

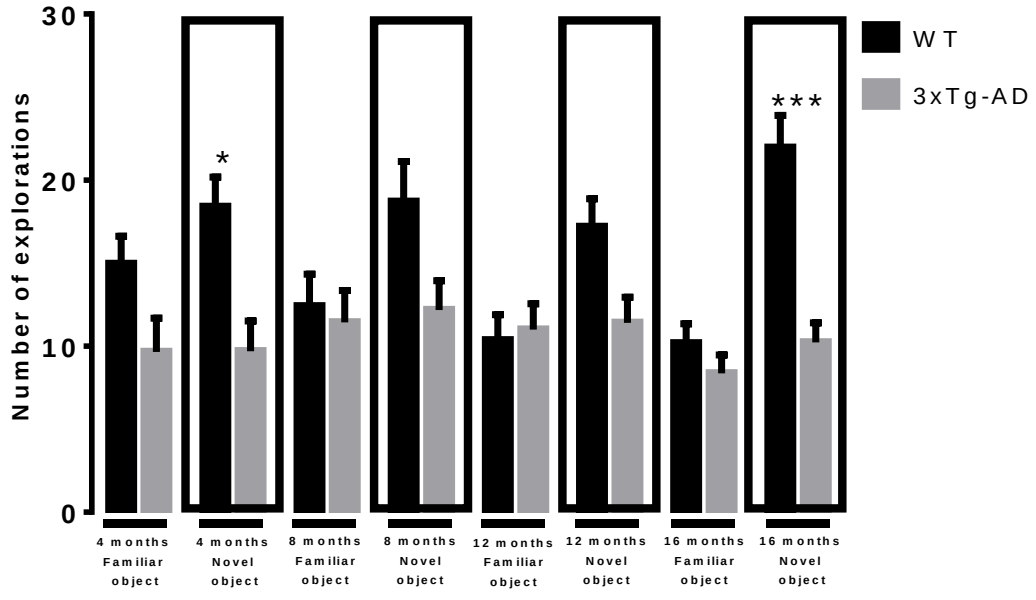

B

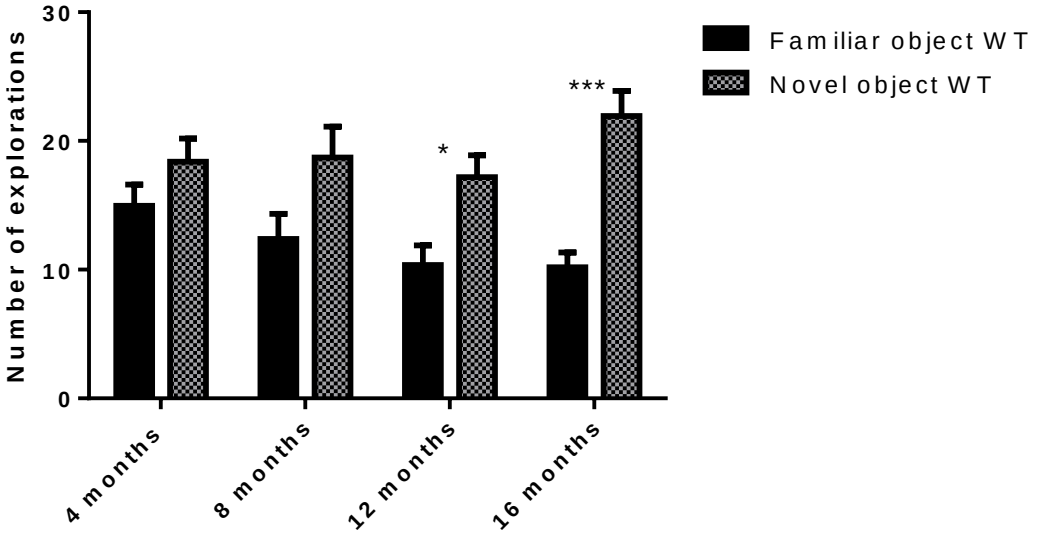

C

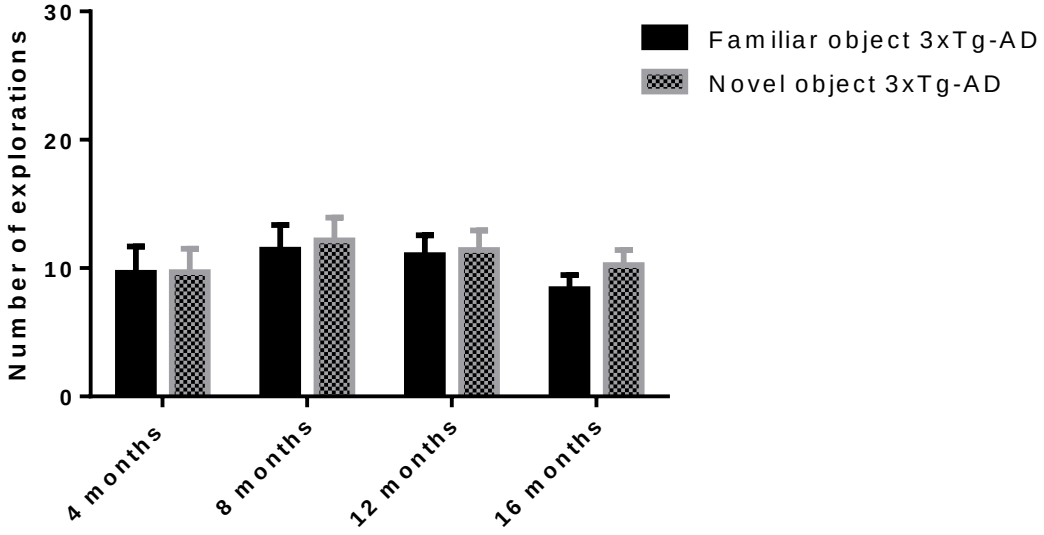

Figure 11 – Number of explorations of WT and 3xTg-AD mice in the novel object recognition test at different time points (4, 8, 12 and 16 months of age). (A) Number of explorations of both groups is compared; (B) Number of explorations of WT in familiar and novel object; (C) Number of explorations of 3xTg-AD in familiar and novel object. Results are presented as mean ± SEM and were analyzed with the Student´s t-test; *P<0.05, **P<0.01 and ***P<0.001 ($n_{\text{WT at 4 months}}$=21, $n_{\text{WT at 8 months}}$=20, $n_{\text{WT at 12 months}}$=17, $n_{\text{WT at 16 months}}$=17, $n_{\text{3xTg-AD at 4 months}}$=20, $n_{\text{3xTg-AD at 8 months}}$=23, $n_{\text{3xTg-AD at 12 months}}$=22, $n_{\text{3xTg-AD at 16 months}}$=22).

A

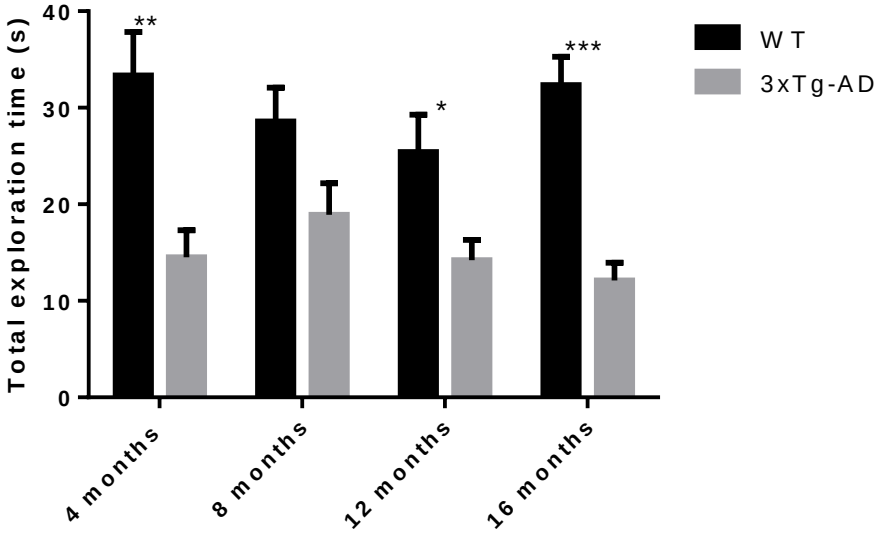

B

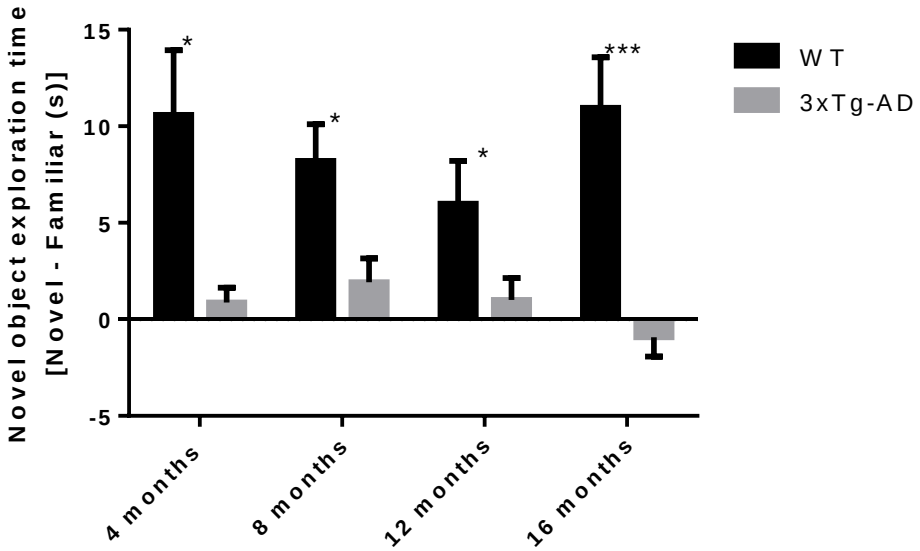

Figure 12 – Total exploration time (A) and novel object exploration time (B) of WT and 3xTg-AD mice at different time points (4, 8, 12 and 16 months of age). Results are presented as mean ± SEM and were analyzed with the Student´s t-test; *P<0.05, **P<0.01 and ***P<0.001 ($n_{WT\ at\ 4\ months}$=21, $n_{WT\ at\ 8\ months}$=20, $n_{WT\ at\ 12\ months}$=17, $n_{WT\ at\ 16\ months}$=17, $n_{3xTg\text{-}AD\ at\ 4\ months}$=20, $n_{3xTg\text{-}AD\ at\ 8\ months}$=23, $n_{3xTg\text{-}AD\ at\ 12\ months}$=22, $n_{3xTg\text{-}AD\ at\ 16\ months}$=22).

1.4.2. Increased Aβ and p-tau protein levels in the hippocampus of 3xTg-AD mice

The two major hallmarks of AD are the diffuse and neuritic plaques which are predominantly composed by Aβ, and the neurofibrillary tangles, formed by aggregates of hyperphosphorylated tau protein (p-tau) (Selkoe 2001). The protein levels of Aβ monomers in the hippocampus of 3xTg-AD mice increased, comparing with age-matched WT, at 4 months

(373.4±63.3% of WT, P<0.01), 8 months (717.1±174.7% of WT, P<0.01), 12 months (1434.9±196.1% of WT, P<0.05) and 16 months (9447.5±1338.9% of WT, P<0.05), reaching a maximum peak at 16 months of age (Figure 13A). We also detected an increase of p-tau levels in the hippocampus of 3xTg-AD at 4 months (434.8±138.2% of WT, P<0.01), 8 months (360.7±69.4% of WT, P<0.01), 12 months (147.4±7.0% of WT, P<0.01) and 16 months (230.2±27.3% of WT, P<0.01) (Figure 13B). Contrarily to what was observed for Aβ, p-tau levels were higher at early time points and decreased with age.

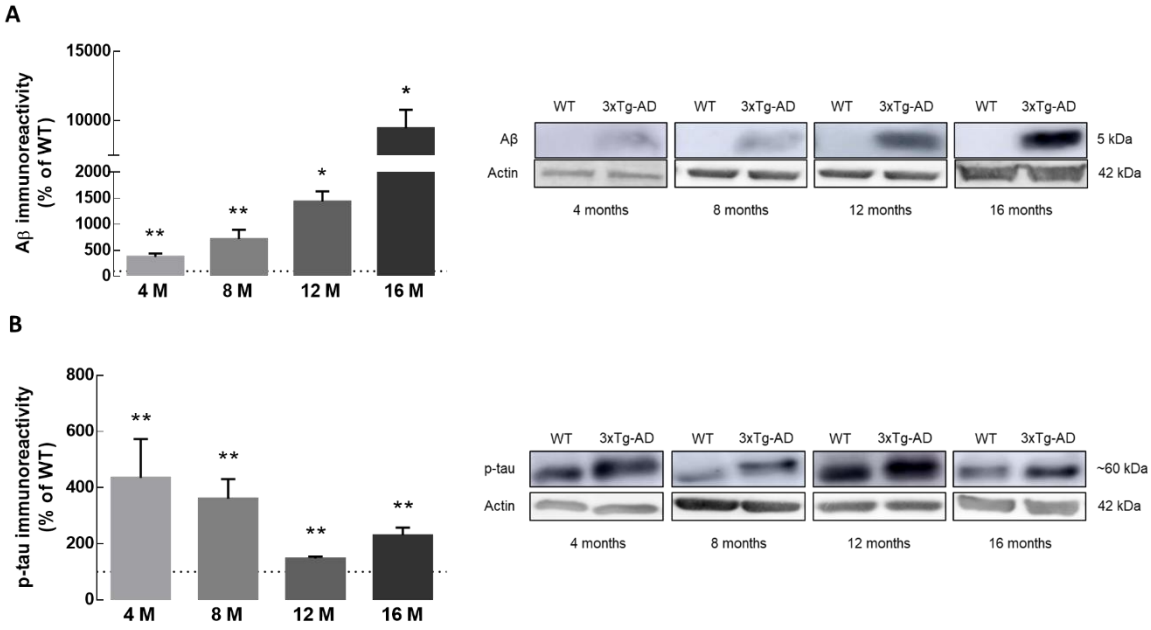

Figure 13 – Increase of Aβ and p-tau protein levels in the hippocampus of 3xTg-AD mice. The protein levels of Aβ (A) and p-tau (B) in total hippocampal extracts from 3xTg-AD and age-matched WT mice were analyzed by Western blotting. Representative images for Aβ, p-Tau and β-actin (loading control) for each time point (4, 8, 12 and 16 months of age) are presented. The results are expressed as percentage of age matched WT animals, and are presented as mean ± SEM of 4–6 animals. *P<0.05 and **P<0.01, different from WT, Mann-Whitney test.

1.4.3. Hippocampal structural impairment in 3xTg-AD mice

When evaluating the structural integrity of the hippocampus, volumetric analysis showed that the 3xTg-AD mice had reduced hippocampal volumes starting at 4 months, which was accentuated during disease progression towards 16 months. Statistical tests showed significant between group effects ($F_{(1,8)}$=268.230, P<0.001) and the post-hoc analyses revealed that the volume of the transgenic mice hippocampi was significantly reduced at all time points compared to the WT group (P<0.001) as shown in Figure 14. Regression curves suggested a more pronounced volumetric reduction occurring in the 3xTg-AD animals ($\beta 1_{3xTg-}$

$_{AD}$=-0.091 mm^3/month; $\beta1_{WT}$=-0.012 mm^3/month) with a trend for significance when comparing the slopes ($F_{(1,36)}$=3.704, P=0.062), (Figure 14, solid lines).

Morphometric analyses, which assess differences in GM volume in a voxel-by-voxel basis, further corroborate these observations showing that clusters of significantly reduced GM volume are already present at 4 months of age in the 3xTg-AD group in the right and left hippocampus (Figure 15A). At later stages, clusters are more prevalent and spread across the hippocampus with emerging clusters of GM volume reductions in the anterior regions englobing CA1, CA2, CA3 and dentate gyrus subfields, as illustrated in Figure 15B.

Regarding perfusion imaging, which is useful to evaluate the BBB permeability (Wang, Golob et al. 2006), results revealed a time dependent increased permeability index and decreased vascular volume (as measured by the peak amplitude) in transgenic animals at later stages of the disease, i.e. 16 months (Figure 16). We found a significant main effect detected with ANOVA for peak amplitude (F=3.41, P=0.034) and differences between groups were visible at 16 months ($F_{(1,8)}$=23.06, P=0.001, Figure 16A). Regarding BBBi, that represents the leakage/permeability of the brain barrier, the longitudinal analysis did not detect a time*group interaction. Post-hoc analysis showed that 3xTg-AD animals had increased BBBi in comparison to WT at 16 months ($F_{(1,8)}$=25.47, P=0.001; Figure 16B).

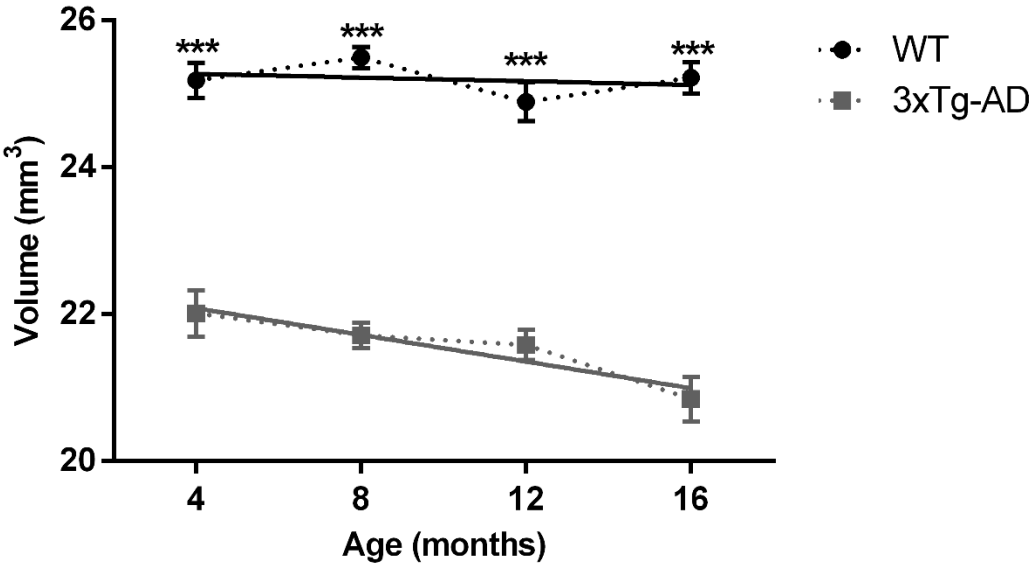

Figure 14 - Hippocampal volumes of WT and 3xTg-AD mice at different time points (4, 8, 12 and 16 months). Solid lines represent the regression curves showing the temporal evolution of the hippocampal volumes. Regression curves: WT, $\boldsymbol{V = -0.01244t + 25.32}$; 3xTg-AD, $\boldsymbol{V = -0.09071t + 22.45}$. V, volume; t, time. Results are presented as mean ± SEM and were analyzed with an ANOVA repeated measures (mixed-effect) followed by a Bonferroni post-hoc test, ***P<0.001, and a linear regression analysis (n $_{WT\ at\ 4,\ 8,\ 12\ and\ 16\ months}$ =4, n $_{3xTg\text{-}AD\ at\ 4,\ 8,\ 12\ and\ 16\ months}$ =6).

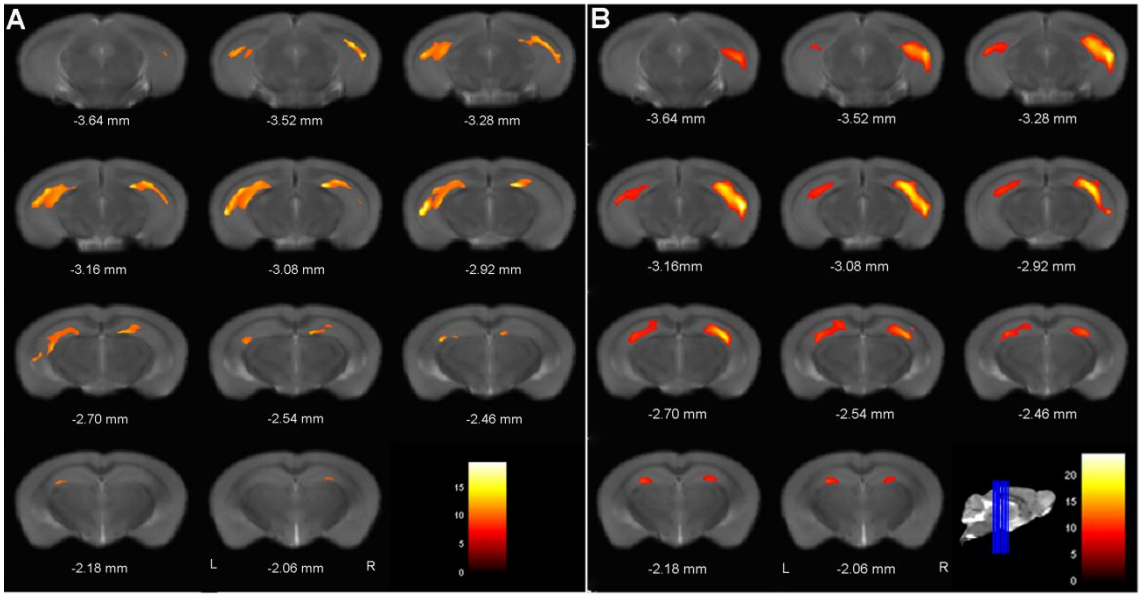

Figure 15 – Voxel based morphometry results in a coronal view at 4 (A) and 16 months (B). Colour bar denotes the T-score magnitude, at the voxel level, with a threshold level of P<0.05 FWE corrected ($n_{WT\ at\ 4,\ 8,\ 12\ and\ 16\ months}$=6, $n_{3xTg\text{-}AD\ at\ 4,\ 8,\ 12\ and\ 16\ months}$=7).

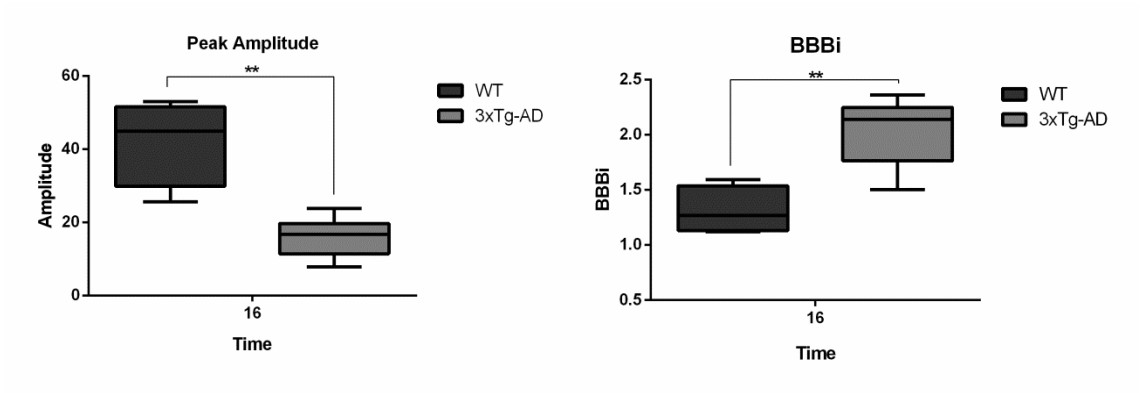

Figure 16 - Perfusion peak amplitude and blood brain barrier index at 16 months of age. Left panel: Perfusion peak amplitude. Right panel: BBB permeability index. Results are presented as mean ± SEM and were analyzed with an ANOVA repeated measures (mixed-effect) followed by a pairwise comparison employing a Bonferroni post-hoc test; **P<0.01 ($n_{WT\ at\ 4,\ 8,\ 12\ and\ 16\ months}$ =4, $n_{3xTg\text{-}AD\ at\ 4,\ 8,\ 12\ and\ 16\ months}$ =6).

1.4.4. Decreased levels of taurine in the hippocampus of 3xTg-AD mice

The spectra enabled a reliable quantification of taurine and its levels were found significantly reduced in the 3xTg-AD animals compared to the WT ($F_{(1,8)}$=45.804, P<0.001) at 4 months ($F_{(1,8)}$=18.470, P<0.003), 8 months ($F_{(1,8)}$=8.573, P<0.019) and 16 months ($F_{(1,8)}$=21.635, P<0.002), as summarized in Figure 16.

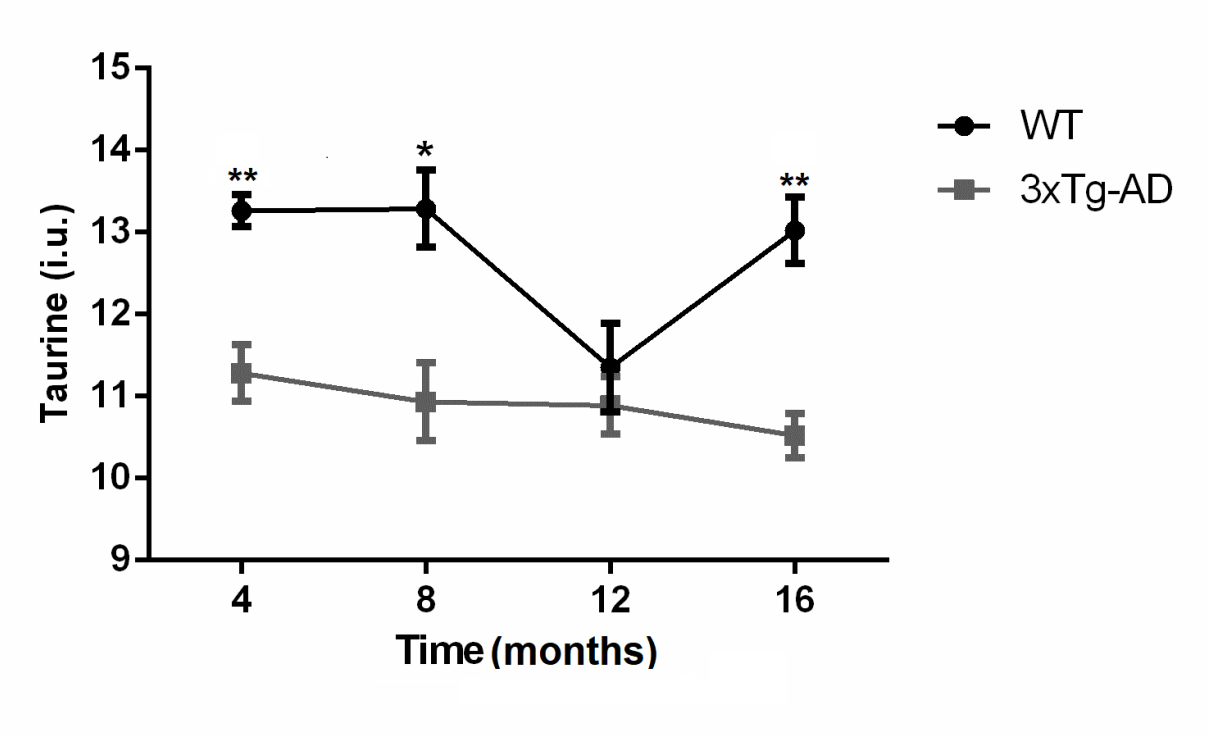

Figure 16 - Taurine levels of 3xTg-AD and WT mice at different time points (4, 8, 12 and 16 months of age). Results are presented as mean ± SEM and were analyzed with an ANOVA repeated measures (mixed-effect) followed by a pairwise comparison employing a Bonferroni post-hoc test; *P<0.05 and **P<0.01 ($n_{WT\ at\ 4,\ 8,\ 12\ and\ 16\ months}$=4 and $n_{3xTg\text{-}AD\ at\ 4,\ 8,\ 12\ and\ 16\ months}$=6).

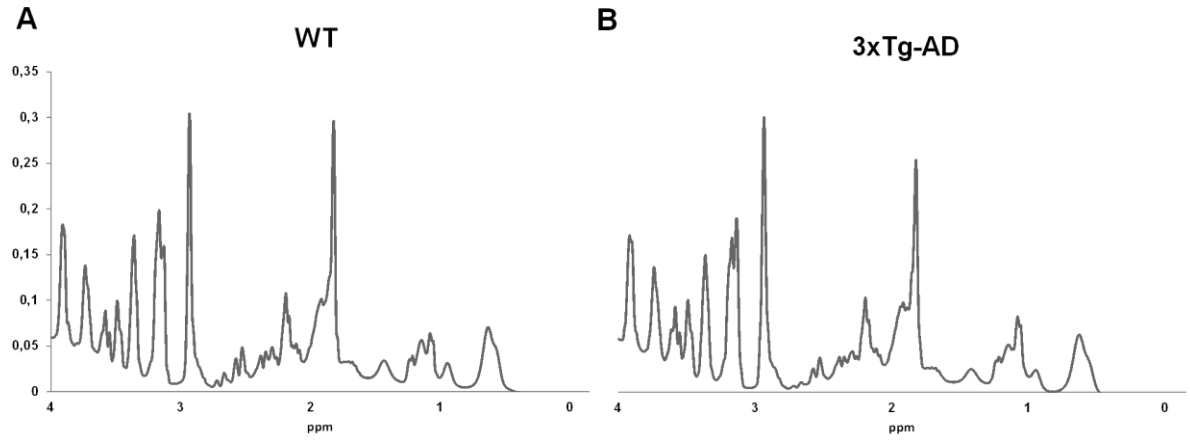

Figure 17 – Representative ^{1}H-MRS spectra of WT (A) and 3xTg-AD (B) mice acquired at 16 months.

1.4.5. No changes in amyloid load and inflammation evaluated by PET

No significant differences were found neither for the uptake values of ^{11}C-PIB (a marker of amyloid, Figure 18A, $F_{(2,9)}$=0.241, P=0.791) or ^{11}C-PK11195 (a marker of inflammatory processes, Figure 18B, $F_{(2,8)}$=1.828, P=0.222) between groups.

A

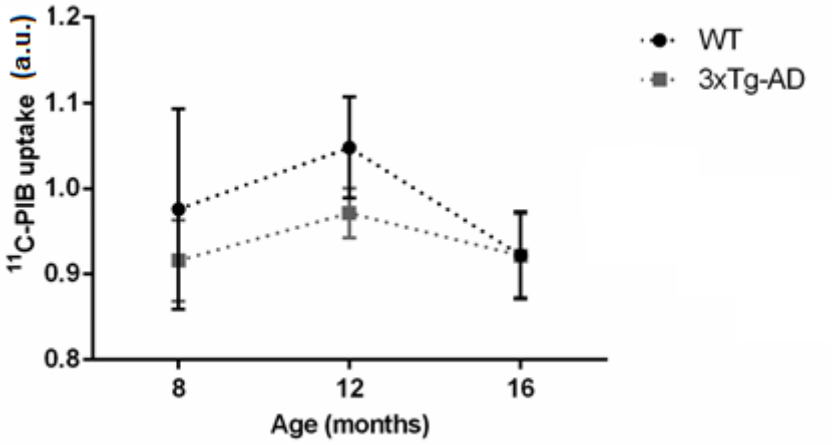

B

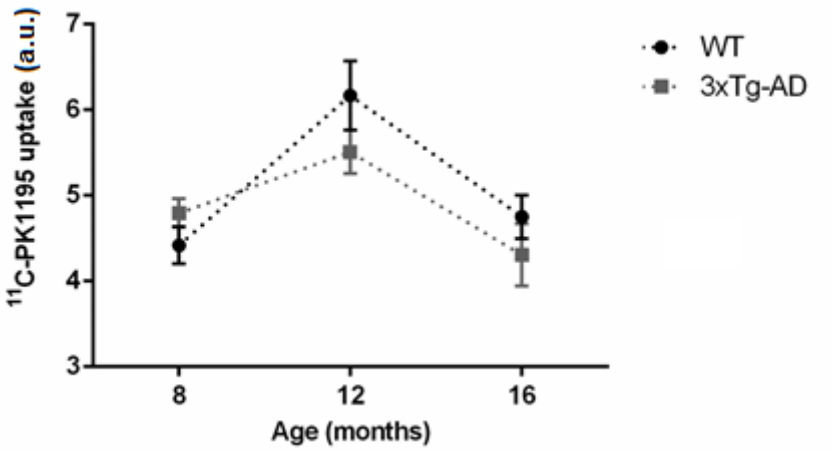

Figure 18 - PET ^{11}C-PIB (A) and ^{11}C-PK11195 (B) uptake of 3xTg-AD and WT mice at different time points (4, 8, 12 and 16 months of age). Results are presented as mean ± SEM and were analyzed with an ANOVA repeated measures (mixed-effect) followed by a pairwise comparison employing a Bonferroni post-hoc test; $P>0.05$ ($n_{\text{WT at 4, 8, 12 and 16 months}}=4$ and $n_{\text{3xTg-AD at 4, 8, 12 and 16 months}}=6$).

1.4.6. Body weight and cumulative proportion of survival

In 3xTg-AD mice the body weight was smaller than in WT animals at all time points (Figure 19). WT and 3xTg-AD animals used in this study did not differ in the cumulative proportion of survival recorded between 4 and 16 months (Figure 20).

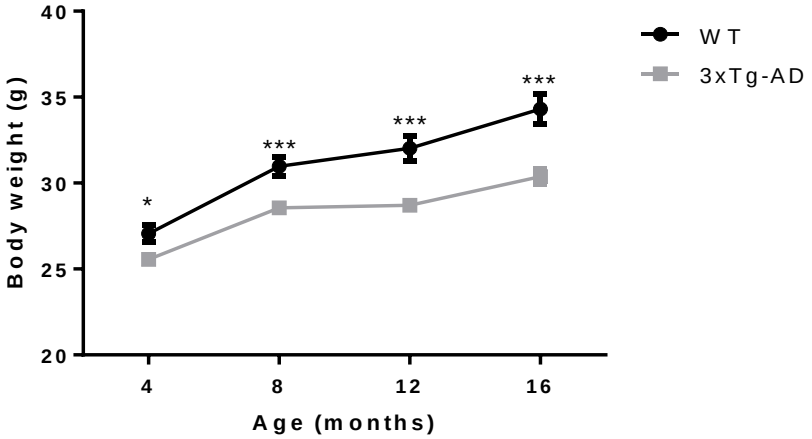

Figure 19 - Body weight of WT ($n_{WT\ at\ 4\ months}$=21, $n_{WT\ at\ 8\ months}$=20, $n_{WT\ at\ 12\ months}$=17, $n_{WT\ at\ 16\ months}$=17) and 3xTg-AD mice ($n_{3xTg\text{-}AD\ at\ 4\ months}$=20, $n_{3xTg\text{-}AD\ at\ 8\ months}$=23, $n_{3xTg\text{-}AD\ at\ 12\ months}$=22, $n_{3xTg\text{-}AD\ at\ 16\ months}$=22). Data represent the mean ± SEM and were analyzed with the Student´s t-test, **P<0.05, **P<0.01 and ***P<0.001.

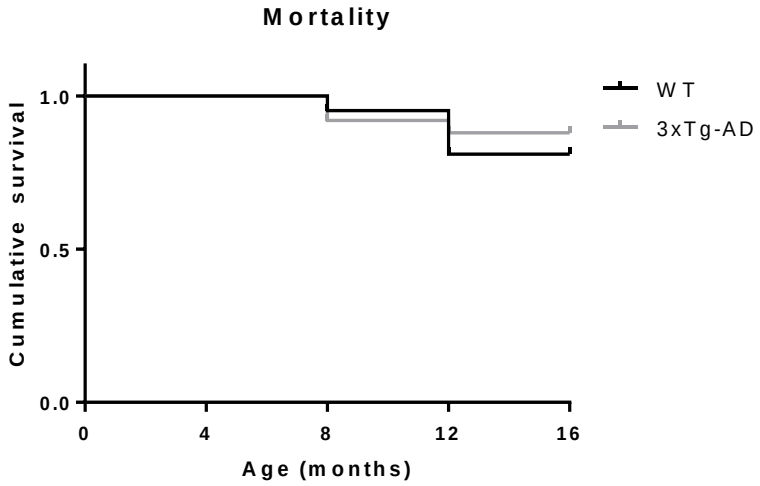

Figure 20 - Survival curve of WT and 3xTg-AD mice. Survival curves of the two strains are not significantly different. This graph represents 21 WT mice and 25 3xTg-AD mice: 4 WT mice and 3 3xTg-AD mice died.

1.5. Discussion

In this study we found that neurobehavioral deficits that are the hallmark of human AD can also be identified using multimodal molecular imaging techniques in animals, along with the novel finding of reduced levels of taurine over several time points. In particular, we found evidence for early hippocampal structural damage, local reduced levels of taurine and recognition memory deficits which paralleled increased hippocampal Aβ and p-tau levels.

Interestingly *in vivo* MRI measures of hippocampal parameters proved to be much more sensitive in this model than PET imaging. Moreover, we found no *in vivo* PET evidence for microglia activation and parameters of BBB integrity were only affected in late stages (16 months). Since motor activity can influence the outcome measurements of subsequent tests it needs to be evaluated in order to determine its influence in tasks designed for assessing cognitive deficits that depend on motor function. Locomotor activity deficits have already been detected in 3xTg-AD mice, but also in APP-deficient mice and APP23 mice (Zheng, Jiang et al. 1995, Van Dam, D'hooge et al. 2003, Halagappa, Guo et al. 2007, Filali, Lalonde et al. 2012, Carvalho, Machado et al. 2013). The 3xTg-AD animal model used in this study shows similar deficits, as shown by measuring the velocity and distance traveled in the open field test. Similar impairments have also been observed in AD patients and this functional impairment progresses as cognition declines (Bridenbaugh, Monsch et al. 2012). The novel object recognition test describes the ability of mice to preferentially explore a novel object than a familiar one. This memory test requires that vision is used to guide behavior towards objects that are discriminated based on their novelty and specific visual features and so it can be used to evaluate cognitive deficits related with recognition memory in several preclinical models of neurodegenerative disorders, including AD. Similarly to humans several brain regions are involved in rodent recognition memory including the hippocampus, prefrontal, perirhinal and entorhinal cortex. Therefore, the study of recognition memory impairments in mouse models of AD may provide important insights regarding AD pathology in humans (Eichenbaum, Yonelinas et al. 2007, Arsenault, Julien et al. 2011, Cohen and Stackman Jr 2015, Morici, Bekinschtein et al. 2015, Warburton and Brown 2015). Recognition memory test deficits suggest that the hippocampus or other structures of the medial temporal lobe are impaired, a behavioral pattern that is characteristic of AD (Gold and Budson 2008). Consequently, the impairment observed in the object recognition memory test in 3xTg-AD mice suggests that the episodic memory system typically impaired in AD was also impaired in this animal model. The hippocampus plays a pivotal role in the process of memory encoding and retrieval. Besides the hippocampus, other brain structures may also be affected such as the striatum and frontal cortex. In particular, the interaction between these brain regions is important in recognition memory (Seger and Cincotta 2005, Herweg, Apitz et al. 2016, Headley and Paré 2017). Oddo and colleagues detected synaptic dysfunction in the hippocampus of 3xTg-AD mice at 6 months of age. This structure is well known to have an impact in memory and cognition in AD patients. A possible explanation for this event is the intraneuronal accumulation of Aβ species. Intracellular immunoreactive Aβ species have been observed in 3xTg-AD mice in the neocortex between 3 and 4 months of age (Oddo, Caccamo et al. 2003). Therefore, it is not surprising that we were able to observe object recognition memory impairment already at 4 months. Furthermore, structural differences between WT and 3xTg-AD groups were detected

with volumetry and voxel based morphometry in the hippocampus as early as 4 months of age which corroborates the behavioral results. This is equivalent to a human age of about 26 years (Flurkey, Currer et al. 2007), which shows that this measure is really an early sensitive marker. Importantly MR volumetry of the hippocampus in humans is a valuable diagnostic criterion. Therefore, these results can be useful for further characterization of animal models of neurodegenerative diseases, and are in line with evidence reporting hippocampal atrophy in AD patients (Hsu, Shou et al. 2015). This is also in line with previous works in humans that reported alterations in the hippocampus volume of the same magnitude as we found here (Henneman, Sluimer et al. 2009, Schuff, Woerner et al. 2009).

Despite the observation that several mouse models of AD have normal BBB permeability (Bien-Ly, Boswell et al. 2015) we found differences in BBB permeability at 16 months, probably being a late consequence of the disease progression. Moreover, the decreased peak amplitude in the transgenic animals may be a sign of hypoperfusion. We also found that the hippocampus has increased levels of Aβ and p-tau. Contrarily to what has been reported in AD patients (Edison, Archer et al. 2008, Okello, Edison et al. 2009, Schuitemaker, Kropholler et al. 2013), using PET imaging we did not detect significant differences in amyloid deposition and neuroinflammatory status in the hippocampus. The reasons why amyloid load is difficult to detect using ^{11}C-PIB in this particular model, unlike other models, remain to be elucidated, given that we found molecular evidence for such accumulation. Also, we did not find evidence for microglia activation using a neuroinflammation marker (^{11}C-PK11195), suggesting that this is not a prominent feature underlying neurodegeneration in this model.

Regarding magnetic resonance spectroscopy we found that taurine levels in 3xTg-AD mice were reduced in the hippocampus. Since taurine prevents the neurotoxicity of Aβ reduced levels of taurine imply lower neuroprotection, which is relevant when amyloid plaques load is high in transgenic animals (Louzada, Lima et al. 2004). Indeed, Louzada and colleagues demonstrated that taurine prevents the neurotoxicity of β-amyloid and glutamate receptor agonists, and its low levels early on in the disease process suggests failure of endogenous neuroprotection. The temporal pattern of change in taurine is quite distinct from the rate of change in hippocampus volume. Moreover, we also found reduced taurine levels in regions such as the striatum at time points while volume was still preserved. This renders unlikely that changes in taurine levels are due to volume changes.

Finally, concerning other metabolites we would have expected to observe decreased levels of glutamate in the hippocampus as was observed in the Ts2 mouse model of Down syndrome (Kaur, Sharma et al. 2014). However, we did not find glutamatergic abnormalities in our mouse model. Future studies should address these differences across models.

In summary, our findings provide interesting homologies between human and animal models and pave the way for studies involving early neurodegeneration, including therapeutic ones. In

AD brain atrophy is enhanced in comparison with normal aging. It has been shown that 11 month old 3xTg-AD animals have a decrease in the brain weight and in the brain to body weight ratio (Carvalho, Cardoso et al. 2012, Carvalho, Machado et al. 2013). This brain shrinkage can be due to the loss of synaptic connections, reduction of neuronal arborization and neuronal loss. Consequently, the observation of a reduction of the volume of the hippocampus and recognition memory impairment in 3xTg-AD mice represents a valuable indicator in line with its use in AD diagnosis and management. However, most of the current mouse models of AD fail to show visible brain neuronal loss, a hallmark present in AD patients (Ashe and Zahs 2010, Karran, Mercken et al. 2011, Onos, Rizzo et al. 2016). Thus, the 3xTg-AD mouse model seems to be valuable in this context.

1.6. Conclusions

In this multimodal molecular imaging study of the 3xTg-AD mouse model, in the presence of the major hallmarks of AD, increased Aβ and p-tau, we measured early abnormal hippocampal volumetry that progressed along all time points. MR neurospectroscopy also showed loss of taurine, which is an important endogenous neuroprotector. PET imaging of amyloid load was less sensitive than MR, and the use of the PET marker ^{11}C-PK11195 did not reveal microglia activation. The BBB was preserved until late stages. This shows that MR signatures of hippocampal volumetry and neurochemistry represent early valuable biomarkers which parallel neurobehavioral deficits, thus providing an *in vivo* multimodal validation of the 3xTg-AD mouse as an early disease model that may be applied in preclinical research using these biomarkers.

2. Retinal thinning of inner sub-layers is associated with cortical atrophy in a mouse model of Alzheimer's disease: a longitudinal *in vivo* study

*Samuel Chiquita[1,2], *João Castelhano[2,3,4], Mário Ribeiro[2,3,4], José Sereno[2,3,4], Elisa J. Campos[1,2], Paula I. Moreira[2,5,6], ‡Miguel Castelo-Branco[2,3,4], ‡António Francisco Ambrósio[1,2]

[1]Coimbra Institute for Clinical and Biomedical Research (iCBR), Faculty of Medicine, University of Coimbra, 3000-548 Coimbra, Portugal; [2]CNC.IBILI Consortium, University of Coimbra, 3000-504 Coimbra, Portugal; [3]Coimbra Institute for Biomedical Imaging and Translational Research (CIBIT), University of Coimbra, 3000-548 Coimbra, Portugal; [4]Institute for Nuclear Sciences Applied to Health (ICNAS), University of Coimbra, 3000-548 Coimbra, Portugal; [5]Center for Neuroscience and Cell Biology (CNC), University of Coimbra, 3004-517 Coimbra, Portugal; [6]Institute of Physiology, Faculty of Medicine, University of Coimbra, 3004-517 Coimbra, Portugal

* These authors contributed equally to this work

‡ These authors contributed equally to this work, as senior authors

Corresponding Authors:

Dr. António Francisco Ambrósio
Principal Investigator
Coimbra Institute for Clinical and Biomedical Research (iCBR)
Faculty of Medicine
University of Coimbra
3000-548 Coimbra, Portugal
Email: afambrosio@fmed.uc.pt
Phone: +351239480093

Dr. Miguel Castelo-Branco
Associate Professor
Coimbra Institute for Biomedical Imaging and Translational Research (CIBIT)
Institute for Nuclear Sciences Applied to Health (ICNAS)
Faculty of Medicine
University of Coimbra
3000-548 Coimbra, Portugal
Email: mcbranco@fmed.uc.pt
Phone: +351239488514

2.1. Abstract

It has been claimed that the retina can be used as a window to study brain disorders. However, concerning Alzheimer's disease (AD), it still remains controversial whether changes occurring in the brain and retina are associated and there is an urgent need to clarify whether the retina can indeed mirror changes occurring in the brain. We aim to understand when changes start appearing in the retina and brain, how changes progress and if they are correlated. To fill in the gaps concerning these missing links between the retina and brain pathology in AD, we carried out a longitudinal study using a triple transgenic mouse model of AD (3xTg-AD) and age matched wild type (WT) mice. Several parameters were evaluated in the same animals *in vivo* at 4, 8, 12 and 16 months of age both in the retina and brain. Retinal structure was evaluated by optical coherence tomography (OCT), which allows performing segmentation of retinal layers and identifying affected layers. Retinal physiology was evaluated with flash electroretinography (ERG) and with pattern electroretinography (PERG). Brain visual cortex structure was evaluated *in vivo* with magnetic resonance imaging (MRI). We found that there was a reduction of retinal thickness in 3xTg-AD mice when compared with WT animals at all time points, except for the outer nuclear layer where the opposite pattern was found. ERG recordings showed higher scotopic b-wave and photopic flicker responses in 3xTg-AD mice, matching the increased outer nuclear layer thickness. PERG recordings, reflecting the activity of cells in the inner retina, did not show different responses between 3xTg-AD and WT mice. Brain structural analysis revealed a significant reduction of the visual cortex grey matter volume in 3xTg-AD mice. Cortical measures were correlated with retinal thickness and electrophysiological responses. These results show that the retina is indeed a mirror to the brain and that models resulting from genetic manipulations can combine neural changes (reflected in retinal and brain thinning) with alterations of possible neurodevelopmental origin, such as increased outer nuclear layer thickness. The concept that the retina is a mirror of AD progression supports the possibility of using the eye as an additional noninvasive tool for early AD diagnostic and therapeutic monitoring.

Keywords: Alzheimer's disease, 3xTg-AD mouse model, retina, brain.

Graphical abstract

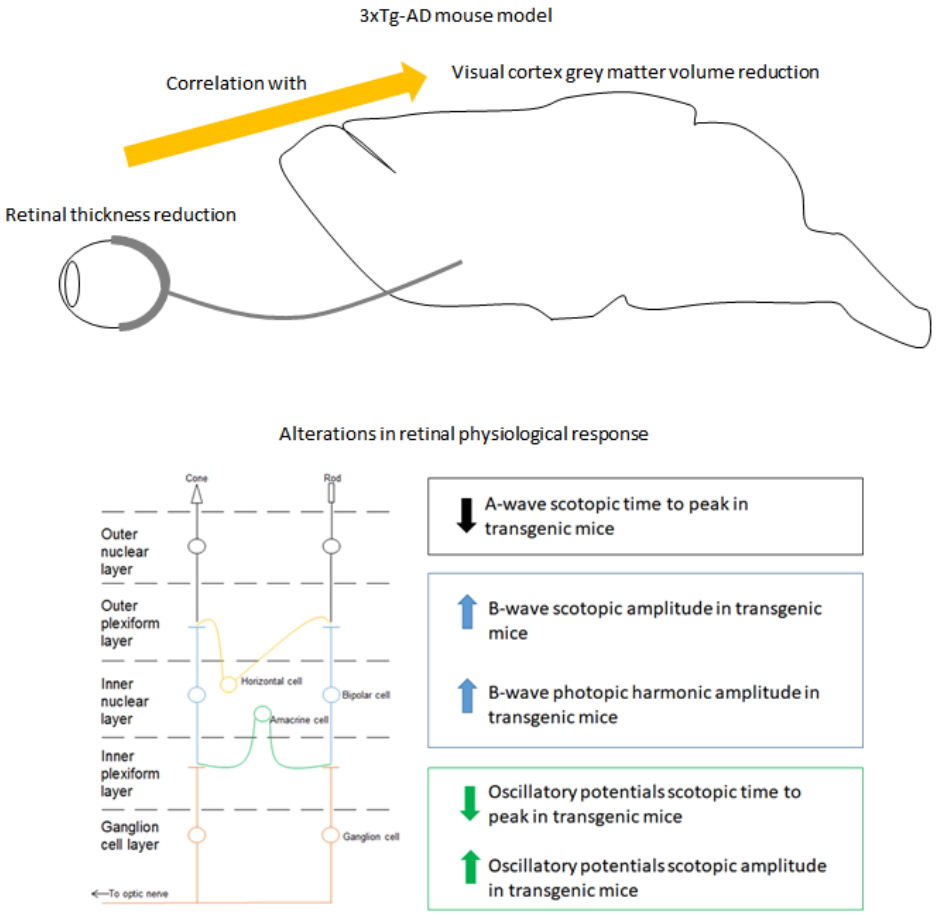

Main points

- Structural analysis reveals significant retinal thickness and visual cortex grey matter volume reduction at 4, 8, 12 and 16 months of age in 3xTg-AD mice.
- Functional analysis reveals that 3xTg-AD mice have higher scotopic b-wave and photopic flicker amplitudes at 4, 8, 12 and 16 months of age.
- Changes in retinal thickness and electrophysiological responses are significantly correlated with a reduction in visual cortex grey matter volume.

2.2. Introduction

The concept of “the retina as a window to the brain” has emerged with possible implications in various diseases such as Alzheimer’s disease (AD), Parkinson´s disease and multiple sclerosis (London, Benhar et al. 2013). In AD it is still difficult to identify subclinical biomarkers that can predict the subsequent appearance of symptoms (Sperling, Aisen et al. 2011). Moreover, in order to have a definitive diagnosis of AD it is needed to identify Aβ plaques and neurofibrillary tangles *postmortem* (Jack, Knopman et al. 2013, Sutphen, Fagan et al. 2014, Lim, He et al. 2016). To achieve better and earlier treatments for AD patients it is ideal to target earlier diagnosis. Thus there is an urgent need to identify new biomarkers that can reliably help in diagnosing early AD onset (Frost, Martins et al. 2010). Visual alterations have been detected in AD patients, and those alterations can be associated with structural and functional changes in the retina (Iseri, Altinas et al. 2006, Lu, Li et al. 2010, Satue, Obis et al. 2016). Retinal imaging and electrophysiology can be used to evaluate structural and functional abnormalities in the retina, a more accessible structure for a potential early AD detection (Parisi, Restuccia et al. 2001, Parisi 2003). The eye enables to perform noninvasive, inexpensive and *in vivo* tests, which is often not the case concerning the brain. In particular, optical coherence tomography (OCT) measurements have shown that there is a thinning of the retina in AD patients (Chang, Lowe et al. 2014, Tzekov and Mullan 2014, Hart, Koronyo et al. 2016, Javaid, Brenton et al. 2016). Actually, retinal manifestations in AD, Parkinson’s disease and multiple sclerosis have been reported with the aid of OCT quantifications (Frohman, Fujimoto et al. 2008, Marziani, Pomati et al. 2013, Bayhan, Aslan Bayhan et al. 2014, Garcia-Martin, Larrosa et al. 2014, Cunha, Proença et al. 2017). Retinal nerve fiber layer thickness reduction has been observed in AD patients (Paquet, Boissonnot et al. 2007, Lu, Li et al. 2010, Shi, Zhu et al. 2016). However, others have reported that there are no differences in retinal nerve fiber layer thickness between mild cognitive impairment or AD patients and control groups (Cronin-Golomb, Rizzo et al. 1991, Justino, Kergoat et al. 2001, Kergoat, Kergoat et al. 2001, Lad, Mukherjee et al. 2018). With the aim of clarifying the controversy related with the possible use of the eye as a window to the brain in AD, longitudinal studies with large cohorts need to be carried out. Mouse models of AD provide the possibility of performing longitudinal studies in a much shorter time scale than in AD patients. There are several studies designed to assess retinal structural and functional changes in AD murine models (Perez, Lumayag et al. 2009, Ioshimoto, Nagy et al. 2012, Antes, Ezra-Elia et al. 2013, Liu, Cao et al. 2015, Gupta, Chitranshi et al. 2016, Lim, He et al. 2016, Millar, Webber et al. 2016, Joly, Lamoureux et al. 2017). However, there are only a few studies that assess the pathophysiology of AD in animal models simultaneously in the retina and brain, trying to establish possible correlations between these structures (Shimazawa, Inokuchi et al. 2008, Gao, Chen et al. 2015, Leinonen, Lipponen

et al. 2016, Lim, He et al. 2016, Mazzaro, Barini et al. 2016, Criscuolo, Cerri et al. 2018). Taking into account the limitations of those studies, because they only assessed few structural and functional parameters without expressing the inner sub-layers detail as it is presented in our study, we aimed to get further insight into the pathophysiology of AD and particularly to understand how changes in the retina correlate with changes in the visual cortex. To achieve these goals, we performed a longitudinal study using the 3xTg-AD mouse model and assessing retinal and visual cortex alterations at 4, 8, 12 and 16 months of age. The combination of structural and functional changes either in the retina and brain regions such as the visual cortex might be used as biomarkers for early AD diagnosis.

2.3. Materials and methods

2.3.1. Animals

Experiments were performed in 3xTg-AD mice harboring three human mutant genes, presenilin 1 ($PS1_{M146V}$), amyloid precursor protein (APP_{SWE}) and tau (Tau_{P301L}), and in age matched WT animals (C57BL6/129S background). WT mice used in this study have the same genetic background of the presenilin knockin embryos used to generate the 3xTg-AD mouse model, but instead of expressing mutant presenilin 1 gene they express the endogenous WT mouse presenilin 1 gene (Oddo, Caccamo et al. 2003). Male 3xTg-AD and WT mice were used to evaluate *in vivo* structural and/or functional changes in the retina and visual cortex at 4, 8, 12 and 16 months of age. The animals were maintained at 22 ± 1 ºC, 68% relative humidity, on a 12 h light/12 h dark cycle, with access to water and food *ad libitum*. In order to assess age related changes the animals were tagged. All procedures involving animals were approved by the Animal Welfare Committee of the Coimbra Institute for Clinical and Biomedical Research (iCBR), Faculty of Medicine, University of Coimbra. The animal experimentation was conducted in accordance with the European Community directive guidelines for the use of animals in laboratory (2010/63/EU), transposed into the Portuguese law in 2013 (Decreto-Lei 113/2013) and was in agreement with the Association for Research in Vision and Ophthalmology (ARVO) statement for animal use.

2.3.2. Optical coherence tomography measurements

Retinal structure was evaluated by OCT, which allows performing the segmentation of retinal layers. In order to evaluate *in vivo* structural changes, a longitudinal study was carried out at 4, 8, 12 and 16 months of age using 3xTg-AD and WT mice. *In vivo* OCT line and circular scans were acquired with Phoenix OCT2 together with Phoenix Micron IV retinal imaging microscope (Phoenix Research Laboratories, San Ramon, CA, USA). Retinal thickness was measured with the Insight eye segmentation software (Voxeleron LLC - Image analysis

solutions, Chabot Drive, CA, USA) between the inner limiting membrane and the retinal pigment epithelium. For each eye, one OCT scan was performed around the optic nerve head and six scans were performed above and below the optic nerve head (Figure 21). Subsequently, measurements of ganglion cell layer (GCL) plus inner plexiform layer (IPL), inner nuclear layer (INL) plus outer plexiform layer (OPL), outer nuclear layer (ONL), inner segments (IS) plus outer segments (OS) and total retinal thickness were obtained both for 3xTg-AD and WT animals (Figure 22). Circular and line scan thickness values for each animal correspond to the average value of measurements for both eyes. To perform OCT animals were anesthetized with an intraperitoneal injection of ketamine (80 mg/kg, Imalgene 1000, Merial, Lyon, France) and xylazine (5 mg/kg, Rompum®, Bayer, Leverkusen, Germany) in 0.1 mL of saline under dim red light illumination. Pupils were dilated with topical tropicamide (1 %), the corneas were locally anesthetized with topical anesthetic eye drops (4 mg/ml oxybuprocaine hydrochloride, Anestocil®, Laboratório Edol, Carnaxide, Portugal). The corneas were kept hydrated and optically cleared with hydroxypropyl methylcellulose (2% Methocel, Dávi II – Farmacêutica S.A., Barcarena, Portugal) during the whole procedure.

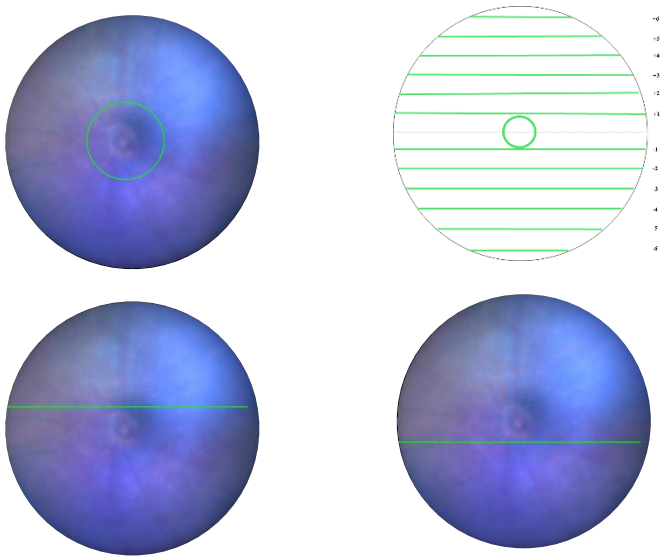

Figure 21 – Procedure implemented to acquire OCT circle and line scans from mice retinas. Firstly, a circular scan was acquired around the optic nerve head (ONH). After, six line scans were acquired above and below the optic nerve head. The figure depicts representative images with scans above and below the ONH. The green line represents where the scan was performed.

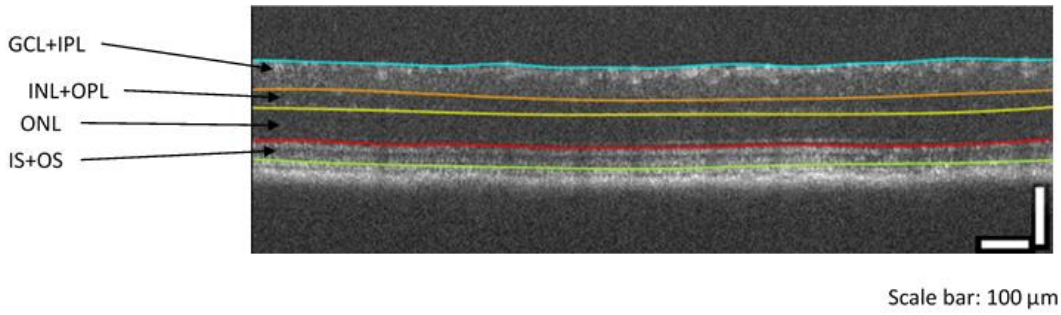

Figure 22 – Retinal layers visualized by optical coherence tomography either in line or circle scan mode. GCL: ganglion cell layer; IPL: inner plexiform layer; INL: inner nuclear layer; OPL: outer plexiform layer; ONL: outer nuclear layer; IS: inner segments; OS: outer segments. Scale bar: 100 µm.

2.3.3. Electroretinography

Retinal physiology was evaluated by flash and pattern electroretinography, which measures the electrical response of retinal cells. With PERG we assessed the function of retinal ganglion cells (RGCs).

2.3.3.1. Flash electroretinogram

After 12 h overnight dark adaptation mice were anesthetized with an intraperitoneal injection of ketamine (80 mg/kg, Imalgene 1000, Merial, Lyon, France) and xylazine (5 mg/kg, Rompum®, Bayer, Leverkusen, Germany) in 0.1 mL saline solution under dim red light illumination. Pupils were dilated with topical phenylephrine (2.5 %), the corneas were locally anesthetized and kept hydrated as described above. The body temperature was maintained with a heating pad set to 37ºC. ERG recordings were performed with the RETIport System (Roland Consult Electrophysiological Diagnostic Systems, Brandenburg, Germany) by placing a custom made gold ring electrode (gold wire 0.25 mm, 2.5 mm diameter) at the corneal surface, a reference electrode placed at the head and a ground electrode in the tail of the animal. With a Ganzfeld stimulator a series of white flashes (0.0095 to 9.49 cd·s/m^2) in scotopic and photopic conditions were applied. Photopic adaption to a white background (25 cd/m^2) was carried out during 16 min and light flashes with intensity of 9.49 cd·s/m^2 were applied. For the photopic flicker white bright flashes (0.95, 3.00 and 9.49 cd·s/m^2) were applied for ten times at 6.3 Hz. ERGs were recorded with a bandwidth of 1-300 Hz at a sampling rate of 3.4 kHz (0.8 kHz for flicker test). Measurements of negative a-wave, positive b-wave and individual oscillatory potentials (OP) amplitude and time to peak were made with the RETIport software (Roland Consult Electrophysiological Diagnostic Systems, Brandenburg, Germany). Scotopic a-wave and b-wave were extracted for seven light intensities from 0.0095 to 9.49 cd·s/m^2. Four

oscillatory potentials were extracted for six light intensities between 0.030 to 9.49 cd·s/m^2. During photopic adaptation flashes of 9.49 cd·s/m^2 were delivered at 0, 2, 4, 8 and 16 minutes and the b-wave was measured. B-wave photopic luminance responses were measured for 3.00 and 9.49 cd·s/m^2. OFF-line digital filters were applied on the b-wave (high frequency cut-off of 50 Hz) and oscillatory potentials (low frequency cut-off of 60 Hz for scotopic ERGs and 55 Hz for photopic ERGs). Flicker responses were evaluated by determining the amplitude and phase of the base wave (6.33 Hz), first (12.7 Hz) and second harmonics (19 Hz) with the Fast Fourier Transform. Tests were performed at 4, 8, 12 and 16 months of age in 3xTg-AD and age matched WT animals.

2.3.3.2. Pattern electroretinogram

Animals were anesthetized, pupils were dilated, corneas were locally anesthetized, hydrated and mice body temperature was maintained as previously described. Light adapted PERG recordings were obtained with the RETIport System (Roland Consult Electrophysiological Diagnostic Systems, Brandenburg, Germany) by placing a custom made gold ring electrode (gold wire 0.25 mm, 2.5 mm diameter) at the corneal surface, a reference electrode placed at the head and a ground electrode in the tail of the animal. Stimuli were dark and light gratings displayed on a monitor whose center was aligned with the projection of the pupil and presented from a short distance (typically 20 cm) to stimulate a large retinal area. Stimuli were displayed for 200 sweeps of contrast reversals with 1 Hz temporal frequency, contrast between 95%-100%. After PERG recording of the right eye a new electrode was placed on the left eye and the procedure repeated. Ganglion cell activity was evaluated by measuring an initial corneal positive response, referred to as P50, followed by a corneal negative response, referred to as N95. An evaluation of the amplitude and time to peak of the major positive (P50/P1) and negative (N95/N2) deflection was performed. Signals were band pass filtered (1-40 Hz) and artefact rejection was set at 100 µV peak to peak with a sample frequency of 1.136 kHz. Tests were performed at 4, 8, 12 and 16 months of age in 3xTg-AD and age matched WT animals.

2.3.4. MRI acquisitions

MRI experiments were performed in a BioSpec 9.4T scanner with a standard cross coil setup using a volume coil for excitation (with 86/112 mm of inner/outer diameter, respectively) and quadrature mouse surface coil for signal detection (Bruker Biospin, Ettlingen, Germany). Mice (WT: n=6; 3xTg-AD: n=7) were kept anesthetized by isoflurane (1.5%) with 100% O_2 and body temperature and respiration monitoring (SA Instruments SA, Stony Brook, NY, USA). T2-weighted images were acquired in coronal planes using a Rapid Acquisition with Relaxation Enhancement (RARE) sequence with the following parameters: TR=3800 ms; TE=33 ms; 10

averages; pixel size of 0.078 mm x 0.078 mm and slice thickness of 0.5 mm without spacing between slices (total head volume: 256 pixels x 256 pixels x 34 slices).

2.3.5. MRI analysis

Voxel based morphometry (VBM) was performed using the statistical parametric mapping software (SPM, Welcome Department of Cognitive Neurology, London, UK), the SPMMouse toolbox (Sawiak, Wood et al. 2013) and a homemade script involving the following steps: a) T2-weighted images were corrected for the magnetic field inhomogeneity generated by the surface coil and this was done using intensity curves from T2-weighted images obtained for an homogeneous phantom and acquired with the same coil and system configuration; b) the rigid body was aligned by registering (affine transformation) the images to the template space; c) tissue segmentation was carried out by means of the grey matter (GM), white matter (WM) and cerebrospinal fluid (CSF) tissue probability maps as provided in the toolbox; d) GM images were non-linearly normalized to the template space and were modulated to correct for volume changes that might have occurred during normalization; e) a binary mask, corresponding to the visual cortex, was drawn in the template space and placed in each aligned GM image; f) finally, the GM volume was quantified by multiplying the GM volume in each voxel by the number of voxels. All steps were done using the default settings of the toolbox.

2.3.6. Statistical analysis

Statistical analysis was performed with GraphPad Prism Version 6 (GraphPad Software, San Diego, CA, USA) and SPSS 22.0 (SPSS Inc., Chicago, IL, USA). The normality of the data was assessed with D´Agostino and Pearson omnibus normality tests. Alterations in the thickness of retinal layers between groups were assessed by a Student´s t-test analysis. Alterations in retinal function between groups were assessed by a Student´s t-test analysis and linear regressions with analysis of covariance (ANCOVA). Alterations in GM volumes of the visual cortex along time and between groups were assessed by an ANOVA repeated measures (mixed-effects) followed by a Bonferroni post-hoc. Data were considered to be significant at *P<0.05, **P<0.01, ***P<0.001 and results are presented as mean ± SEM.

2.4. Results

2.4.1. Reduction of retinal thickness in 3xTg-AD mice

The thickness of total retina, as well as the thickness of GCL+IPL, obtained from both circle and line scans, was significantly decreased in 3xTg-AD mice at all time points (Figure 23A, B, C and D). At 16 months, the total retinal thickness in WT mice, 196.3 µm, decreased to 176.1 µm in 3xTg-AD mice, and the thickness of GGL+IPL decreased from 69.5 µm in WT mice to

53.5 µm in 3xTg-AD mice (circle scan). In line scans, the thickness of INL+OPL was also significantly reduced in 3xTg-AD mice at all time points (Figure 23F), but in circle scans the INL+OPL thickness was significantly decreased only at 8, 12 and 16 months (Figure 23E). Similarly, the IS+OS thickness (circle and line scans) was significantly reduced only at 8, 12 and 16 months (Figure 23I and J). However, contrary to the results obtained for the layers described above, the ONL thickness in 3xTg-AD mice was significantly higher in comparison with WT animals at 12 and 16 months (Figure 23G and H). At 4, 8, 12 and 16 months of age there is a reduction of 3xTg-AD mice retinal thickness observed with line scans and circular scans. This reduction can be observed at total retinal thickness and at several layers of the retina, including ganglion cell layer (Table 5).

A

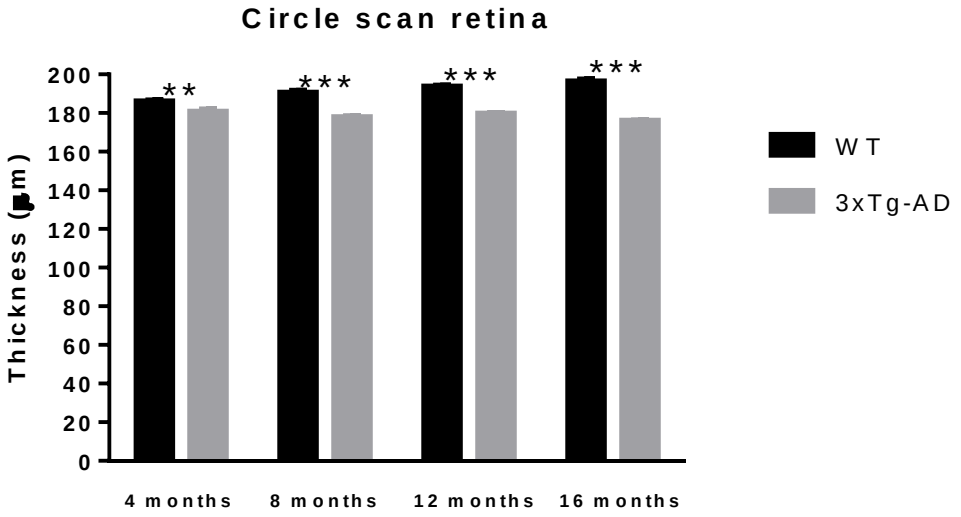

B

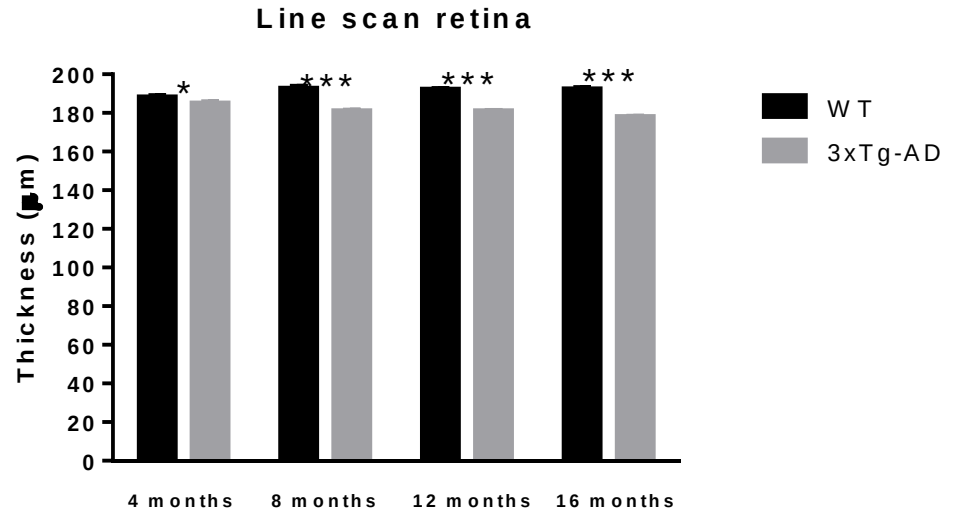

C

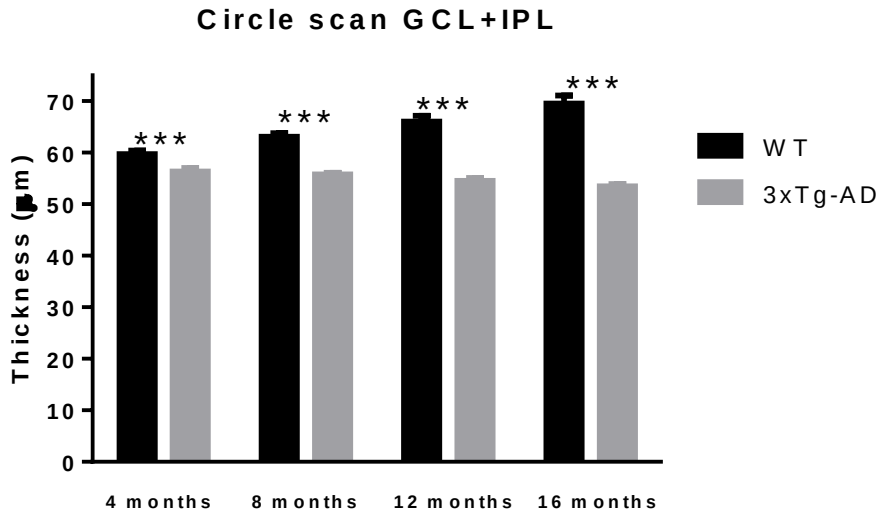
Circle scan GCL+IPL
Thickness (µm)
0
10
20
30
40
50
60
70
***
***
***
***
4 months
8 months
12 months
16 months
WT
3xTg-AD

D

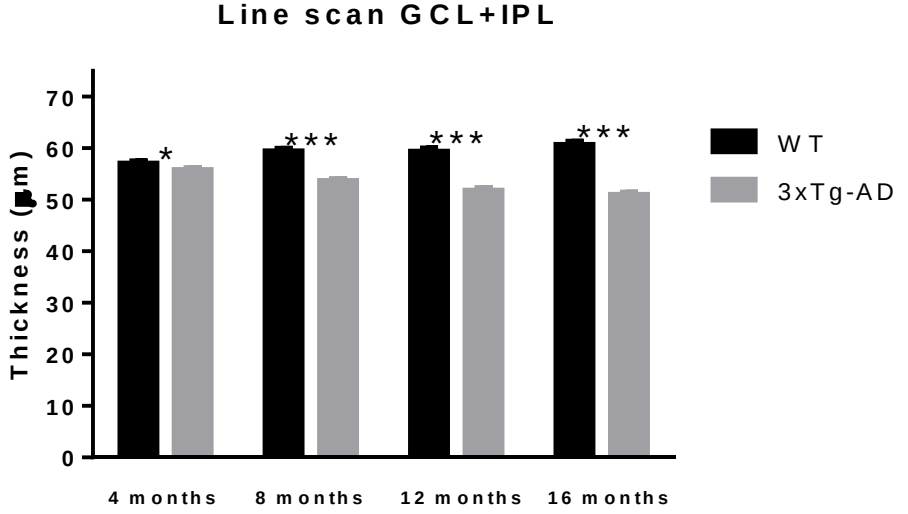
Line scan GCL+IPL
Thickness (µm)
0
10
20
30
40
50
60
70
*
***
***
***
4 months
8 months
12 months
16 months
WT
3xTg-AD

E

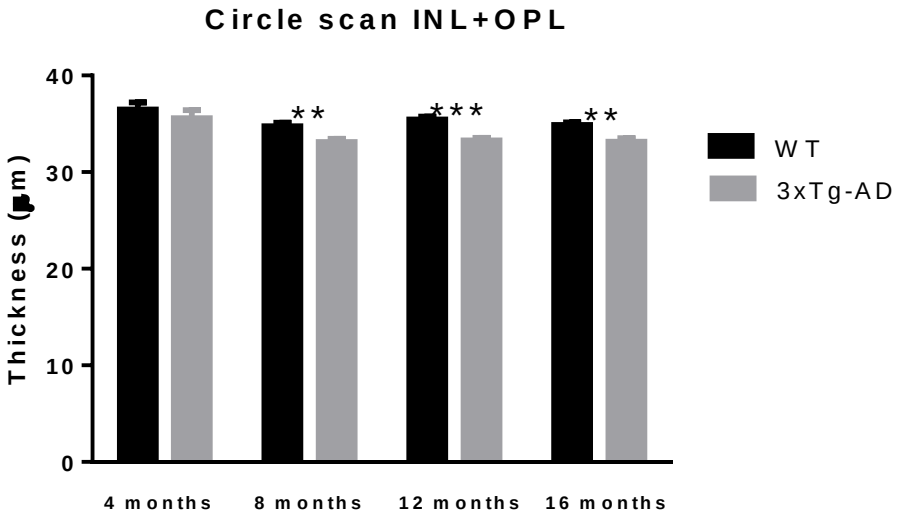
Circle scan INL+OPL
Thickness (µm)
0
10
20
30
40
**
***
**
4 months
8 months
12 months
16 months
WT
3xTg-AD

F

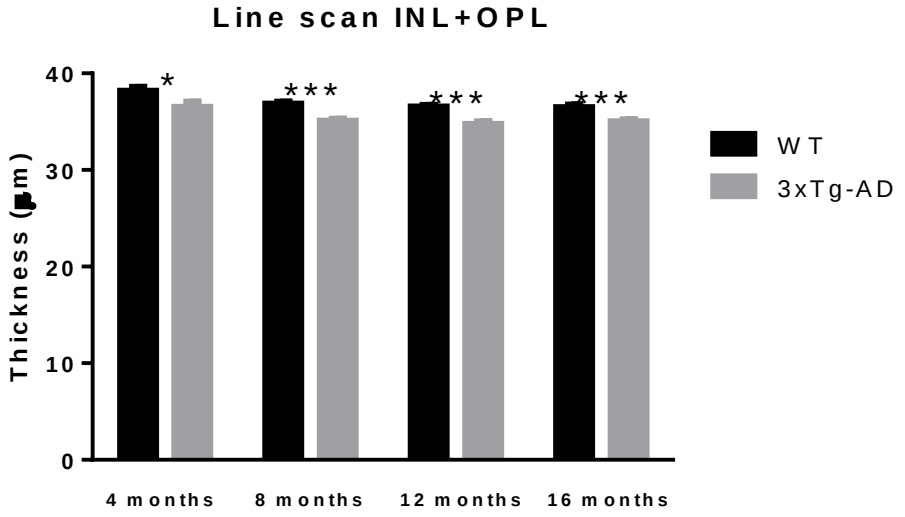
Line scan INL+OPL
Thickness (µm)
40
30
20
10
0
*
***
***
***
4 months
8 months
12 months
16 months
WT
3xTg-AD

G

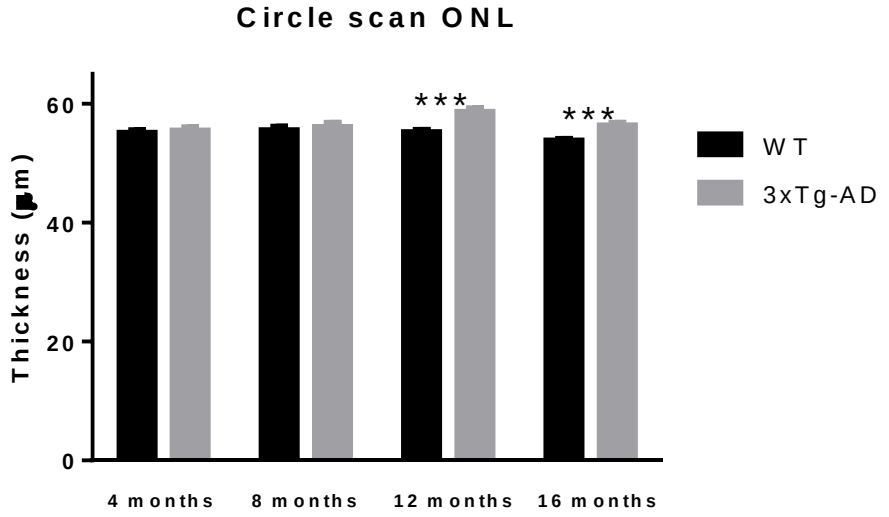
Circle scan ONL
Thickness (µm)
60
40
20
0
***
***
4 months
8 months
12 months
16 months
WT
3xTg-AD

H

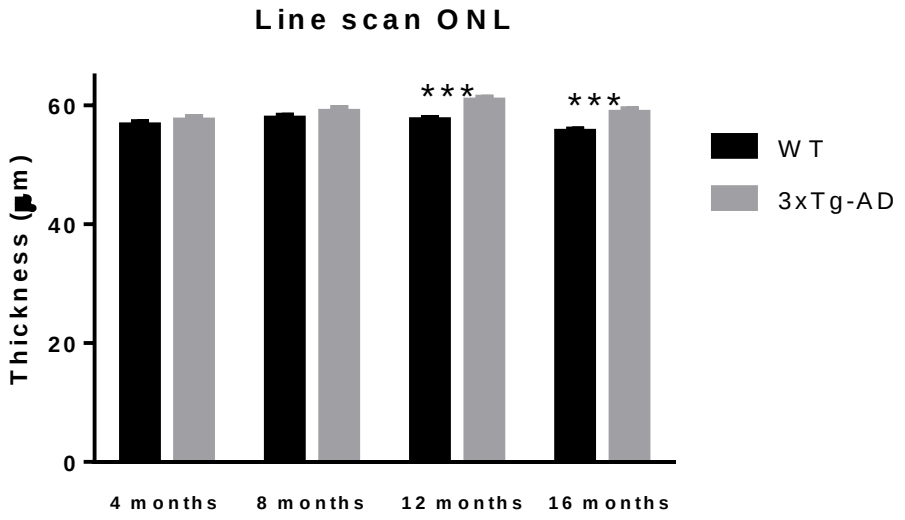
Line scan ONL
Thickness (µm)
60
40
20
0
***
***
4 months
8 months
12 months
16 months
WT
3xTg-AD

I

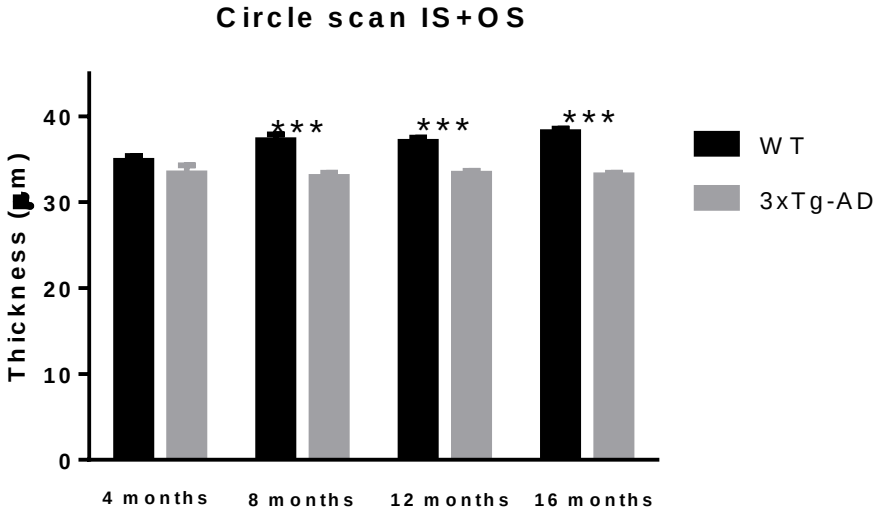

J

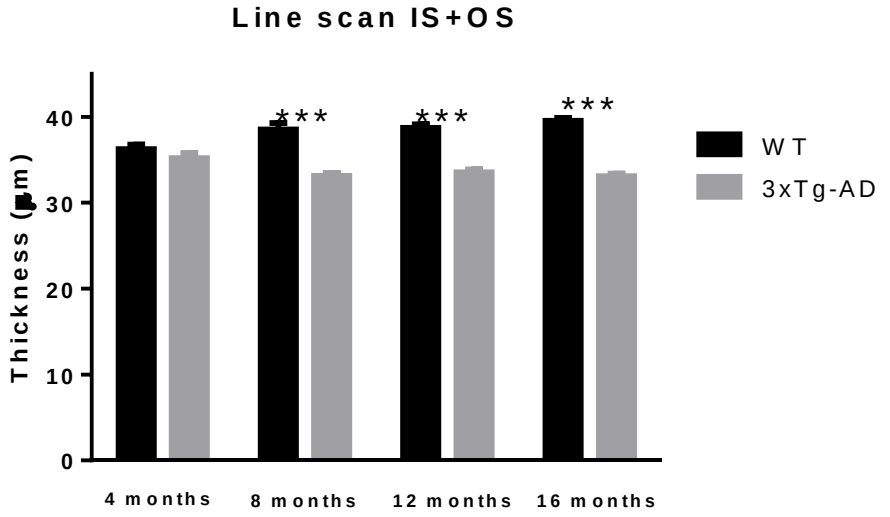

Figure 23 – Thickness of different retinal layers in 3xTg-AD and WT mice at 4, 8, 12 and 16 months of age. *In vivo* optical coherence tomography circle and line scans were obtained using the Phoenix OCT2 together with Phoenix Micron IV retinal imaging microscope. The thickness of retinal layers was measured using the InSight software. (A) Retina thickness – circle scan, (B) Retina thickness – line scan, (C) GCL+IPL thickness – circle scan, (D) GCL+IPL thickness – line scan, (E) INL+OPL thickness – circle scan, (F) INL+OPL thickness – line scan, (G) ONL thickness – circle scan, (H) ONL thickness – line scan, (I) IS+OS thickness – circle scan, (J) IS+OS thickness – line scan. The results are presented as mean ± SEM and were analyzed with the Student´s t-test; *P<0.05, **P<0.01 and ***P<0.001 ($n_{\text{WT 4 months with line scan}}$=21 and $n_{\text{3xTg-AD at 4 months with line scan}}$= 19, $n_{\text{WT at 4 months with circle scan}}$=19 and $n_{\text{3xTg-AD at 4 months with circle scan}}$= 18; $n_{\text{WT at 8 months with line scan}}$=19 and $n_{\text{3xTg-AD at 8 months with line scan}}$=22, $n_{\text{WT at 8 months with circle scan}}$=19 and $n_{\text{3xTg-AD at 8 months circle line scan}}$=22; $n_{\text{WT at 12 months with line scan}}$=17 and $n_{\text{3xTg-AD at 12 months with line scan}}$=22, $n_{\text{WT at 12}}$

months with circle scan=17 and n 3xTg-AD at 12 months circle line scan=22; n WT at 16 months with line scan=17 and n 3xTg-AD at 16 months with line scan=22, n WT at 16 months with circle scan=17 and n 3xTg-AD at 16 months circle line scan=22).

Table 5 - ANOVA repeated measures results summary for retinal layers thickness along time; *P<0.05, **P<0.01 and ***P<0.001.

Circle scan		
WT	F (dFn,DFd)	P value
GCL+IPL	F (2.532, 37.98) = 23.40	P < 0.0001***
INL+OPL	F (1.644, 24.66) = 2.715	P = 0.0947
ONL	F (2.822, 42.33) = 2.778	P = 0.0558
IS+OS	F (2.105, 31.57) = 8.272	P = 0.0011**
Retina	F (2.396, 35.95) = 18.73	P < 0.0001***
3xTg-AD		
GCL+IPL	F (1.986, 31.78) = 6.176	P = 0.0055**
INL+OPL	F (1.681, 26.89) = 7.156	P = 0.0048**
ONL	F (2.379, 38.06) = 12.52	P < 0.0001***
IS+OS	F (1.771, 28.34) = 0.7398	P = 0.4708
Retina	F (2.128, 34.04) = 6.085	P = 0.0048**

Line scan		
WT	F (dFn,DFd)	P value
GCL+IPL	F (2.677, 42.84) = 13.15	P < 0.0001***
INL+OPL	F (2.694, 43.10) = 8.368	P = 0.0003***
ONL	F (1.938, 31.01) = 5.053	P = 0.0133*
IS+OS	F (1.982, 31.72) = 9.154	P = 0.0007***
Retina	F (2.481, 39.70) = 6.874	P = 0.0015***
3xTg-AD		
GCL+IPL	F (1.668, 28.35) = 23.23	P < 0.0001***
INL+OPL	F (1.732, 29.44) = 8.760	P = 0.0016**
ONL	F (2.461, 41.84) = 15.31	P < 0.0001***
IS+OS	F (2.480, 42.15) = 6.162	P = 0.0025**
Retina	F (2.498, 42.46) = 13.36	P < 0.0001***

2.4.2. Alterations in the physiological responses of 3xTg-AD animals

The analysis of the ERGs showed that 3xTg-AD mice had a significantly higher scotopic b-wave amplitude at all time points (4, 8, 12 and 16 months of age; Figure 24A, Figure 25A and C). The a-wave amplitude in 3xTg-AD was not significantly different from WT mice (Figure 24A and Figure 25B), although there was a consistent increase in the a-wave amplitude at all time points. The OP amplitude in 3xTg-AD was significantly higher (*P<0.05) at 12 months. At the other time points (4, 8 and 16 months of age) the OP amplitude also showed a trend for higher values (Figure 24B and Figure 25D). In photopic conditions the electrical activity is mainly cone driven. At 4 and 8 months the b-wave amplitude in 3xTg-AD mice was significantly higher (**P<0.01) than in WT mice (Figure 24D and Figure 25E). As age progresses the differences were attenuated, and at 12 and 16 months of age the increase in the b-wave amplitude in 3xTg-AD mice was not significantly different from WT animals. Regarding the photopic flicker experiments the harmonic amplitude in 3xTg-AD animals was significantly higher (***P<0.001) when compared with WT group at all time points (4, 8, 12 and 16 months of age; Figure 24E and Figure 25F). PERG recordings did not show statistically significant differences between 3xTg-AD and WT mice (Figure 24F and Figure 25G).

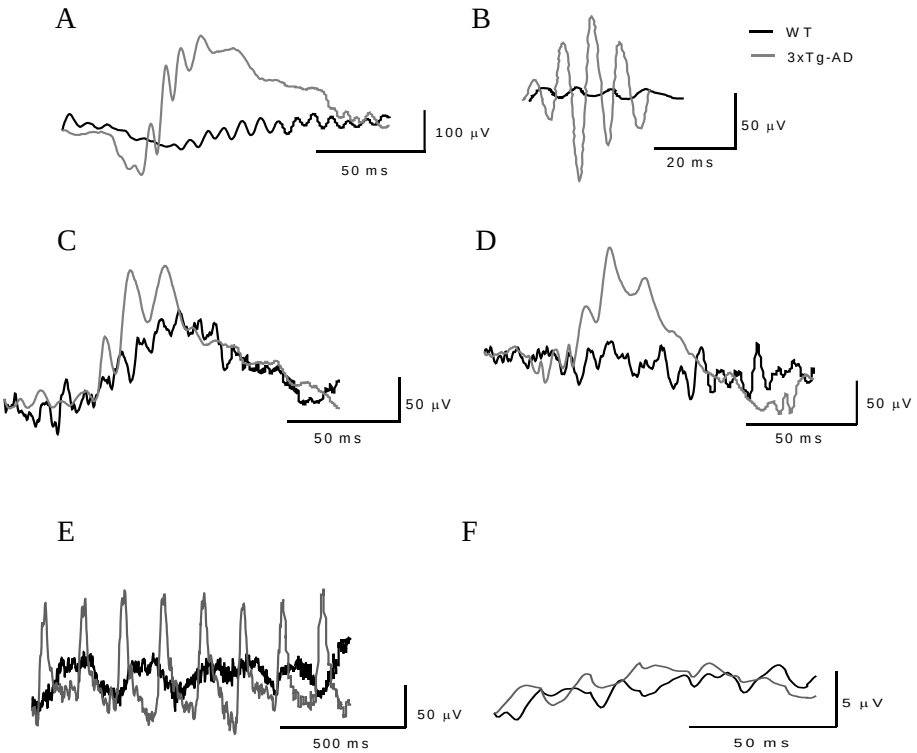

Figure 24 – Representative ERG recordings obtained from 3xTg-AD and WT animals. Retinal function was tested under (A and B) scotopic, (C) photopic adaptation, (D) photopic, (E) photopic flicker and (F) PERG conditions.

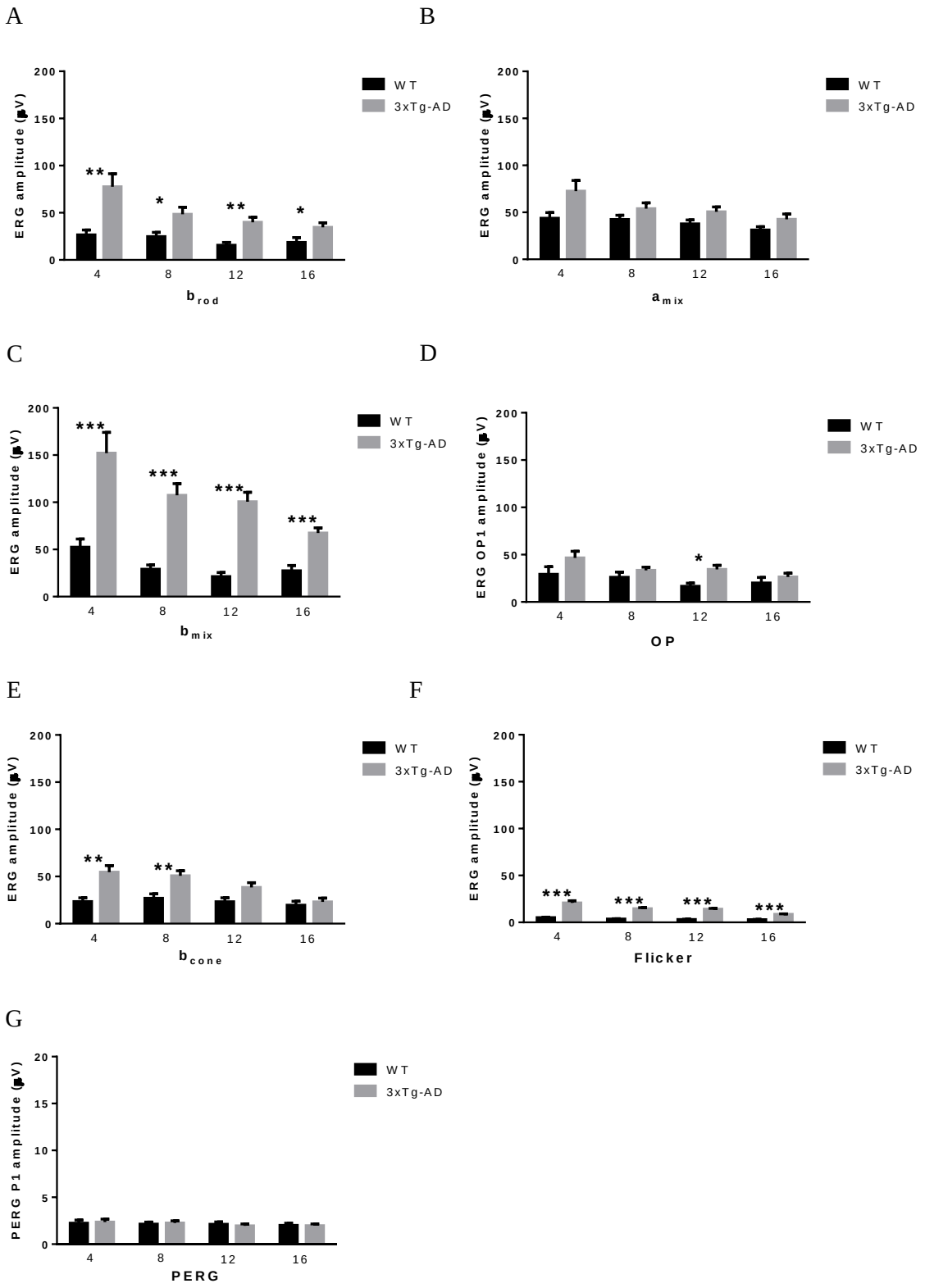

Figure 25 – Higher retinal activity in 3xTg-AD mice. Retinal function was tested under scotopic and photopic conditions at 4, 8, 12 and 16 months of age. Rod mediated responses were recorded in response to light stimuli of -2 log cd·s/m^2, while the other parameters were recorded in response to light flashes of 0.98 log cd·s/m^2. (A) Scotopic b_{rod} amplitude, (B) Scotopic a_{mix} amplitude, (C) Scotopic b_{mix} amplitude, (D) Scotopic OP1 amplitude, (E) Photopic b_{cone}

amplitude, (F) Photopic flicker base wave amplitude, (G) PERG amplitude. The results are presented as mean ± SEM and were analyzed with the Student´s t-test; *P<0.05, **P<0.01 and ***P<0.001 ($n_{WT\ at\ 4\ months}$=19 and $n_{3xTg\text{-}AD\ at\ 4\ months}$=18; $n_{WT\ at\ 8\ months}$=19 and $n_{3xTg\text{-}AD\ at\ 8\ months}$=23; $n_{WT\ at\ 12\ months}$=17 and $n_{3xTg\text{-}AD\ at\ 12\ months}$=22; $n_{WT\ at\ 16\ months}$=17 and $n_{3xTg\text{-}AD\ at\ 16\ months}$=22).

2.4.3. Higher scotopic luminance responses in 3xTg-AD mice

Our results show that a-wave response is altered in WT animals because they had a higher time to peak value in comparison with 3xTg-AD mice mainly at higher luminous intensities (Figure 26). We can observe that there was a delay in the a-wave in WT mice. OP time to peak was also affected and WT mice had also a delayed OP response (Figure 27). Scotopic response showed an evident difference at b-wave amplitude at 4, 8, 12 and 16 months of age between 3xTg-AD and WT mice (Figure 28 and Figure 29).

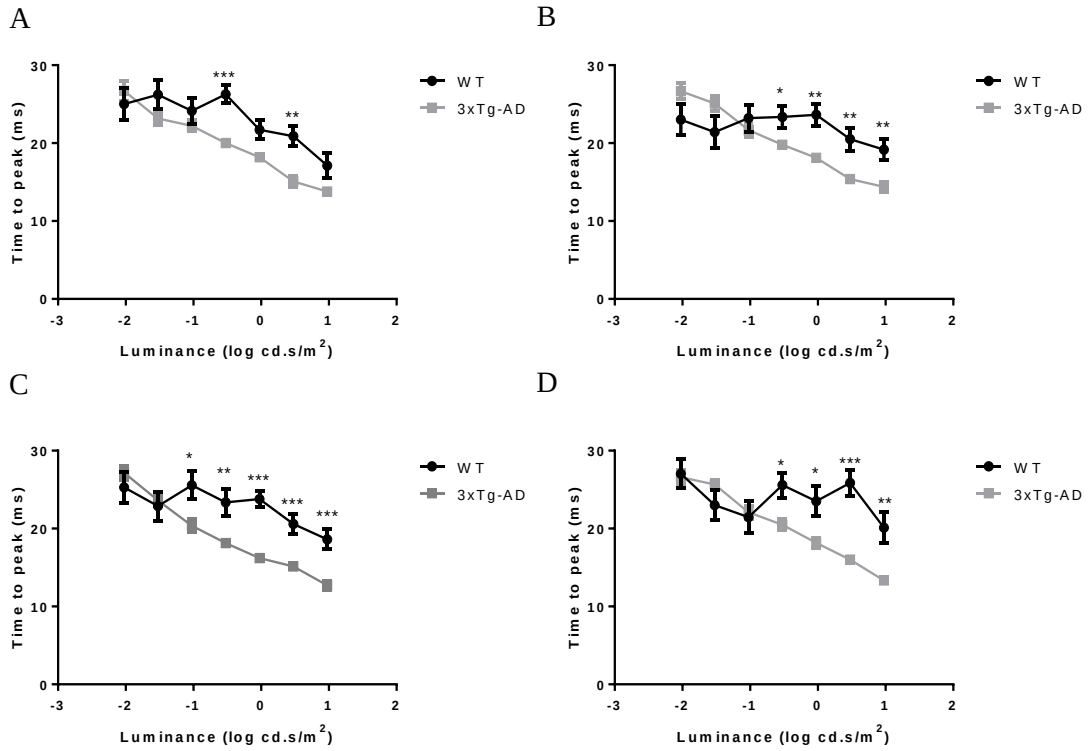

Figure 26 – Scotopic a-wave time to peak at 4 (A), 8 (B), 12 (C) and 16 (D) months of age. The results are presented as mean ± SEM and were analyzed with the Student´s t-test; *P<0.05, **P<0.01 and ***P<0.001 ($n_{WT\ at\ 4\ months}$=19 and $n_{3xTg\text{-}AD\ at\ 4\ months}$=18; $n_{WT\ at\ 8\ months}$=19 and $n_{3xTg\text{-}AD\ at\ 8\ months}$=23; $n_{WT\ at\ 12\ months}$=17 and $n_{3xTg\text{-}AD\ at\ 12\ months}$=22; $n_{WT\ at\ 16\ months}$=17 and $n_{3xTg\text{-}AD\ at\ 16\ months}$=22).

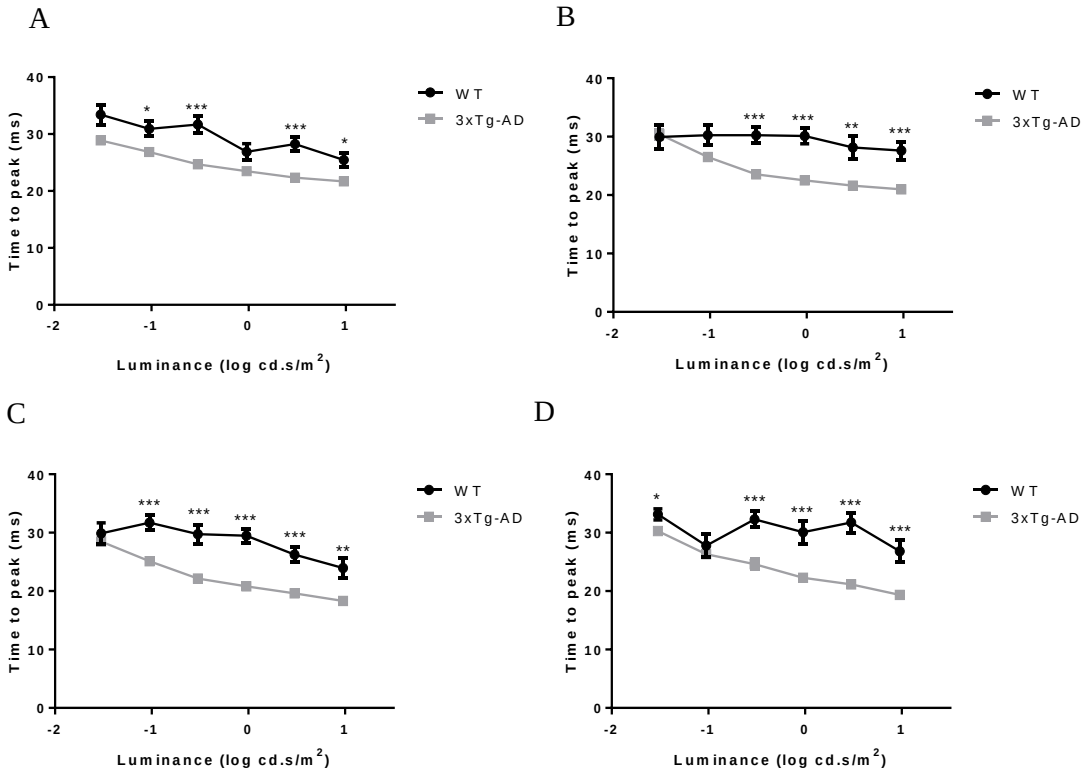

Figure 27 – Scotopic oscillatory potential time to peak at 4 (A), 8 (B), 12 (C) and 16 (D) months of age. The results are presented as mean ± SEM and were analyzed with the Student´s t-test; *P<0.05, **P<0.01 and ***P<0.001 ($n_{WT\ at\ 4\ months}$=19 and $n_{3xTg\text{-}AD\ at\ 4\ months}$=18; $n_{WT\ at\ 8\ months}$=19 and $n_{3xTg\text{-}AD\ at\ 8\ months}$=23; $n_{WT\ at\ 12\ months}$=17 and $n_{3xTg\text{-}AD\ at\ 12\ months}$=22; $n_{WT\ at\ 16\ months}$=17 and $n_{3xTg\text{-}AD\ at\ 16\ months}$=22).

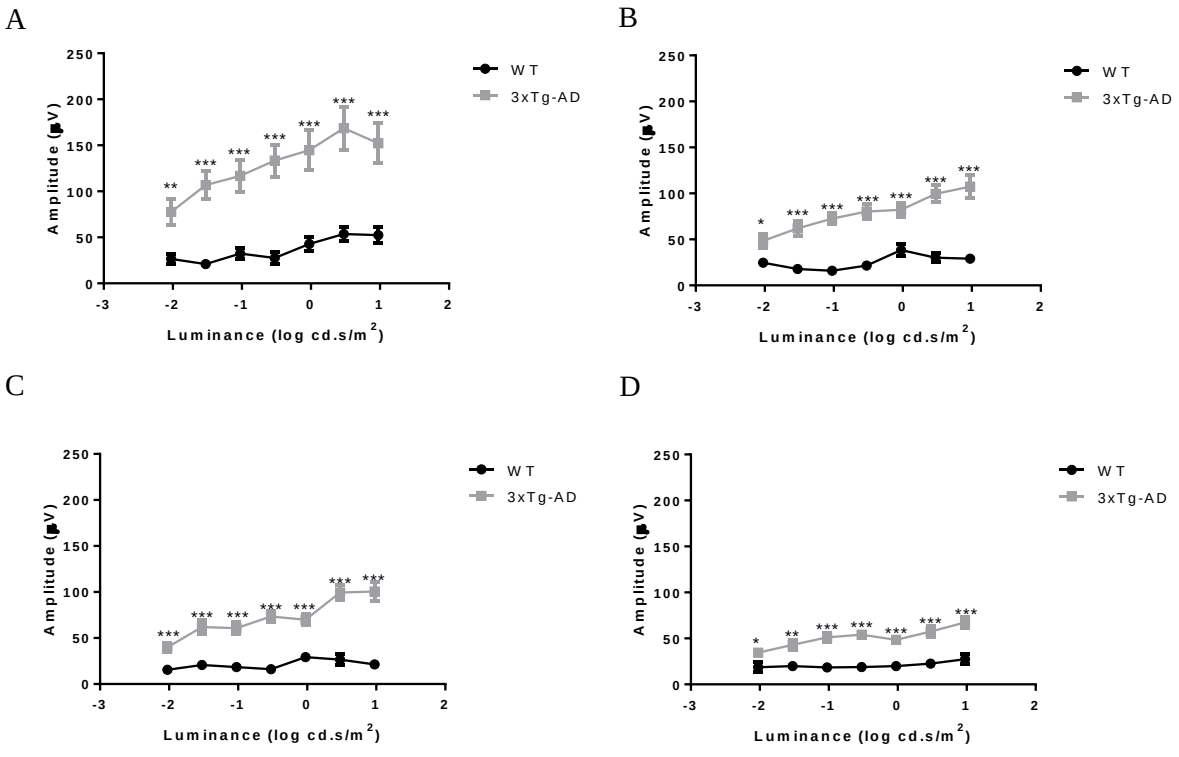

Figure 28 – Scotopic luminance retinal responses in 3xTg-AD and WT animals at 4 (A), 8 (B), 12 (C) and 16 (D) months of age. Graphs present the amplitude of the b-wave at the indicated luminance conditions. The results are presented as mean ± SEM and were analyzed with the Student´s t-test; *P<0.05, **P<0.01 and ***P<0.001 ($n_{WT\ at\ 4\ months}$=19 and $n_{3xTg\text{-}AD\ at\ 4\ months}$=18; $n_{WT\ at\ 8\ months}$=19 and $n_{3xTg\text{-}AD\ at\ 8\ months}$=23; $n_{WT\ at\ 12\ months}$=17 and $n_{3xTg\text{-}AD\ at\ 12\ months}$=22; $n_{WT\ at\ 16\ months}$=17 and $n_{3xTg\text{-}AD\ at\ 16\ months}$=22).

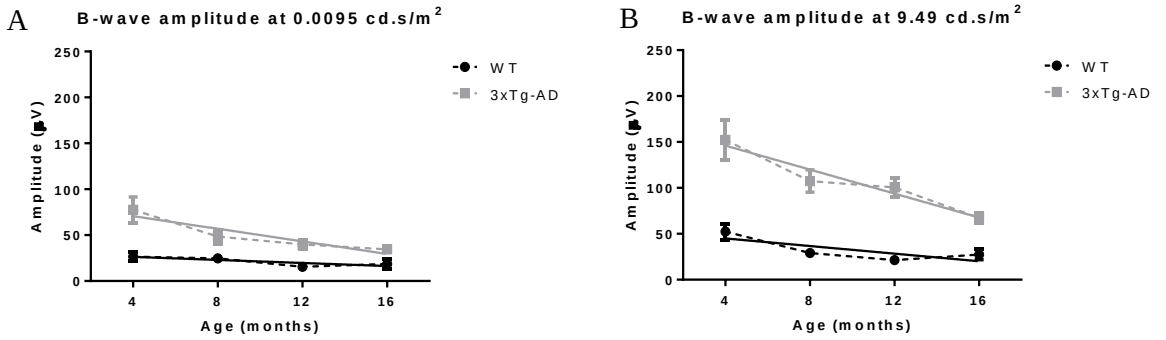

Figure 29 – Linear regression fit to scotopic b-wave amplitude at 0.0095 cd·s/m^2 (A) and 9.49 cd·s/m^2 (B) in 3xTg-AD and WT animals. B-wave amplitude difference between 3xTg-AD and WT animals was assessed by comparing slopes and intercepts with ANCOVA, P<0.05.

2.4.4. Higher photopic flicker harmonic amplitude in 3xTg-AD mice

Photopic flicker results showed that the harmonic amplitude in 3xTg-AD mice was higher when compared with WT animals at base wave, first and second harmonics at all time points (4, 8, 12 and 16 months of age; Figure 30). Moreover, the differences in photopic flicker harmonic amplitude between the slopes and elevations of 3xTg-AD and WT animals are significant at base wave, first and second harmonics (Figure 31). With aging the harmonic amplitude decayed both in 3xTg-AD and WT mice. Moreover, 3xTg-AD animals tend to follow the input base wave frequency (6.33 Hz) more effectively than WT mice leading to a difference in phase responses (Figure 30 and Figure 31A). In the first harmonic phase a similar behavior is seen, despite with a smaller difference between the phase elevations of 3xTg-AD and WT groups meaning that 3xTg-AD had a faster response at first harmonic frequency (12.7 Hz) than WT mice (Figure 30 and Figure 31B). In the second harmonic phase the opposite was observed and WT mice had a faster response at second harmonic frequency (19 Hz; Figure 30 and Figure 31C).

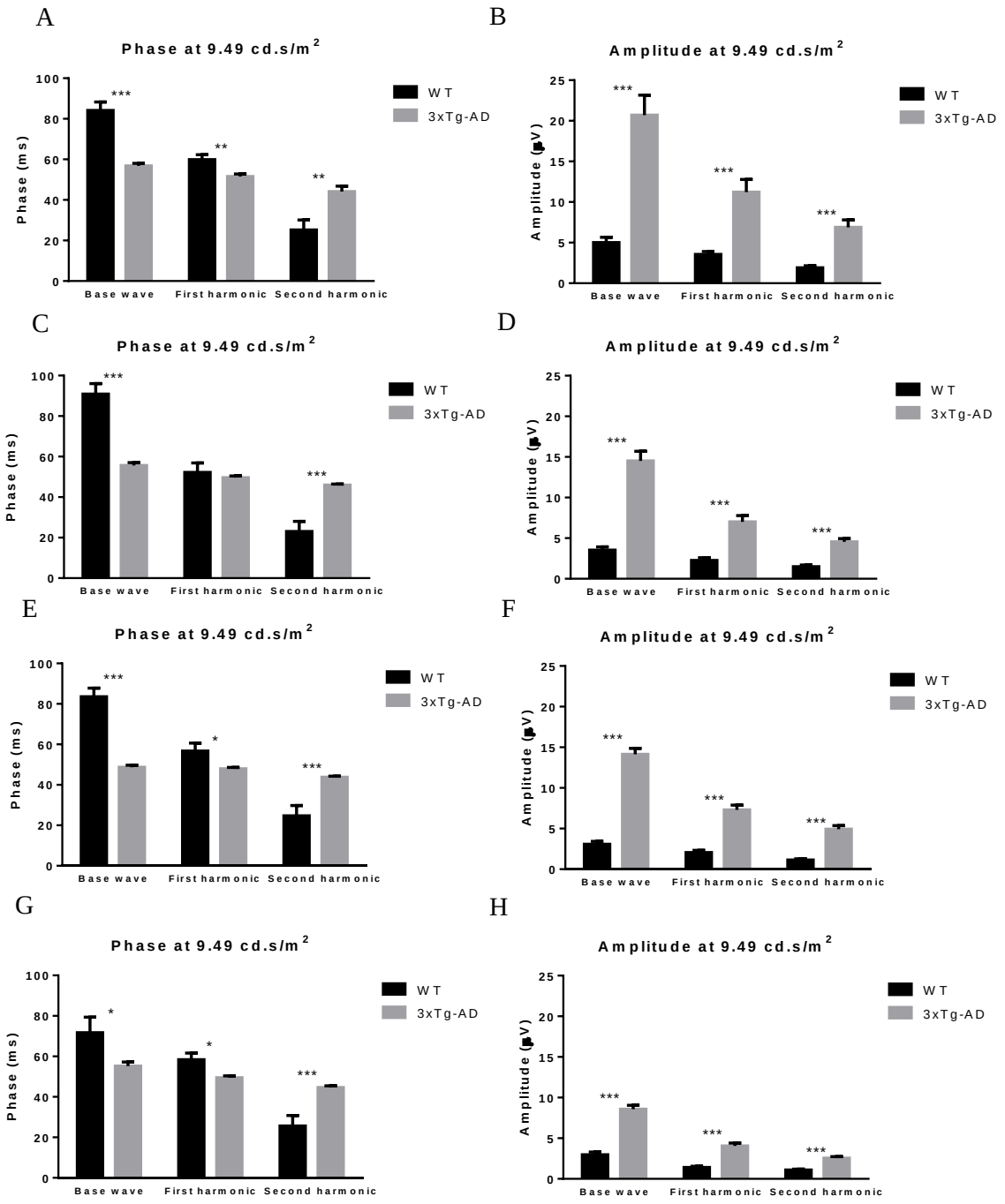

Figure 30 – Photopic flicker retinal response in 3xTg-AD and WT animals at 4 (A,B), 8 (C,D), 12 (E,F) and 16 (G,H) months of age. The amplitude and phase of the signal after Fourier transform were evaluated and are indicated in the respective graph. The results are presented as mean ± SEM and were analyzed with the Student´s t-test; *P<0.05, **P<0.01 and ***P<0.001 ($n_{WT\ at\ 4\ months}$=19 and $n_{3xTg\text{-}AD\ at\ 4\ months}$=18; $n_{WT\ at\ 8\ months}$=19 and $n_{3xTg\text{-}AD\ at\ 8\ months}$=23; $n_{WT\ at\ 12\ months}$=17 and $n_{3xTg\text{-}AD\ at\ 12\ months}$=22; $n_{WT\ at\ 16\ months}$=17 and $n_{3xTg\text{-}AD\ at\ 16\ months}$=22).

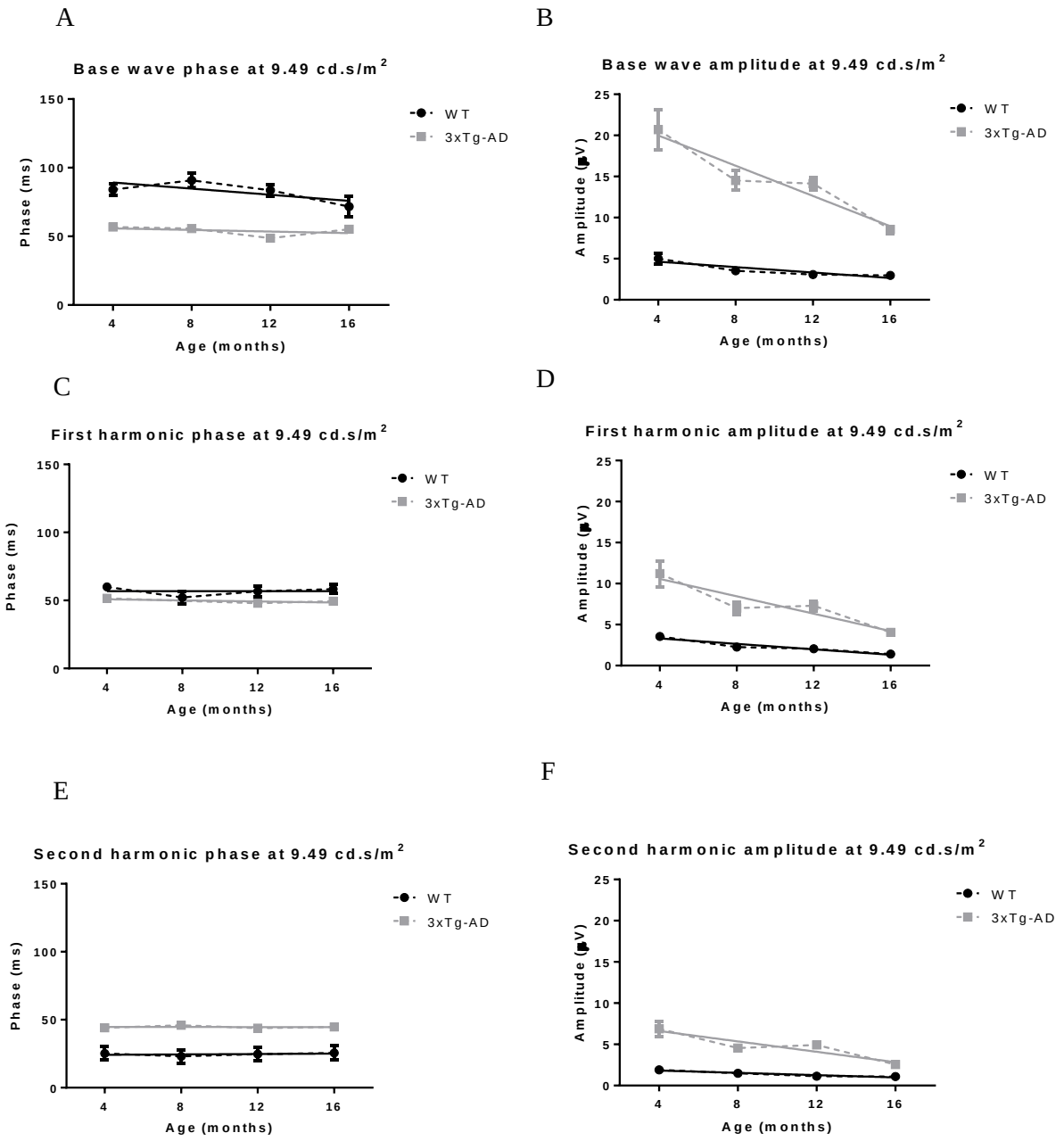

Figure 31 - Linear regression fit to base wave (A, B), first harmonic (C, D) and second harmonic (E, F) amplitudes and phases in 3xTg-AD and WT animals. Photopic flicker harmonic amplitude difference between 3xTg-AD and WT animals was assessed by comparing slopes and intercepts with ANCOVA, $P<0.05$.

2.4.5. Similar pattern electroretinogram responses in 3xTg-AD and WT animals

In PERG experiments we did not observe any significant difference between 3xTg-AD and WT mice. In particular, no significant differences were found between both groups in P1 and N2 implicit time and amplitude at all time points (4, 8, 12 and 16 months of age; Figure 32).

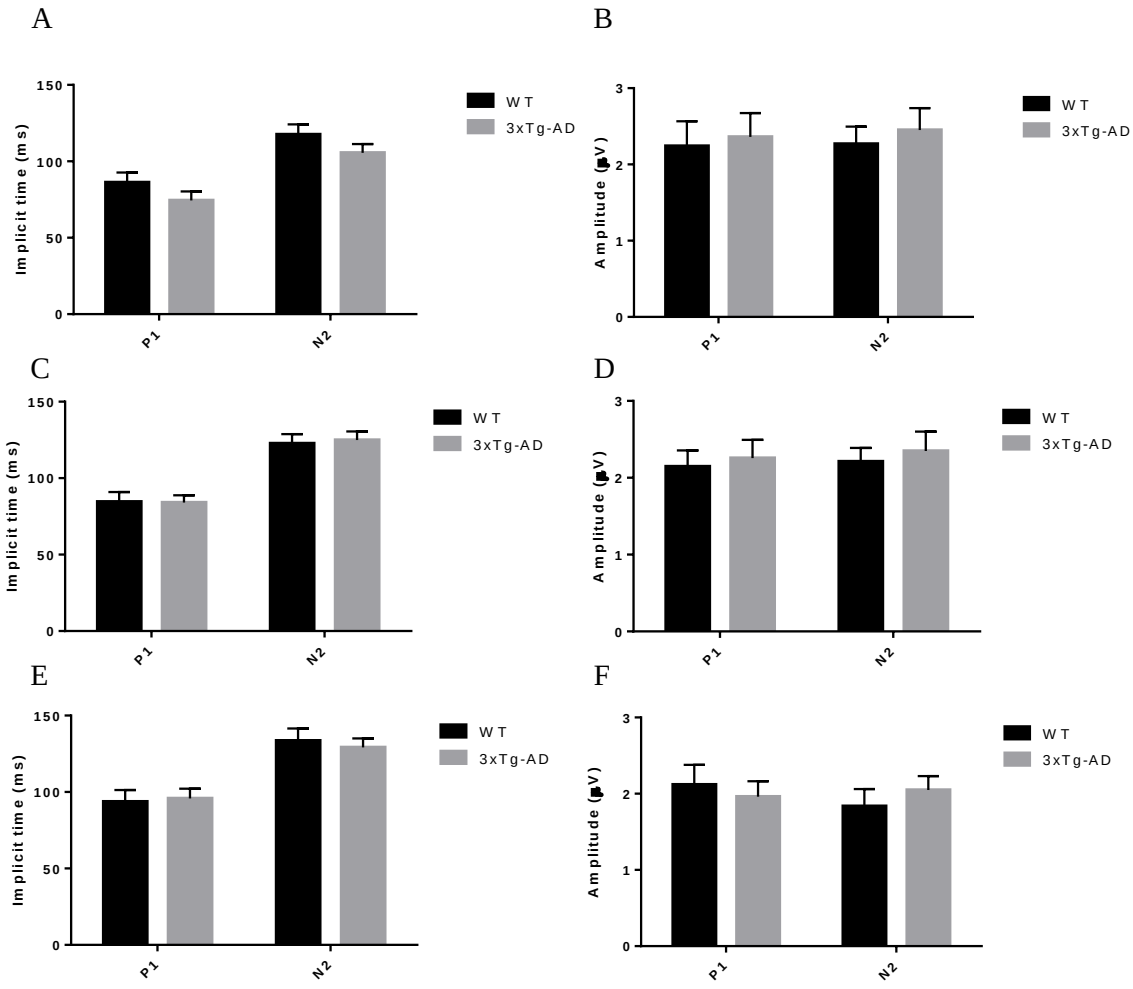

Figure 32 – Pattern electroretinogram retinal response at (A, B) 4, (C, D) 8, (E, F) 12 and (G, H) 16 months of age in 3xTg-AD and WT animals. The parameters amplitude and implicit time were evaluated. The results are presented as mean ± SEM and were analyzed with the Student´s t-test; P>0.05 ($n_{WT\ at\ 4\ months}$=19 and $n_{3xTg\text{-}AD\ at\ 4\ months}$=17; $n_{WT\ at\ 8\ months}$=19 and $n_{3xTg\text{-}AD\ at\ 8\ months}$=22; $n_{WT\ at\ 12\ months}$=17 and $n_{3xTg\text{-}AD\ at\ 12\ months}$=22; $n_{WT\ at\ 16\ months}$=17 and $n_{3xTg\text{-}AD\ at\ 16\ months}$=22).

2.4.6. Reduction of the volume of visual cortex grey matter in 3xTg-AD animals

We acquired whole brain anatomical MRI data to study the potential alterations in the volume of GM between 3xTg-AD and WT groups at different time points (4, 8, 12 and 16 months of age). A whole brain analysis revealed a significant age dependent reduction of the GM volume between both groups ($F_{(1,8)}$=71.04, p<0.0002). Furthermore, an analysis focused in the visual cortex as a region of interest (ROI) also showed a significant reduction in the GM volume of the 3xTg-AD animals in comparison to age matched WT mice ($F_{(1,8)}$=104.95; p<0.0002) for all

time points (Figure 33). VBM analysis, showed a significant reduction in 3xTg-AD animals in comparison to age matched WT mice for all time points (4M: $F_{(1,8)}$=49.66, p<0.0002; 8M: $F_{(1,8)}$=28.49, p=0.001; 12M: $F_{(1,8)}$=23.06, p=0.001; 16M: $F_{(1,8)}$=84.71, p<0.0002; Figure 33).

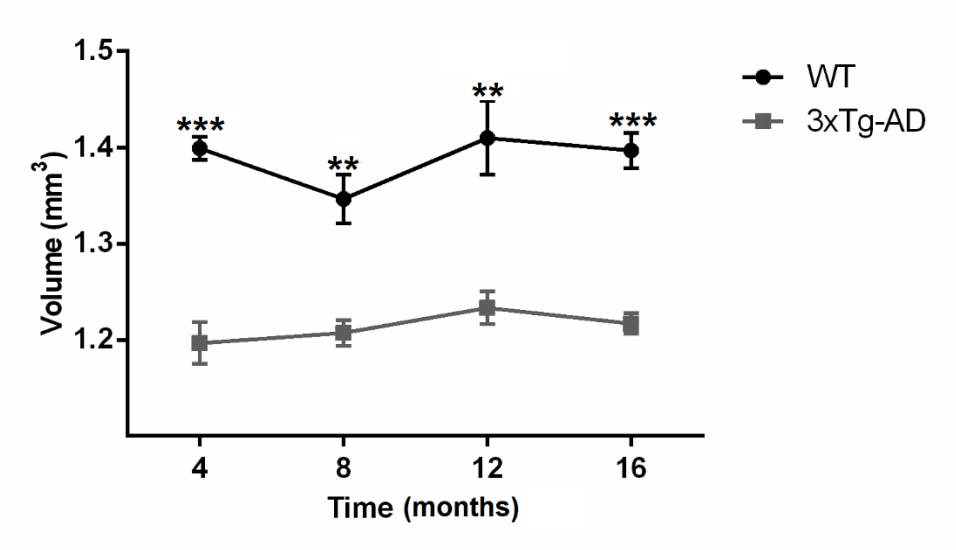

Figure 33 – Grey matter volume in the visual cortex of 3xTg-AD and WT animals measured by VBM analysis. Results are presented as mean ± SEM and the significance of the alterations in GM volumes of the visual cortex along time and between groups was assessed by an ANOVA repeated measures (mixed-effects) followed by a Bonferroni post-hoc test; *P<0.05, **P<0.01 and ***P<0.001 ($n_{\text{WT at 4, 8, 12 and 16 months}}$=6 and $n_{\text{3xTg-AD at 4, 8, 12 and 16 months}}$=7).

2.4.7. Retinal thickness changes and physiological responses are correlated with visual cortex grey matter volume

In order to further elucidate the relation between the alterations in the retina and visual cortex, we performed a correlation analysis between retinal thickness and ERG flicker response with the grey matter volume in the visual cortex. A Spearman correlation test showed a positive correlation between retinal thickness and grey matter volume (retina line scan: r=0.657, p<0.0002, N=52; retina circle scan: r=0.728, p<0.0002, N=49; Figure 34A). Additionally we calculated the Spearman correlation between amplitude values of ERG flicker response and grey matter volume in the visual cortex. We found a significant negative correlation between ERG amplitude and GM volume in the visual cortex (r=-0.790, p<0.0002, N=48; Figure 34B). Also, the correlation of retinal thickness with ERG amplitude was negative at all time points both for circle and line scans in the ganglion cell layer plus the inner plexiform layer (Table 6).

A

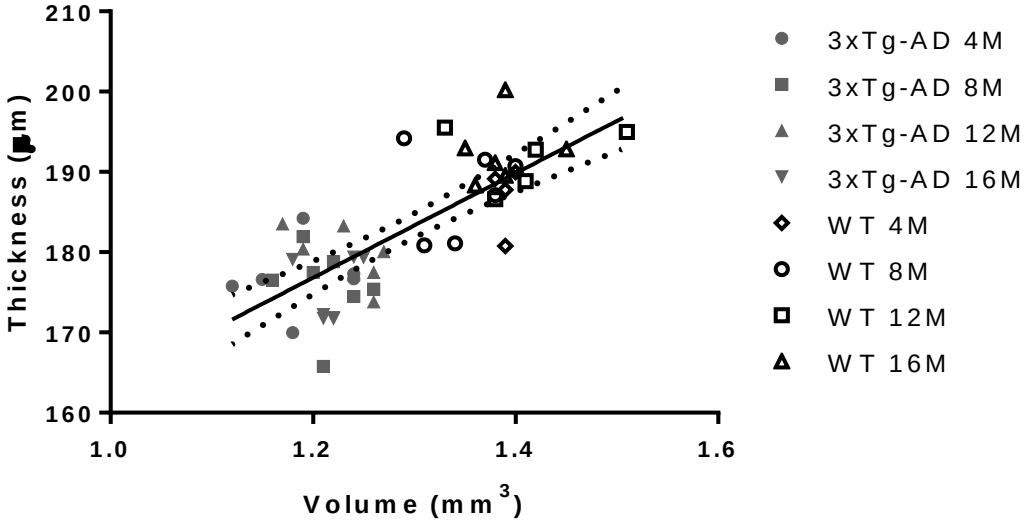

B

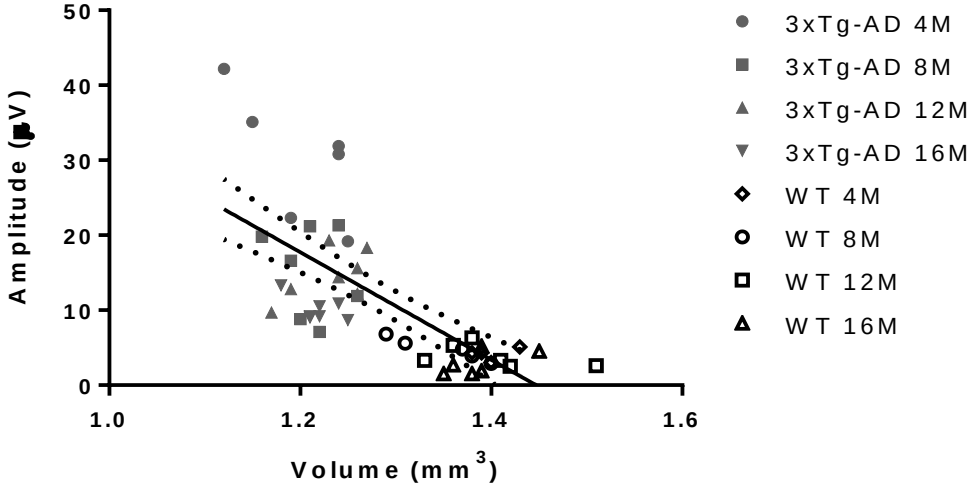

Figure 34 – (A) Spearman correlation of retinal thickness with grey matter volume of the visual cortex. Summary plot of the correlation between retinal thickness as measured by the OCT line scan and GM volume in the visual cortex ($r=0.657$, $p<0.0002$). (B) Spearman correlation between the amplitude of ERG flicker response and grey matter volume of the visual cortex ($r=-0.790$, $p<0.0002$). All animals tested at all time points were included in the graph and for sake of simplicity they are represented with different symbols in the plot ($n_{\text{WT at 4, 8, 12 and 16 months}}=6$ and $n_{\text{3xTg-AD at 4, 8, 12 and 16 months}}=7$).

Table 6 - Correlations of ERG flicker amplitude with retina and retinal cell layers thickness ($N_{circle\ scan}$=30, $N_{line\ scan}$=32). In this table r quantifies Spearman correlation, *P<0.05, **P<0.01 and ***P<0.001 are considered to be significant.

	4 months	8 months	12 months	16 months
Retina (line scan)	r= -0.2401; P= 0.1855	r= -0.6554; P< 0.0001***	r= -0.6920; P< 0.0001***	r= -0.6822; P< 0.0001***
Retina (circle scan)	r= -0.5258; P= 0.0028**	r= -0.6276; P= 0.0002***	r= -0.7620; P< 0.0001***	r= -0.7157; P< 0.0001***
GCL+IPL (line scan)	r= -0.3833; P= 0.0303*	r=-0.6554; P< 0.0001***	r= -0.6317; P= 0.0001***	r= -0.6763; P < 0.0001***
GCL+IPL (circle scan)	r= -0.4070; P= 0.0256*	r= -0.6970; P< 0.0001***	r= -0.6937; P< 0.0001***	r= -0.7108; P< 0.0001***
INL+OPL(line scan)	r= -0.2372; P= 0.1911	r= -0.5290; P= 0.0019**	r= -0.5396; P= 0.0014**	r= -0.3801; P= 0.0319*
INL+OPL (circle scan)	r= -0.0345; P= 0.8564	r= -0.3232; P= 0.0814	r= -0.5885; P= 0.0006***	r= -0.4265; P= 0.0188*
ONL (line scan)	r= -0.0108; P= 0.9532	r= -0.0792; P= 0.6666	r= 0.5521; P=0.0011**	r= 0.4663; P= 0.0071**
ONL (circle scan)	r= 0.0296; P= 0.8766	r= -0.0016; P= 0.9935	r= 0.3765; P= 0.0403*	r= 0.5493; P= 0.0017**
IS+OS (line scan)	r= -0.1039; P= 0.5713	r= -0.7188; P < 0.0001***	r= -0.7614; P < 0.0001***	r= -0.6525; P< 0.0001***
IS+OS (circle scan)	r= -0.3707; P= 0.0437*	r= -0.6885; P< 0.0001***	r= -0.8194; P< 0.0001**	r= -0.7771; P< 0.0001***

2.5. Discussion

This study is a unique longitudinal *in vivo* assessment using the 3xTg-AD mouse model, at four different time points (4, 8,12 and 16 months of age), both in the retina and brain. Here, correlations between changes in the retina and brain were performed, based on different physiological and structural approaches in association with MRI. This study also represents not only a completely new approach in animals models to tackle the potential links between retinal and brain changes in the context of AD pathology, but also gives new clues about the pathology and confirms some findings that have already been observed in humans. Several studies in AD patients, in which retinal thickness was evaluated by OCT, have reported a thinning in the retina (Paquet, Boissonnot et al. 2007, Kesler, Vakhapova et al. 2011, Thomson,

Yeo et al. 2015, Cunha, Proença et al. 2017). Here we replicated this finding in an animal model, suggesting that OCT may be useful for an early diagnosis of AD and also for the evaluation of the response to treatment in such preclinical models. Our work does therefore corroborates the notion that animal models of AD can be used to assess retinal changes and the impact of neurodegeneration (Lim, He et al. 2016). At 4 months of age, there was a thinning of GCL+IPL and of total retina both for circle and lines scans in 3xTg-AD mice. We also detected a thinning in the INL+OPL thickness for line scan acquisitions. These observations suggest that the first signs of retinal impairment in AD start at the innermost layers. With this observation we cannot discard the possibility that transsynaptic degeneration from the brain to the retina can occur. Another possibility is that some changes start occurring in the retina, even before or at least at the same time they start occurring in the brain, although this could not be ascertained. At 8 months and after we observed a thinning of GCL+IPL, INL+OPL, IS+OS and total retina in 3xTg-AD mice. The thinning observed at the inner retina at an early time point, 4 months, had spread to almost all quantified layers. This might be due to secondary degeneration, a phenomenon in which synapses and neurons in the neighborhood of originally affected neurons are also affected. This retinal thinning, even at early time points, is an important finding that corroborates previous results obtained with humans in which OCT results clearly show that there is retinal thinning in AD patients (Parisi, Restuccia et al. 2001, Liu, Zhang et al. 2015, Thomson, Yeo et al. 2015). Despite the generalized thinning of several layers of the retina, there was also an increase in the thickness of the ONL in 3xTg-AD mice that had an increased thickness in comparison with WT animals. This thickening of the ONL is not easy to explain, but we cannot exclude that it has a developmental cause.

The aim of this research work was to perform a longitudinal *in vivo* study, using the same animals for the different experimental techniques applied at each time point. We did not aim to go deeper in the structural changes of the retina and the visual cortex. We believe that a longitudinal *in vivo* study has much more relevance for the clinical setting. Moreover, OCT is the technique widely used in clinical retinal evaluation, particularly retinal layers thickness assessment. In the context of our study, in which we observed thickness changes in the µm range, histological examination would not be a good approach. Actually, it would be unlikely to detect significant changes using histology. Histological analysis also requires the use of different animals at each time point, which would preclude the implementation of a longitudinal study. Moreover, it would be difficult to obtain slices exactly in the same region of the retina whereas by using OCT we were able to analyze the same region of the retina. Also, tissue collection and preparation for histological analysis affects retinal structure, therefore thickness measurement would not be as reliable. We can say the same for the brain. We evaluated the volume of the visual cortex *in vivo* by using MRI and this is much more reliable than calculating the volume based on histological analysis of the brain.

Regarding retinal electrophysiology, scotopic and photopic b-wave amplitudes of 3xTg-AD and WT mice were significantly different at various time points. There was an altered b-wave amplitude in 3xTg-AD mice at 4, 8, 12 and 16 months of age ($P<0.05$), which indicates that there was a physiological alteration at bipolar cells. These increased responses of flash ERG, which originate in the outer retina, are not inconsistent with the increased ONL thickness that we found. Moreover, the scotopic time to peak in the a-wave and oscillatory potentials was faster in 3xTg-AD mice. Abnormal scotopic b-wave implicit time and decreased a-wave amplitude have been also reported in 3xTg-AD mice (Ioshimoto, Nagy et al. 2012). Furthermore, higher scotopic and photopic b-wave amplitudes have been observed in a mouse model of Down syndrome where layer specific changes in thickness were also found (Laguna, Barallobre et al. 2013). In fact, Aβ deposition has been detected both in AD and Down syndrome individuals (Gyure, Durham et al. 2001). In people with trisomy 21 the neurodegenerative processes associated with AD are also expressed. Moreover, APP gene is located at chromosome 21 and Down syndrome individuals have an extra copy of this chromosome, thus leading to the development of early onset dementia with AD characteristics (Hardy and Selkoe 2002, Huang and Mucke 2012). This may entail that there is a common phenotype in the retina between AD and Down syndrome individuals.

The difference in the ERG response between 3xTg-AD and WT starts at the photoreceptor level. In this study, WT animals were chosen according to the genetic background from which 3xTg-AD mice were generated and it seems that the introduction of human genes that have been associated with AD had an effect that was contrary to what was expected, if one assumes that the effects of this genetic manipulation only impacts on neurodegeneration. However, if developmental effects are also present, as suggested by the increased thickness of ONL, then this might explain increased flash ERG responses in 3xTg-AD mice. In general, the flash evoked ERG signal, which mainly originated from the outer retina, was larger in 3xTg-AD mice than the one obtained in WT animals. Moreover, regarding the inner retinal responses from ganglion cell populations evaluated with PERG we did not observe any significant difference between both groups. In previous humans studies there are contradictory results regarding PERG recordings. Several studies show abnormal pattern electroretinograms and visual evoked potentials in AD patients (Katz, Rimmer et al. 1989, Nesher and Trick 1991, Krasodomska, Lubiński et al. 2010, Sartucci, Borghetti et al. 2010). On the other hand, reports of normal retinal function have also been published (Strenn, Dal-Bianco et al. 1991, Prager, Schweitzer et al. 1993, Justino, Kergoat et al. 2001). Moreover, in PERG recordings, P1 is driven by ON pathway while N2 is driven by OFF pathway (Miura, Wang et al. 2009). Because we did not observe any difference in P1 and N2 parameters between 3xTg-AD and WT mice this suggests that retinal ganglion cell function is not significantly impaired in this animal model of AD.

Since both structural and functional changes were observed in the retina at all time points the possible causal links (early neurodegenerative or neurodevelopmental) on structure and function remain somehow elusive. According to ERG evaluation 3xTg-AD mice had higher b-wave and harmonic amplitude responses than WT mice. In order to depict more accurately what is happening in terms of retinal physiological changes in this model it would be essential to perform either multielectrode array or patch clamp recordings which enable to determine more precisely the changes in retinal response properties to a given light stimulus. Visual evoked potentials recordings would enable to determine if visual information transmitted from the retina to the brain is impaired. Our results show that there is a positive correlation between retinal thickness and grey matter volume of the visual cortex, while ERG flicker amplitude is negatively correlated with retinal and cortical structural measurements. These associations further suggest that enhanced ERG responses may actually reflect an impairment, as also suggested by Laguna and colleagues (Laguna, Barallobre et al. 2013). Therefore, we show that retinal structural and functional changes are associated with visual cortex alterations with potential impact on early AD diagnosis. Similar pathophysiological mechanisms might be occurring in both structures because the retina and the visual cortex are part of the central nervous system. However, it is not easy to explain how structural changes occurring in the visual cortex can contribute for retinal changes because what is happening in the visual cortex does not necessarily affect, at least directly, the retina.

2.6. Conclusions

In this longitudinal multimodal study the 3xTg-AD mouse model allowed to identify structural and neurophysiological alterations in the retina that mirrored changes in grey matter volume in the visual cortex. These retinocortical alterations showed early onset and remained persistent over time. Some of these changes were of neurodegenerative nature (as expressed by retinal and brain thinning). Since the retina is an optically accessible part of the brain OCT may become a feasible, noninvasive, low cost method and an additional tool for preclinical research in AD. The 3xTg-AD mouse model may be used as a tool for preclinical studies in which retinal structural and functional changes can be correlated with brain impairments detected with neuroimaging, which may be quite useful for preclinical drug trials. The results emerging from the present research assume particular importance because they enable to establish a model in which retinal manifestations of AD are observed at an early time point. Moreover, our results emphasize the possibility for using retinal biomarkers in AD.

Chapter 3 | General discussion, conclusions and future perspectives

3. General discussion, conclusions and future perspectives

The 3xTg-AD mouse model used in this study mimics both Aβ plaques and tau neurofibrillary tangles deposition found in AD patients. Indeed, previous results show a connection between Aβ and tau in which Aβ deposition leads to downstream tau hyperphosphorylation and tangles formation (Oddo, Billings et al. 2004). Therefore, this 3xTg-AD mouse model may be a valuable tool for preclinical studies. In order to be able to deliver the appropriate therapeutics for AD we need to understand the processes that lead to AD and if possible perform a diagnosis at an early phase. Several factors will ultimately contribute to cognitive decline, namely Aβ accumulation, neurofibrillary tangles deposition, synaptic/neuronal loss, glial activation and age. Since most AD patients suffer from sporadic pathology the mechanisms that lead to AD inception are still a matter of debate (Sperling, Aisen et al. 2011). Moreover, clinical trials of AD treatments have been disappointing (Weiner, Veitch et al. 2015). Thus, there is an urgent need to have a model in which candidate biomarkers are accurately characterized enabling to determine the efficacy of candidate drugs. Transgenic mouse models provide the possibility to mimic human AD pathophysiology (Sutphen, Fagan et al. 2014). As a research tool mouse models resemble familial AD. Nevertheless, the most common form is sporadic AD. Therefore, preclinical tests of novel therapeutics in AD mouse models serve as a screening tool and results need to be carefully validated in human clinical trials (Hall and Roberson 2012).

In this research work a multimodal, longitudinal and *in vivo* study was performed in order to characterize retinal and brain alterations in the 3xTg-AD mouse model. Results were compared between 3xTg-AD mice and WT animals enabling to determine differences that are due to AD. In both groups aging produces changes at an exponential rate due to the accumulation of various risk factors along life (Gerashchenko 2002). Aging exponential nature can be observed in the locomotor activity of the animals. Both distance and speed exhibit an exponential nature at the time points tested both in WT and 3xTg-AD mice. Therefore, the differences observed between both groups are likely due to AD related pathology and not due to aging. Regarding novel object recognition test there are some differences between the protocols used in distinct laboratories and results may not be comparable. Moreover, the age of 3xTg-AD mice is not always the same. This leads to distinct results in which some authors claim that there are no novel object recognition memory deficits while others state that there are recognition memory impairments (Clinton, Billings et al. 2007, Martinez-Coria, Green et al. 2010, Arsenault, Julien et al. 2011, Onishi, Iwashita et al. 2011, Filali, Lalonde et al. 2012, Guzmán-Ramos, Moreno-Castilla et al. 2012, Davis, Easton et al. 2013, Grayson, Leger et al. 2015, Stover, Campbell et al. 2015). During behavioral tests WT mice behaved normally and indeed had a better object recognition performance than 3xTg-AD mice. Because in 3xTg-AD mice there are recognition memory impairments visual recognition memory assessment may

become a biomarker for AD diagnosis. The ventral visual stream and the medial temporal lobe memory system can interact in order to obtain a memory representation of the visual world. This interaction leads to a conjugation between memory and perception. The hippocampus may act as a structure that integrates information about visual and spatial features (Bussey and Saksida 2007). The role of the hippocampus in spatial and recognition memory was confirmed experimentally. Evidence for the requirement of the hippocampus in spatial memory overwhelms that from recognition memory. However, the hippocampus also has a role in recognition memory (Broadbent, Squire et al. 2004). Other structures also have been involved in the recognition of objects, namely the perirhinal cortex (Winters, Forwood et al. 2004). Indeed, it was proposed to regard the ventral visual stream as a continuum between ventral visual pathway, perirhinal cortex and hippocampus with impact in visual memory and perception (Bussey and Saksida 2007). Besides the accumulation of Aβ and tau in hippocampal regions previously described, in AD patients amyloid and neurofibrillary pathologies have been observed in the visual cortex. Amyloid firstly deposits in the neocortex and after progresses to the hippocampus. Neurofibrillary pathology goes from transentorhinal, entorhinal and hippocampal areas to the neocortex (Braak and Braak 1991, Braak, Alafuzoff et al. 2006). Therefore, the pathological hallmarks of AD may be the basis of object recognition memory impairment observed at all time points.

Regarding structural and functional evaluation of the retina we used OCT, ERG and PERG assessments. OCT has been used for imaging animal models with retinal diseases. With animal models it is possible to quantify structural alterations in longitudinal studies. This aspect is important since it allows to perform preclinical studies and drug tests without sacrificing animals (Drexler and Fujimoto 2008, Drexler and Fujimoto 2008). Retinal mouse models in which quantification was performed include models of retinal vein occlusion (Ebneter, Agca et al. 2015), retinoblastoma (Ruggeri, Wehbe et al. 2007), diabetes (Antony, Jeong et al. 2014), retinitis pigmentosa and Leber's congenital amaurosis (Huber, Beck et al. 2009, Pennesi, Magee et al. 2011, Pennesi, Michaels et al. 2012). Several neurodegenerative conditions benefit from the use of OCT namely multiple sclerosis, optic neuritis, neuromyelitis optica, Parkinson's disease and AD (Raftopoulos and Trip 2012). Regarding OCT measurements performed in animal models of AD publications are scarce. Results from our group for the 3xTg-AD mouse model show its potential use for preclinical studies. Therefore, OCT may contribute to an early diagnosis of AD when therapeutic agents have the potential to refrain the impairments observed in AD. Automated segmentation algorithms for measuring retinal thickness are already available. Nevertheless, some discrepancies between manual segmentation measurements in mice and automated segmentation algorithms were detected (Dysli, Enzmann et al. 2015). Typical dimension of wild type C57BL/6 mouse retina thickness is around 200 µm (Ferguson, Dominguez II et al. 2013). Total retinal thickness values in

C57BL6/129S mice varies between 186-196 µm around the optic nerve head and between 188-192 µm above and below the optic nerve head. The obtained values are thus in agreement with measurements previously reported.

At 4 months the thinning in the GCL+IPL detected with circle scan around the optic nerve head has a higher statistical significance (***P<0.001). This highlights the possibility that there is transsynaptic (transneuronal) degeneration from the brain to the retina. Synaptic dysfunction and loss has long been recognized as the basis of AD. Early alterations are observed in the hippocampus and neocortex. Therefore, synaptic degeneration is associated with AD onset and progression (Arendt 2009). We hypothesize that structural changes in the brain may lead to structural changes in the retina. Several researchers demonstrated that retrograde transsynaptic degeneration was responsible for a reduction of the inner retina (Gills and Wadsworth 1967, Chauhan, Stevens et al. 2012, Keller, Sánchez-Dalmau et al. 2014). It is known that tau pathology progresses from limbic regions to the neocortex and that this pathology correlates better with AD progression than amyloid plaque burden (Braak and Braak 1991). Progressive anterograde transneuronal degeneration was described in *postmortem* hippocampal tissue from patients with mild and severe AD (Su, Deng et al. 1997). Both anterograde and retrograde degeneration may be present in AD. While in anterograde degeneration the postsynaptic neuron degenerates after presynaptic atrophy in retrograde degeneration is the other way around. Retrograde degeneration may be a process concomitant with anterograde degeneration resulting in the spread of AD. Furthermore, Aβ deposition, tau accumulation and functional alterations in the retina of transgenic mouse models were detected even before they were detected in other brain regions (Koronyo-Hamaoui, Koronyo et al. 2011, Chiasseu, Alarcon-Martinez et al. 2017, Criscuolo, Cerri et al. 2018). In AD Aβ and tau characteristic proteinopathies may spread through transsynaptic exosome transmission to neighboring cells (Rajendran, Honsho et al. 2006, Wang, Balaji et al. 2017, Xiao, Zhang et al. 2017). Since in the 3xTg-AD mouse model we observe retinal and brain changes at 4 months it is difficult to state what is really happening in terms of retinal and brain AD onset and progression.

Besides ganglion cell loss, loss of cells at the INL and ONL may result from a secondary process initiated due to retrograde transsynaptic degeneration. Previously, secondary degeneration was reported after partial optic nerve transection (Levkovitch–Verbin, Quigley et al. 2001, Levkovitch-Verbin, Quigley et al. 2003, Li, Ruan et al. 2014). Degeneration leads to synaptic and neuronal loss that probably underlies the observed retinal thinning. In glaucoma beyond typical retinal ganglion cell degeneration the INL and ONL may also degenerate due to retrograde transneuronal degeneration (Calkins 2012). Since at 8, 12 and 16 months we observe a thinning in GCL+IPL, INL+OPL and in IS+OS we imply that there is a more generalized degeneration that affects both the inner and outer retina. Neuronal and synapse

loss occurs in AD being the later associated with disease progression and cognitive decline. Brain regions important for memory are impaired in AD and synaptic dysfunction and structural changes certainly influences this outcome. Synaptic changes in AD patients and mouse models suggest that structural alterations in brain connectivity may lead to cognitive deficits. Early onset familial AD mouse models enable to study in detail synaptic dysfunction and loss. With these mouse models dendritic spine alterations were reported, thus emphasizing the importance of synaptic changes in memory impairment (Pozueta, Lefort et al. 2013). At 12 and 16 months the ONL in 3xTg-AD mice has an increased thickness in comparison with WT animals. This thickening of the ONL is not easy to explain, but it may be partly due to retinal gliosis. In particular, microglia may play an important contribution for this thickness increase. Microglia contributes to synaptic pruning and in AD gliosis leads to synapse loss due to the engulfment of spines (Spires-Jones and Hyman 2014). Therefore, infiltration of cells at the outer retina may happen due to trigger signals present in AD mouse retina. These signals may be related to the pathophysiology of AD, namely Aβ and tau proteinopathies. Previously, Lim and colleagues reported functional and structural alterations in the retina of 5xFAD mice. Moreover, Aβ was detected in the hippocampus, cortex and retina (Lim, He et al. 2016). Noninvasive *in vivo* retinal imaging also showed the presence of Aβ plaques in the retina (Koronyo, Salumbides et al. 2012). Tau pathology expression in the retina was reported with a reduction of INL layer thickness in a transgenic mouse model with mutant tau (Ho, Leung et al. 2015). Furthermore, hyperphosphorylated tau accumulation and functional changes were reported in retinal ganglion cells of P301S tau transgenic mice (Gasparini, Crowther et al. 2011, Mazzaro, Barini et al. 2016). Thus, there is already some evidence in the literature that tau and Aβ disturb retinal structure and function. But what about the role of glia in AD retinal degeneration? Neuroinflammation, microglia and astrocytes activation play a role in AD neurodegeneration. Chronic inflammation with microglial over activation can contribute to neuronal degeneration. Moreover, activated microglia can phagocytose cell debris and protein aggregates. In AD brains activated astrocytes and microglia were detected surrounding amyloid plaques with implications in Aβ phagocytosis. In the retina of AD transgenic mouse models microglial activation was observed related with Aβ and tau proteinopathies (Parnell, Guo et al. 2012, Ramirez, de Hoz et al. 2017). In addition, macroglial activation was observed in the retina of 3xTg-AD mice. Retinal astrocytes and Müller cells were detected around amyloid deposits emphasizing the importance of glial activation in AD retinal alterations (Edwards, Rodríguez et al. 2014). Consequently, ONL retinal thickness increase may be partly due to the recruitment of microglial cells in response to Aβ and tau proteinopathies. This increase only starts to be detected at 12 months, which means that at early age neuroinflammation with glial cell activation and recruitment may not be clearly established. Therefore, this effect seems to be due to AD progression being detected only when mice are

older. A significant microglial cells increase around old amyloid plaques was observed in APP transgenic mice brains (Wegiel, Imaki et al. 2003). Moreover, in age-related macular degeneration microglial activation was observed in ONL (Madeira, Boia et al. 2015). Since the retina is an extension of the brain similar mechanisms may act in both structures. Other possible explanation for ONL thickness increase in 3xTg-AD animals relies on a neurodevelopmental effect, contrarily to the neurodegeneration observed in the other retinal layers. While in 3xTg-AD mice a neurodevelopmental effect may lead to a higher thickness in the ONL, a neurodegenerative effect leads to a generalized retinal thinning. Our results suggest that in fact retinal alterations are detected in 3xTg-AD mice. With the exception of the ONL, we observed a generalized thinning of the retina. This probably means that there is an atrophy of retina neural cells, namely at the synaptic level. Neuronal loss may also contribute to this process, something that was already observed in the retina (Blanks, Schmidt et al. 1996, Blanks, Torigoe et al. 1996). Nevertheless, with the 3xTg-AD used in this study there was no evidence for synaptic loss and cell death (Neves, Chiquita et al. 2017). Having this said, it does not seem reasonable that there is a reduction of retinal thickness in 3xTg-AD mice without any synaptic loss or cell death. Probably the techniques used to assess synaptic loss and cell death, namely Western blotting and terminal deoxynucleotidyl transferase dUTP nick end labeling (TUNEL), fail to detect small changes that lye below its detection level. Spectral domain OCT can be used to image the rodent retina allowing to quantify retinal layers thickness *in vivo* (Fischer, Huber et al. 2009, Huber, Beck et al. 2009, Berger, Cavallero et al. 2014). OCT is a highly sensitive technique that detects changes in the µm range allowing to unmask the differences between 3xTg-AD and WT mice and may become a feasible, noninvasive and low cost method for early AD diagnosis.

Regarding the evaluation of structural changes at the retina level, the evidence based in AD patients overwhelms the evidence based in AD mouse models. This is probably due to the fact that animal models containing the genes that mimic some of the most important features of AD only became available recently. In particular, the publications describing the 3xTg-AD mouse model used in this study were only published in 2003 (Oddo, Caccamo et al. 2003, Oddo, Caccamo et al. 2003). The practical difficulties in order to clearly establish retinal structural alterations as an early biomarker for AD are related with the existence of some overlap between the changes observed in AD with the changes observed in other pathological conditions that also affect the retina. This does not means that OCT measurements are not a valuable tool for future AD diagnosis and treatment. This only means that OCT measurements should be done in conjugation with other tests used for AD diagnosis and assessment of cognitive status, such as the Mini-Mental State Examination (MMSE). The results obtained with 3xTg-AD mice clearly emphasize its possible use for preclinical studies. In fact, there is an ongoing project funded by the European Research Council that is using OCT to image

mouse models of AD pathology (OPTIMALZ 2015). Since there are visual symptoms due to distinct neurodegenerative diseases it is important to have a model in which we are sure that the pathological hallmarks observed are due to a specific disorder. Murine models constitute a valuable tool for assessing retinal disorders pathogenesis. Particularly, mouse models of AD play a crucial role because they allow to envisage possible early diagnosis and assess response to treatments before translating them into AD patients.

Several reports of retinal function in mouse models of AD were done for scotopic and photopic conditions (Perez, Lumayag et al. 2009, Ioshimoto, Nagy et al. 2012, Antes, Ezra-Elia et al. 2013, Joly, Lamoureux et al. 2017). These recordings reflect the contribution of the rod and cone systems, respectively. Given the differences observed at a-wave, b-wave and oscillatory potentials between WT and 3xTg-AD mice results suggest that there is a mechanism acting at first and second order retinal neurons with implications in amplitude and time to peak measurements. Thus, scotopic ERG results suggest that in 3xTg-AD mice signal transmission seems to be faster at the photoreceptor level and at a postsynaptic level both b-wave and oscillatory potentials are affected with a higher amplitude and smaller time to peak when compared with WT mice. The concerted activity of excitatory and inhibitory transmitters leads to membrane potential changes of retinal neurons due to alterations of ions flux. While glutamate and acetylcholine are related to an excitatory function, GABA and glycine have an inhibitory role. Since 3xTg-AD mice oscillatory potentials have higher amplitude and smaller time to peak the typical acetylcholine deficit observed in AD may not explain these results. Amacrine cells modulate signal transmission to ganglion cells both with excitatory and inhibitory transmitters. The resulting potential recording reflects the balance between neurotransmitters release with opposite effects. Glutamate release from photoreceptors leads to second order bipolar cells activity that receive inhibitory inputs at axonal terminals via GABA and glycine. Ganglion cells receive excitatory and inhibitory neurotransmission mediated through similar mechanisms acting upon bipolar cells adding also acetylcholine inputs. In the inner retina amacrine cells modulate electrical signal flow by the release of GABA, glycine and acetylcholine that can act upon bipolar or ganglion cells (Kolb 2009). In photopic conditions the electrical activity response is mainly cone driven. At 4 and 8 months we can observe differences at b-wave amplitude. Moreover, at 12 months oscillatory potentials have distinct amplitudes. Thus, both cone driven bipolar cells and amacrine cells may have altered function. The results obtained under dark adaptation are confirmed in photopic conditions, with implications in functional responses of second order neurons. Both bipolar and amacrine cells seem to be involved. Flicker ERG is a powerful technique for determining bipolar cells contribution to retinal activity. By using a Fourier transform the time domain signal can be analyzed in the frequency domain enabling to evaluate amplitude and phase at base wave, first harmonic and second harmonic. Photopic flicker ERG results clearly show that 3xTg-AD

amplitude is higher when compared with WT group. This is similar to what was previously discussed for b-wave results both in scotopic and photopic conditions. This means that bipolar cells have a higher response in 3xTg-AD mice. At base wave 3xTg-AD mice have a faster response but at second harmonic this pattern is reversed. In mice light response above a given frequency is mediated by ON cone bipolar cells and by OFF cone bipolar cells (Tanimoto, Sothilingam et al. 2015). Therefore, the reverse in phase response at higher frequencies may be related with distinct retinal activity of ON and OFF pathways at different frequencies, with OFF pathway dominating at higher frequencies. Pattern contrast reversals stimuli at a given frequency originate synchronous retinal ganglion cell responses that can be measured at the corneal electrode. PERG technique can be used to assess functional status of the inner retina both in mice and in humans making possible to determine the effect of retinal disorders in ganglion cell function (Hull and Thompson 1989, Porciatti 2007, Porciatti, Saleh et al. 2007). Since in AD there may be ganglion cell dysfunction and loss with PERG we aim to understand the functional implications of AD at the retinal output neurons. WT and 3xTg-AD groups do not show statistically significant differences in P1 and N2 amplitude and implicit time at all time points. This means that, despite there is a difference originating from photoreceptor, bipolar and amacrine cells responses, this difference is not observed at ganglion cell level. Correlations between retina and brain recordings may be obtained, by performing recordings in whole mount retinas and hippocampal slices. The disadvantage of these techniques in comparison with PERG is that they do not permit to perform *in vivo* longitudinal evaluations in the same animals, being necessary to sacrifice animals in order to extract the retina and brain. The output retinal signal to the brain detected via PERG is similar for both groups. This result is in opposition to the result obtained with photopic flicker ERG that assesses outer retinal function. Since both flicker ERG and PERG were done in light adapted conditions both are cone driven signals. Therefore, bipolar cell transmission to ganglion cells may be modulated by amacrine inhibitory feedback mechanisms leading to a similar recording between groups. With the exception of the ONL, there is a negative correlation between retinal thickness and ERG flicker amplitude. While in WT animals there is a retinal thickness increase due to normal growth that is associated with a reduced ERG response, in 3xTg-AD mice the generalized retinal thickness decrease is related with a higher ERG response. This suggests that compensatory mechanisms may be present at the retina, trying to balance the functional response and structural changes imbalance. Weight loss was also observed in AD patients (Guyonnet, Nourhashemi et al. 1998, Gillette-Guyonnet, Nourhashémi et al. 2000, Power, Noel et al. 2001). Moreover, a statistically significant correlation between weight loss and AD progression was already reported in the literature (White, Pieper et al. 1998). The difference observed in body weight between 3xTg-AD and WT mice is more evident at 8, 12 and 16 months of age than at 4 months. Nevertheless, both groups exhibit an increase in body weight

with age which means that this increase is probably due to animal normal growth. Both animal groups were given access to water and food *ad libitum* both exhibiting this increase in body weight. Thus, the difference between WT and 3xTg-AD mice body weight is likely due to AD. The 3xTg-AD mouse model may be used as a tool for preclinical tests in which brain impairments detected with neuroimaging can be correlated with retinal structural and functional changes. Indeed, retinal structure and function is correlated with visual cortex grey matter. Furthermore, hippocampal and visual cortex volumes reduction has been detected in 3xTg-AD mice. In AD patients structural measurements reveal an eminent brain atrophy and retinal neurodegeneration (Li, Wang et al. 2012, Hsu, Shou et al. 2015, Mutlu, Colijn et al. 2017). Consequently, the observation of a reduction of the volumes of the hippocampus and visual cortex in conjugation with a decrease in the thickness of the retina in 3xTg-AD mice may become a valuable indicator for AD diagnosis and treatment. We can argue that the impairments in the retina are likely to be due to the genes associated with human AD expressed in the 3xTg-AD mouse model. Therefore, OCT evaluations in combination with possible treatments for AD can pave the way forward in AD research field. Electrophysiology recordings may also be useful for the early diagnosis of AD, since with this technique we can evaluate the function of various neural cells in the retina. As previously discussed, the alterations in the ERG recordings in the 3xTg-AD animal model are similar to those observed in a mouse model of Down syndrome. In order to further evaluate possible correlations between the retina and brain in AD patch clamp or multielectrode recordings in the retina and brain would be useful. In particular, it would be interesting to obtain recordings from retinal ganglion cells since recordings obtained with PERG technique have a low signal amplitude and some variability. Moreover, recordings from hippocampal brain slices could be obtained and alterations observed at the hippocampal level (Oddo, Caccamo et al. 2003) could be eventually correlated with alterations at ganglion cell level, the neuronal cells that project to the brain.

The main findings obtained in this research work using the 3xTg-AD mouse model are described below:

- Behavioral tests show that there are recognition memory and locomotor activity impairments in 3xTg-AD mice;
- OCT thickness measurements reveal that there is a reduction of retinal thickness in 3xTg-AD mice at all time points. This reduction can be observed at total retinal thickness and at several layers of the retina, being more pronounced in the inner retinal layers;
- Functional analysis reveals that 3xTg-AD mice have higher retinal response in scotopic and photopic flicker amplitudes at all time points, which indicates that there is a

physiological alteration at bipolar cells. PERG recordings do not show any statistically significant difference between 3xTg-AD and WT mice;

- MRI brain structural analysis reveals substantial hippocampal and visual cortex grey matter volumes reduction at all time points in 3xT-AD mice;
- Neurospectroscopy assessment shows that hippocampal taurine levels are reduced in 3xTg-AD mice;
- PET results for amyloid accumulation and neuroinflammation do not show any significant differences between 3xTg-AD and WT mice;
- Retinal thickness and electroretinogram response are correlated with visual cortex grey matter volume.

Regarding the question asked at the beginning of this work “The changing brain in Alzheimer's disease: is the retina a mirror of disease onset and progression?” the results obtained suggest that the retina is a window to the brain and can be assessed noninvasively as a tool to monitor AD onset and progression. In particular, OCT acquisitions and ERG recordings in combination with other techniques used in the clinics to diagnose AD might enable to perform an early and better diagnosis of this disease. The assessment of cognitive function with the MMSE and diagnosis of probable AD with the National Institute of Neurological and Communicative Disorders and Stroke/Alzheimer’s Disease and Related Disorders Association (NINCDS-ADRDA) criteria in conjugation with OCT measurements and ERG recordings in AD patients may become a valuable approach (Folstein, Folstein et al. 1975, McKhann, Drachman et al. 1984). A combination of structural, functional and molecular measurements of the retina and brain, together with cognitive assessments may increase the potential for an early and reliable AD diagnosis and treatment.

To sum up, results indicate that there are structural and functional changes in the retina of 3xTg-AD mice, which are associated with brain and behavioral alterations. These changes might mirror AD progression creating the possibility of using the eye as a noninvasive model for early AD diagnosis. Future longitudinal clinical studies will enable to establish accurate biomarkers for early AD diagnosis and possible therapeutic approaches for this threatening condition.

Chapter 4 | References

4. References

Alzheimer, A. (1907). "Ueber eine einartige Erkrankung der Hirnrinde." Zblatt fur ges Neurologie u Psychiatrie **18**: 177-179.

Amram, S. and D. Frenkel (2016). "Animal Models of Alzheimer's." Neuroprotection in Alzheimer's Disease: 31.

Antes, R., R. Ezra-Elia, D. Weinberger, A. Solomon, R. Ofri and D. M. Michaelson (2013). "ApoE4 induces synaptic and ERG impairments in the retina of young targeted replacement apoE4 mice." PloS one **8**(5): e64949.

Antony, B. J., W. Jeong, M. D. Abramoff, J. Vance, E. H. Sohn and M. K. Garvin (2014). "Automated 3D segmentation of intraretinal surfaces in SD-OCT volumes in normal and diabetic mice." Translational vision science & technology **3**(5): 8-8.

Arendt, T. (2009). "Synaptic degeneration in Alzheimer's disease." Acta neuropathologica **118**(1): 167-179.

Arsenault, D., C. Julien, C. Tremblay and F. Calon (2011). "DHA improves cognition and prevents dysfunction of entorhinal cortex neurons in 3xTg-AD mice." PLoS One **6**(2): e17397.

Ashe, K. H. and K. R. Zahs (2010). "Probing the biology of Alzheimer's disease in mice." Neuron **66**(5): 631-645.

Aytan, N., J.-K. Choi, I. Carreras, V. Brinkmann, N. W. Kowall, B. G. Jenkins and A. Dedeoglu (2016). "Fingolimod modulates multiple neuroinflammatory markers in a mouse model of Alzheimer's disease." Scientific reports **6**: 24939.

Bachatene, L., V. Bharmauria and S. Molotchnikoff (2012). Adaptation and Neuronal Network in Visual Cortex. Visual Cortex-Current Status and Perspectives, InTech.

Baden, T., P. Berens, K. Franke, M. R. Rosón, M. Bethge and T. Euler (2016). "The functional diversity of retinal ganglion cells in the mouse." Nature **529**(7586): 345.

Baek, H., M. Ye, G. Kang, C. Lee, G. Lee and D. Choi (2016). "Neuroprotective effects of CD4+CD25+Foxp3+ regulatory T cells in a 3xTg-AD Alzheimer's disease model. Oncotarget." Oncotarget. **7**: 69347–69357.

Ballard, C. e. a. (2011). "Alzheimer's disease." The Lancet **377**(9770): 1019 - 1031.

Bayhan, H. A., S. Aslan Bayhan, N. Tanık and C. Gürdal (2014). "The association of spectral-domain optical coherence tomography determined ganglion cell complex parameters and disease severity in Parkinson's disease." Current eye research **39**(11): 1117-1122.

Berger, A., S. Cavallero, E. Dominguez, P. Barbe, M. Simonutti, J.-A. Sahel, F. Sennlaub, W. Raoul, M. Paques and A.-P. Bemelmans (2014). "Spectral-domain optical coherence tomography of the rodent eye: highlighting layers of the outer retina using signal averaging and comparison with histology." PloS one **9**(5): e96494.

Berisha, F., G. T. Feke, C. L. Trempe, J. W. McMeel and C. L. Schepens (2007). "Retinal abnormalities in early Alzheimer's disease." Investigative ophthalmology & visual science **48**(5): 2285-2289.

Bien-Ly, N., C. A. Boswell, S. Jeet, T. G. Beach, K. Hoyte, W. Luk, V. Shihadeh, S. Ulufatu, O. Foreman and Y. Lu (2015). "Lack of widespread BBB disruption in Alzheimer's disease models: focus on therapeutic antibodies." Neuron **88**(2): 289-297.

Billings, L. M., S. Oddo, K. N. Green, J. L. McGaugh and F. M. LaFerla (2005). "Intraneuronal Aβ causes the onset of early Alzheimer's disease-related cognitive deficits in transgenic mice." Neuron **45**(5): 675-688.

Blanks, J. C., S. Y. Schmidt, Y. Torigoe, K. V. Porrello, D. R. Hinton and R. H. Blanks (1996). "Retinal pathology in Alzheimer's disease. II. Regional neuron loss and glial changes in GCL." Neurobiology of aging **17**(3): 385-395.

Blanks, J. C., Y. Torigoe, D. R. Hinton and R. H. Blanks (1996). "Retinal pathology in Alzheimer's disease. I. Ganglion cell loss in foveal/parafoveal retina." Neurobiology of aging **17**(3): 377-384.

Braak, H., I. Alafuzoff, T. Arzberger, H. Kretzschmar and K. Del Tredici (2006). "Staging of Alzheimer disease-associated neurofibrillary pathology using paraffin sections and immunocytochemistry." Acta neuropathologica **112**(4): 389-404.

Braak, H. and E. Braak (1991). "Neuropathological stageing of Alzheimer-related changes." Acta neuropathologica **82**(4): 239-259.

Bridenbaugh, S., A. U. Monsch and R. W. Kressig (2012). "How does gait change as cognitive decline progresses in the elderly?" Alzheimer's & Dementia: The Journal of the Alzheimer's Association **8**(4): P131-P132.

Broadbent, N. J., L. R. Squire and R. E. Clark (2004). "Spatial memory, recognition memory, and the hippocampus." Proceedings of the National Academy of Sciences of the United States of America **101**(40): 14515-14520.

Bryan, K. J., H.-g. Lee, G. Perry, M. A. Smith and G. Casadesus (2009). "Transgenic mouse models of Alzheimer's disease: behavioral testing and considerations."

Buccarello, L., A. Sclip, M. Sacchi, A. M. Castaldo, I. Bertani, A. ReCecconi, S. Maestroni, G. Zerbini, P. Nucci and T. Borsello (2017). "The c-jun N-terminal kinase plays a key role in ocular degenerative changes in a mouse model of Alzheimer disease suggesting a correlation between ocular and brain pathologies." Oncotarget **8**(47): 83038.

Bussey, T. and L. Saksida (2007). "Memory, perception, and the ventral visual-perirhinal-hippocampal stream: thinking outside of the boxes." Hippocampus **17**(9): 898-908.

Calkins, D. J. (2012). "Critical pathogenic events underlying progression of neurodegeneration in glaucoma." Progress in retinal and eye research **31**(6): 702-719.

Carvalho, C., S. Cardoso, S. C. Correia, R. X. Santos, M. S. Santos, I. Baldeiras, C. R. Oliveira and P. I. Moreira (2012). "Metabolic alterations induced by sucrose intake and Alzheimer's disease promote similar brain mitochondrial abnormalities." Diabetes **61**(5): 1234-1242.

Carvalho, C., N. Machado, P. C. Mota, S. C. Correia, S. Cardoso, R. X. Santos, M. S. Santos, C. R. Oliveira and P. I. Moreira (2013). "Type 2 diabetic and Alzheimer's disease mice present similar behavioral, cognitive, and vascular anomalies." Journal of Alzheimer's Disease **35**(3): 623-635.

Chang, L. Y., J. Lowe, A. Ardiles, J. Lim, A. C. Grey, K. Robertson, H. Danesh-Meyer, A. G. Palacios and M. L. Acosta (2014). "Alzheimer's disease in the human eye. Clinical tests that identify ocular and visual information processing deficit as biomarkers." Alzheimer's & Dementia **10**(2): 251-261.

Chauhan, B. C., K. T. Stevens, J. M. Levesque, A. C. Nuschke, G. P. Sharpe, N. O'Leary, M. L. Archibald and X. Wang (2012). "Longitudinal in vivo imaging of retinal ganglion cells and retinal thickness changes following optic nerve injury in mice." PloS one **7**(6): e40352.

Cheung, C. Y.-l., Y. T. Ong, M. K. Ikram, S. Y. Ong, X. Li, S. Hilal, J.-A. S. Catindig, N. Venketasubramanian, P. Yap and D. Seow (2014). "Microvascular network alterations in the retina of patients with Alzheimer's disease." Alzheimer's & Dementia **10**(2): 135-142.

Chiasseu, M., L. Alarcon-Martinez, N. Belforte, H. Quintero, F. Dotigny, L. Destroismaisons, C. V. Velde, F. Panayi, C. Louis and A. Di Polo (2017). "Tau accumulation in the retina promotes early neuronal dysfunction and precedes brain pathology in a mouse model of Alzheimer's disease." Molecular neurodegeneration **12**(1): 58.

Chiu, K., T.-F. Chan, A. Wu, I. Y.-P. Leung, K.-F. So and R. C.-C. Chang (2012). "Neurodegeneration of the retina in mouse models of Alzheimer's disease: what can we learn from the retina?" Age **34**(3): 633-649.

Clarka, R. E. and L. R. Squirea (2013). "Similarity in form and function of the hippocampus in rodents, monkeys, and humans." Sciences **10**: 12.

Clinton, L. K., L. M. Billings, K. N. Green, A. Caccamo, J. Ngo, S. Oddo, J. L. McGaugh and F. M. LaFerla (2007). "Age-dependent sexual dimorphism in cognition and stress response in the 3xTg-AD mice." Neurobiology of disease **28**(1): 76-82.

Cohen, S. J. and R. W. Stackman Jr (2015). "Assessing rodent hippocampal involvement in the novel object recognition task. A review." Behavioural brain research **285**: 105-117.

Criscuolo, C., E. Cerri, C. Fabiani, S. Capsoni, A. Cattaneo and L. Domenici (2018). "The retina as a window to early dysfunctions of Alzheimer's disease following studies with a 5xFAD mouse model." Neurobiology of aging **67**: 181-188.

Cronin-Golomb, A., J. F. Rizzo, S. Corkin and J. H. Growdon (1991). "Visual function in Alzheimer's disease and normal aging." Annals of the New York Academy of Sciences **640**(1): 28-35.

Cunha, J. P., R. Proença, A. Dias-Santos, R. Almeida, H. Águas, M. Alves, A. L. Papoila, C. Louro and A. Castanheira-Dinis (2017). "OCT in Alzheimer's disease: thinning of the RNFL and superior hemiretina." Graefe's Archive for Clinical and Experimental Ophthalmology **255**(9): 1827-1835.

Danesh-Meyer, H., H. Birch, J.-F. Ku, S. Carroll and G. Gamble (2006). "Reduction of optic nerve fibers in patients with Alzheimer disease identified by laser imaging." Neurology **67**(10): 1852-1854.

Davis, K. E., A. Easton, M. J. Eacott and J. Gigg (2013). "Episodic-like memory for what-where-which occasion is selectively impaired in the 3xTgAD mouse model of Alzheimer's disease." Journal of Alzheimer's Disease **33**(3): 681-698.

de Haan, E. H. and A. Cowey (2011). "On the usefulness of 'what'and 'where'pathways in vision." Trends in cognitive sciences **15**(10): 460-466.

Dhande, O. S. and A. D. Huberman (2014). "Retinal ganglion cell maps in the brain: implications for visual processing." Current opinion in neurobiology **24**: 133-142.

Drexler, W. and J. G. Fujimoto (2008). Optical coherence tomography: technology and applications, Springer Science & Business Media.

Drexler, W. and J. G. Fujimoto (2008). "State-of-the-art retinal optical coherence tomography." Progress in retinal and eye research **27**(1): 45-88.

Dutescu, R. M., Q.-X. Li, J. Crowston, C. L. Masters, P. N. Baird and J. G. Culvenor (2009). "Amyloid precursor protein processing and retinal pathology in mouse models of Alzheimer's disease." Graefe's Archive for Clinical and Experimental Ophthalmology **247**(9): 1213-1221.

Dysli, C., V. Enzmann, R. Sznitman and M. S. Zinkernagel (2015). "Quantitative analysis of mouse retinal layers using automated segmentation of spectral domain optical coherence tomography images." Translational vision science & technology **4**(4): 9-9.

Ebneter, A., C. Agca, C. Dysli and M. S. Zinkernagel (2015). "Investigation of retinal morphology alterations using spectral domain optical coherence tomography in a mouse model of retinal branch and central retinal vein occlusion." PloS one **10**(3): e0119046.

Edison, P., H. A. Archer, A. Gerhard, R. Hinz, N. Pavese, F. E. Turkheimer, A. Hammers, Y. F. Tai, N. Fox and A. Kennedy (2008). "Microglia, amyloid, and cognition in Alzheimer's disease: An [11C](R) PK11195-PET and [11C] PIB-PET study." Neurobiology of disease **32**(3): 412-419.

Edwards, M. M., J. J. Rodríguez, R. Gutierrez-Lanza, J. Yates, A. Verkhratsky and G. A. Lutty (2014). "Retinal macroglia changes in a triple transgenic mouse model of Alzheimer's disease." Experimental eye research **127**: 252-260.

Eichenbaum, H., A. P. Yonelinas and C. Ranganath (2007). "The medial temporal lobe and recognition memory." Annu. Rev. Neurosci. **30**: 123-152.

Elder, G. A., M. A. Gama Sosa, R. De Gasperi, D. L. Dickstein and P. R. Hof (2010). "Presenilin transgenic mice as models of Alzheimer's disease." Brain Structure and Function **214**(2): 127-143.

Ferguson, L. R., J. M. Dominguez II, S. Balaiya, S. Grover and K. V. Chalam (2013). "Retinal thickness normative data in wild-type mice using customized miniature SD-OCT." PloS one **8**(6): e67265.

Filali, M., R. Lalonde, P. Theriault, C. Julien, F. Calon and E. Planel (2012). "Cognitive and non-cognitive behaviors in the triple transgenic mouse model of Alzheimer's disease expressing mutated APP, PS1, and Mapt (3xTg-AD)." Behavioural brain research **234**(2): 334-342.

Fischer, M. D., G. Huber, S. C. Beck, N. Tanimoto, R. Muehlfriedel, E. Fahl, C. Grimm, A. Wenzel, C. E. Remé and S. A. van de Pavert (2009). "Noninvasive, in vivo assessment of mouse retinal structure using optical coherence tomography." PloS one **4**(10): e7507.

Flurkey, K., J. Currer and D. Harrison (2007). The mouse in aging research, pp. 637–672 in The Mouse in Biomedical Research, edited by JG Fox. American College Laboratory Animal Medicine, Elsevier), Burlington, MA.

Folstein, M. F., S. E. Folstein and P. R. McHugh (1975). ""Mini-mental state": a practical method for grading the cognitive state of patients for the clinician." Journal of psychiatric research **12**(3): 189-198.

Frohman, E. M., J. G. Fujimoto, T. C. Frohman, P. A. Calabresi, G. Cutter and L. J. Balcer (2008). "Optical coherence tomography: a window into the mechanisms of multiple sclerosis." Nature Reviews Neurology **4**(12): 664.

Frost, S., R. N. Martins and Y. Kanagasingam (2010). "Ocular biomarkers for early detection of Alzheimer's disease." Journal of Alzheimer's Disease **22**(1): 1-16.

Gao, L., X. Chen, Y. Tang, J. Zhao, Q. Li, X. Fan, H. Xu and Z. Q. Yin (2015). "Neuroprotective effect of memantine on the retinal ganglion cells of APPswe/PS1ΔE9 mice and its immunomodulatory mechanisms." Experimental eye research **135**: 47-58.

Garcia-Martin, E., J. M. Larrosa, V. Polo, M. Satue, M. L. Marques, R. Alarcia, M. Seral, I. Fuertes, S. Otin and L. E. Pablo (2014). "Distribution of retinal layer atrophy in patients with Parkinson disease and association with disease severity and duration." American journal of ophthalmology **157**(2): 470-478. e472.

Gasparini, L., R. A. Crowther, K. R. Martin, N. Berg, M. Coleman, M. Goedert and M. G. Spillantini (2011). "Tau inclusions in retinal ganglion cells of human P301S tau transgenic mice: effects on axonal viability." Neurobiology of aging **32**(3): 419-433.

Gerashchenko, B. (2002). "Philosophy of aging." Medical hypotheses **58**(2): 157-158.

Gillette-Guyonnet, S., F. Nourhashémi, S. Andrieu, I. de Glisezinski, P. J. Ousset, D. Rivière, J.-L. Albarède and B. Vellas (2000). "Weight loss in Alzheimer disease." The American journal of clinical nutrition **71**(2): 637S-642S.

Gills, J. P. and J. A. Wadsworth (1967). "Retrograde transsynaptic degeneration of the inner nuclear layer of the retina." Investigative Ophthalmology & Visual Science **6**(4): 437-448.

Gimenez-Llort, L., G. Blazquez, T. Canete, B. Johansson, S. Oddo, A. Tobena, F. LaFerla and A. Fernandez-Teruel (2007). "Modeling behavioral and neuronal symptoms of Alzheimer's disease in mice: a role for intraneuronal amyloid." Neuroscience & Biobehavioral Reviews **31**(1): 125-147.

Gold, C. A. and A. E. Budson (2008). "Memory loss in Alzheimer's disease: implications for development of therapeutics." Expert review of neurotherapeutics **8**(12): 1879-1891.

Gollisch, T. and M. Meister (2010). "Eye smarter than scientists believed: neural computations in circuits of the retina." Neuron **65**(2): 150-164.

Gordon, B. A., T. M. Blazey, Y. Su, A. Hari-Raj, A. Dincer, S. Flores, J. Christensen, E. McDade, G. Wang and C. Xiong (2018). "Spatial patterns of neuroimaging biomarker change in individuals from families with autosomal dominant Alzheimer's disease: a longitudinal study." The Lancet Neurology **17**(3): 241-250.

Götz, J. and L. M. Ittner (2008). "Animal models of Alzheimer's disease and frontotemporal dementia." Nature Reviews Neuroscience **9**(7): 532-544.

Grayson, B., M. Leger, C. Piercy, L. Adamson, M. Harte and J. C. Neill (2015). "Assessment of disease-related cognitive impairments using the novel object recognition (NOR) task in rodents." Behavioural brain research **285**: 176-193.

Gupta, V. K., N. Chitranshi, V. B. Gupta, M. Golzan, Y. Dheer, R. Vander Wall, D. Georgevsky, A. E. King, J. C. Vickers and R. Chung (2016). "Amyloid β accumulation and inner retinal degenerative changes in Alzheimer's disease transgenic mouse." Neuroscience letters **623**: 52-56.

Guyonnet, S., F. Nourhashemi, S. Andrieu, P. Ousset, L. Gray, L. Fitten, B. Vellas and J. Albarede (1998). "A prospective study of chances in the nutritional status of Alzheimer's patients." Archives of Gerontology and Geriatrics **26**: 255-262.

Guzmán-Ramos, K., P. Moreno-Castilla, M. Castro-Cruz, J. L. McGaugh, H. Martínez-Coria, F. M. LaFerla and F. Bermúdez-Rattoni (2012). "Restoration of dopamine release deficits during object recognition memory acquisition attenuates cognitive impairment in a triple transgenic mice model of Alzheimer's disease." Learning & memory **19**(10): 453-460.

Gyure, K. A., R. Durham, W. F. Stewart, J. E. Smialek and J. C. Troncoso (2001). "Intraneuronal Aβ-amyloid precedes development of amyloid plaques in Down syndrome." Archives of pathology & laboratory medicine **125**(4): 489-492.

Halagappa, V. K. M., Z. Guo, M. Pearson, Y. Matsuoka, R. G. Cutler, F. M. LaFerla and M. P. Mattson (2007). "Intermittent fasting and caloric restriction ameliorate age-related behavioral deficits in the triple-transgenic mouse model of Alzheimer's disease." Neurobiology of disease **26**(1): 212-220.

Hall, A. M. and E. D. Roberson (2012). "Mouse models of Alzheimer's disease." Brain research bulletin **88**(1): 3-12.

Hardy, J. and D. J. Selkoe (2002). "The amyloid hypothesis of Alzheimer's disease: progress and problems on the road to therapeutics." science **297**(5580): 353-356.

Harper, A. (2010). "Mouse models of neurological disorders—A comparison of heritable and acquired traits." Biochimica et Biophysica Acta (BBA)-Molecular Basis of Disease **1802**(10): 785-795.

Hart, N. J., Y. Koronyo, K. L. Black and M. Koronyo-Hamaoui (2016). "Ocular indicators of Alzheimer's: exploring disease in the retina." Acta neuropathologica **132**(6): 767-787.

Haxby, J., V. Clark and M. Courtney (2012). "Distributed Hierarchical Neural Systems for Visual Memory in Human Cortex." Connections, Cognition and Alzheimer's Disease: 167.

Headley, D. B. and D. Paré (2017). "Common oscillatory mechanisms across multiple memory systems." npj Science of Learning **2**(1): 1.

Henneman, W., J. Sluimer, J. Barnes, W. Van Der Flier, I. Sluimer, N. Fox, P. Scheltens, H. Vrenken and F. Barkhof (2009). "Hippocampal atrophy rates in Alzheimer disease: added value over whole brain volume measures." Neurology **72**(11): 999-1007.

Herweg, N. A., T. Apitz, G. Leicht, C. Mulert, L. Fuentemilla and N. Bunzeck (2016). "Theta-alpha oscillations bind the hippocampus, prefrontal cortex, and striatum during recollection: evidence from simultaneous EEG–fMRI." Journal of Neuroscience **36**(12): 3579-3587.

Hinton, D. R., A. A. Sadun, J. C. Blanks and C. A. Miller (1986). "Optic-nerve degeneration in Alzheimer's disease." New England Journal of Medicine **315**(8): 485-487.

Ho, W. L., Y. Leung, S. S. Y. Cheng, C. K. M. Lok, Y.-S. Ho, L. Baum, X. Yang, K. Chiu and R. C.-C. Chang (2015). "Investigating degeneration of the retina in young and aged tau P301L mice." Life sciences **124**: 16-23.

Hsu, P. J., H. Shou, T. Benzinger, D. Marcus, T. Durbin, J. C. Morris and Y. I. Sheline (2015). "Amyloid burden in cognitively normal elderly is associated with preferential hippocampal subfield volume loss." Journal of Alzheimer's disease: JAD **45**(1): 27.

Huang, Y. and L. Mucke (2012). "Alzheimer mechanisms and therapeutic strategies." Cell **148**(6): 1204-1222.

Huber, G., S. C. Beck, C. Grimm, A. Sahaboglu-Tekgoz, F. Paquet-Durand, A. Wenzel, P. Humphries, T. M. Redmond, M. W. Seeliger and M. D. Fischer (2009). "Spectral domain optical coherence tomography in mouse models of retinal degeneration." Investigative ophthalmology & visual science **50**(12): 5888-5895.

Huberman, A. D. and C. M. Niell (2011). "What can mice tell us about how vision works?" Trends in neurosciences **34**(9): 464-473.

Hull, B. and D. Thompson (1989). "A review of the clinical applications of the pattern electroretinogram." Ophthalmic and Physiological Optics **9**(2): 143-152.

Ioshimoto, G. L., B. V. Nagy, J. J. Kremers and D. F. Ventura (2012). "Erg Changes In A Triple Transgenic Mouse Model For Alzheimers Disease." Investigative Ophthalmology & Visual Science **53**(14): 5376-5376.

Iseri, P. K., Ö. Altinas, T. Tokay and N. Yüksel (2006). "Relationship between cognitive impairment and retinal morphological and visual functional abnormalities in Alzheimer disease." Journal of neuro-ophthalmology **26**(1): 18-24.

Jack, C. R., D. S. Knopman, W. J. Jagust, R. C. Petersen, M. W. Weiner, P. S. Aisen, L. M. Shaw, P. Vemuri, H. J. Wiste and S. D. Weigand (2013). "Tracking pathophysiological processes in Alzheimer's disease: an updated hypothetical model of dynamic biomarkers." The Lancet Neurology **12**(2): 207-216.

Jahn, H. (2013). "Memory loss in Alzheimer's disease." Dialogues in clinical neuroscience **15**(4): 445.

Janus, C. and D. Westaway (2001). "Transgenic mouse models of Alzheimer's disease." Physiology & behavior **73**(5): 873-886.

Javaid, F. Z., J. Brenton, L. Guo and M. F. Cordeiro (2016). "Visual and ocular manifestations of Alzheimer's disease and their use as biomarkers for diagnosis and progression." Frontiers in neurology **7**.

Jentsch, S., D. Schweitzer, K. U. Schmidtke, S. Peters, J. Dawczynski, K. J. Bär and M. Hammer (2015). "Retinal fluorescence lifetime imaging ophthalmoscopy measures depend on the severity of Alzheimer's disease." Acta ophthalmologica **93**(4): e241-e247.

Joly, S., S. Lamoureux and V. Pernet (2017). "Nonamyloidogenic processing of amyloid beta precursor protein is associated with retinal function improvement in aging male APP swe/PS1ΔE9 mice." Neurobiology of Aging **53**: 181-191.

Justino, L., M.-J. Kergoat, H. Bergman, H. Chertkow, A. Robillard and H. Kergoat (2001). "Neuroretinal function is normal in early dementia of the Alzheimer type." Neurobiology of Aging **22**(4): 691-695.

Kanamori, A., M.-M. Catrinescu, J. M. Belisle, S. Costantino and L. A. Levin (2012). "Retrograde and Wallerian axonal degeneration occur synchronously after retinal ganglion cell axotomy." The American journal of pathology **181**(1): 62-73.

Karran, E., M. Mercken and B. De Strooper (2011). "The amyloid cascade hypothesis for Alzheimer's disease: an appraisal for the development of therapeutics." Nature reviews Drug discovery **10**(9): 698.

Katz, B., S. Rimmer, V. Iragui and R. Katzman (1989). "Abnormal pattern electroretinogram in Alzheimer's disease: evidence for retinal ganglion cell degeneration?" Annals of neurology **26**(2): 221-225.

Kaur, G., A. Sharma, W. Xu, S. Gerum, M. J. Alldred, S. Subbanna, B. S. Basavarajappa, M. Pawlik, M. Ohno and S. D. Ginsberg (2014). "Glutamatergic transmission aberration: a major cause of behavioral deficits in a murine model of Down's syndrome." Journal of Neuroscience **34**(15): 5099-5106.

Keller, J., B. F. Sánchez-Dalmau and P. Villoslada (2014). "Lesions in the posterior visual pathway promote trans-synaptic degeneration of retinal ganglion cells." PLoS One **9**(5): e97444.

Kerbage, C., C. H. Sadowsky, D. Jennings, G. D. Cagle and P. D. Hartung (2013). "Alzheimer's disease diagnosis by detecting exogenous fluorescent signal of ligand bound to beta amyloid in the lens of human eye: an exploratory study." Frontiers in neurology **4**.

Kergoat, H., M. J. Kergoat, L. Justino, H. Chertkow, A. Robillard and H. Bergman (2001). "An evaluation of the retinal nerve fiber layer thickness by scanning laser polarimetry in individuals with dementia of the Alzheimer type." Acta Ophthalmologica **79**(2): 187-191.

Kesler, A., V. Vakhapova, A. D. Korczyn, E. Naftaliev and M. Neudorfer (2011). "Retinal thickness in patients with mild cognitive impairment and Alzheimer's disease." Clinical neurology and neurosurgery **113**(7): 523-526.

Kirbas, S., K. Turkyilmaz, O. Anlar, A. Tufekci and M. Durmus (2013). "Retinal nerve fiber layer thickness in patients with Alzheimer disease." Journal of Neuro-Ophthalmology **33**(1): 58-61.

Kolb, H. (2009). "Neurotransmitters in the Retina." Retrieved 7-4-2018, from https://www.ncbi.nlm.nih.gov/books/NBK11546/.

Kong, V., G. A. Devenyi, D. Gallino, G. Ayranci, J. Germann, C. Rollins and M. M. Chakravarty (2018). "Early-in-life neuroanatomical and behavioural trajectories in a triple transgenic model of Alzheimer's disease." Brain Structure and Function: 1-18.

Koronyo-Hamaoui, M., Y. Koronyo, A. V. Ljubimov, C. A. Miller, M. K. Ko, K. L. Black, M. Schwartz and D. L. Farkas (2011). "Identification of amyloid plaques in retinas from Alzheimer's patients and noninvasive in vivo optical imaging of retinal plaques in a mouse model." Neuroimage **54**: S204-S217.

Koronyo, Y., B. C. Salumbides, K. L. Black and M. Koronyo-Hamaoui (2012). "Alzheimer's disease in the retina: imaging retinal aβ plaques for early diagnosis and therapy assessment." Neurodegenerative Diseases **10**(1-4): 285-293.

Krantic, S. and A. Torriglia (2014). "Retina: source of the earliest biomarkers for Alzheimer's disease?" J Alzheimers Dis **40**(2): 237-243.

Krasodomska, K., W. Lubiński, A. Potemkowski and K. Honczarenko (2010). "Pattern electroretinogram (PERG) and pattern visual evoked potential (PVEP) in the early stages of Alzheimer's disease." Documenta ophthalmologica **121**(2): 111-121.

Lad, E. M., D. Mukherjee, S. S. Stinnett, S. W. Cousins, G. G. Potter, J. R. Burke, S. Farsiu and H. E. Whitson (2018). "Evaluation of inner retinal layers as biomarkers in mild cognitive impairment to moderate Alzheimer's disease." PloS one **13**(2): e0192646.

Laguna, A., M.-J. Barallobre, M.-Á. Marchena, C. Mateus, E. Ramírez, C. Martínez-Cue, J. M. Delabar, M. Castelo-Branco, P. de la Villa and M. L. Arbonés (2013). "Triplication of DYRK1A causes retinal structural and functional alterations in Down syndrome." Human molecular genetics **22**(14): 2775-2784.

Leinonen, H., A. Lipponen, K. Gurevicius and H. Tanila (2016). "Normal Amplitude of Electroretinography and Visual Evoked Potential Responses in AβPP/PS1 Mice." Journal of Alzheimer's Disease **51**(1): 21-26.

Lettvin, J. Y., H. R. Maturana, W. S. McCulloch and W. H. Pitts (1959). "What the frog's eye tells the frog's brain." Proceedings of the IRE **47**(11): 1940-1951.

Levkovitch-Verbin, H., H. A. Quigley, K. R. Martin, D. J. Zack, M. E. Pease and D. F. Valenta (2003). "A model to study differences between primary and secondary degeneration of retinal ganglion cells in rats by partial optic nerve transection." Investigative ophthalmology & visual science **44**(8): 3388-3393.

Levkovitch–Verbin, H., H. A. Quigley, L. A. Kerrigan–Baumrind, S. A. D'Anna, D. Kerrigan and M. E. Pease (2001). "Optic nerve transection in monkeys may result in secondary degeneration of retinal ganglion cells." Investigative ophthalmology & visual science **42**(5): 975-982.

Li, H.-Y., Y.-W. Ruan, C.-R. Ren, Q. Cui and K.-F. So (2014). "Mechanisms of secondary degeneration after partial optic nerve transection." Neural regeneration research **9**(6): 565.

Li, Y., Y. Wang, G. Wu, F. Shi, L. Zhou, W. Lin, D. Shen and A. s. D. N. Initiative (2012). "Discriminant analysis of longitudinal cortical thickness changes in Alzheimer's disease using dynamic and network features." Neurobiology of aging **33**(2): 427. e415-427. e430.

Lim, J. K., Z. He, A. J. Vingrys, H. R. Chinnery, Q.-X. Li, B. V. Bui and C. T. O. Nguyen (2016). "Age-related changes in retinal structure and function in a mouse model of Alzheimer's disease." Investigative Ophthalmology & Visual Science **57**(12): 613-613.

Lipsø, K. W. (2016). A novel MR contrast agent for angiography and perfusion: Hyperpolarized water, Technical University of Denmark, Department of Electrical Engineering.

Liu, B., S. Rasool, Z. Yang, C. G. Glabe, S. S. Schreiber, J. Ge and Z. Tan (2009). "Amyloid-peptide vaccinations reduce β-amyloid plaques but exacerbate vascular deposition and inflammation in the retina of Alzheimer's transgenic mice." The American journal of pathology **175**(5): 2099-2110.

Liu, C., L. Cao, S. Yang, L. Xu, P. Liu, F. Wang and D. Xu (2015). "Subretinal injection of amyloid-β peptide accelerates RPE cell senescence and retinal degeneration." International journal of molecular medicine **35**(1): 169-176.

Liu, D., L. Zhang, Z. Li, X. Zhang, Y. Wu, H. Yang, B. Min, X. Zhang, D. Ma and Y. Lu (2015). "Thinner changes of the retinal never fiber layer in patients with mild cognitive impairment and Alzheimer's disease." BMC neurology(1): 14.

London, A., I. Benhar and M. Schwartz (2013). "The retina as a window to the brain—from eye research to CNS disorders." Nature Reviews Neurology **9**(1): 44-53.

Louzada, P. R., A. C. P. Lima, D. L. Mendonça-Silva, F. NoëL, F. G. De Mello and S. T. Ferreira (2004). "Taurine prevents the neurotoxicity of β-amyloid and glutamate receptor agonists: activation of GABA receptors and possible implications for Alzheimer's disease and other neurological disorders." The FASEB Journal **18**(3): 511-518.

Lu, Y., Z. Li, X. Zhang, B. Ming, J. Jia, R. Wang and D. Ma (2010). "Retinal nerve fiber layer structure abnormalities in early Alzheimer's disease: evidence in optical coherence tomography." Neuroscience letters **480**(1): 69-72.

Madeira, M. H., R. Boia, P. F. Santos, A. F. Ambrósio and A. R. Santiago (2015). "Contribution of microglia-mediated neuroinflammation to retinal degenerative diseases." Mediators of inflammation **2015**.

Maeda, J., B. Ji, T. Irie, T. Tomiyama, M. Maruyama, T. Okauchi, M. Staufenbiel, N. Iwata, M. Ono and T. C. Saido (2007). "Longitudinal, quantitative assessment of amyloid, neuroinflammation, and anti-amyloid treatment in a living mouse model of Alzheimer's disease enabled by positron emission tomography." Journal of Neuroscience **27**(41): 10957-10968.

Maier, F. C., H. F. Wehrl, A. M. Schmid, J. G. Mannheim, S. Wiehr, C. Lerdkrai, C. Calaminus, A. Stahlschmidt, L. Ye and M. Burnet (2014). "Longitudinal PET-MRI reveals β-amyloid deposition and rCBF dynamics and connects vascular amyloidosis to quantitative loss of perfusion." Nature medicine **20**(12): 1485.

Manook, A., B. H. Yousefi, A. Willuweit, S. Platzer, S. Reder, A. Voss, M. Huisman, M. Settles, F. Neff and J. Velden (2012). "Small-animal PET imaging of amyloid-beta plaques with [11C] PiB and its multi-modal validation in an APP/PS1 mouse model of Alzheimer's disease." PloS one **7**(3): e31310.

Marieb, E. N. and K. Hoehn (2007). Human anatomy & physiology, Pearson Education.

Martinez-Coria, H., K. N. Green, L. M. Billings, M. Kitazawa, M. Albrecht, G. Rammes, C. G. Parsons, S. Gupta, P. Banerjee and F. M. LaFerla (2010). "Memantine improves cognition and reduces Alzheimer's-like neuropathology in transgenic mice." The American journal of pathology **176**(2): 870-880.

Martins, P., A. Blanco, P. Crespo, M. F. F. Marques, R. F. Marques, P. M. Gordo, M. Kajetanowicz, G. Korcyl, L. Lopes and J. Michel (2014). "Towards very high resolution RPC-PET for small animals." Journal of Instrumentation **9**(10): C10012.

Marziani, E., S. Pomati, P. Ramolfo, M. Cigada, A. Giani, C. Mariani and G. Staurenghi (2013). "Evaluation of retinal nerve fiber layer and ganglion cell layer thickness in Alzheimer's disease using spectral-domain optical coherence tomography." Investigative ophthalmology & visual science **54**(9): 5953-5958.

Masland, R. H. (1996). "Processing and encoding of visual information in the retina." Current opinion in neurobiology **6**(4): 467-474.

Masland, R. H. (2001). "The fundamental plan of the retina." Nature neuroscience **4**(9): 877-886.

Masland, R. H. (2012). "The neuronal organization of the retina." Neuron **76**(2): 266-280.

Masland, R. H. and P. R. Martin (2007). "The unsolved mystery of vision." Current Biology **17**(15): R577-R582.

Mazzaro, N., E. Barini, M. G. Spillantini, M. Goedert, P. Medini and L. Gasparini (2016). "Tau-driven neuronal and neurotrophic dysfunction in a mouse model of early tauopathy." Journal of Neuroscience **36**(7): 2086-2100.

McKhann, G., D. Drachman, M. Folstein, R. Katzman, D. Price and E. M. Stadlan (1984). "Clinical diagnosis of Alzheimer's disease Report of the NINCDS-ADRDA Work Group* under the auspices of Department of Health and Human Services Task Force on Alzheimer's Disease." Neurology **34**(7): 939-939.

Méndez-Gómez, J. L., M.-B. Rougier, L. Tellouck, J.-F. Korobelnik, C. Schweitzer, M.-N. Delyfer, H. Amieva, J.-F. Dartigues, C. Delcourt and C. Helmer (2017). "Peripapillary retinal nerve Fiber layer Thickness and the evolution of cognitive Performance in an elderly Population." Frontiers in neurology **8**: 93.

Millar, J. C., H. C. Webber, T. Phan, S. Neubauer and A. F. Clark (2016). "PRIMARY OPEN ANGLE GLAUCOMA AND ALZHEIMER'S DISEASE: IS THERE AN ASSOCIATION IN 5XFAD MICE?" Investigative Ophthalmology & Visual Science **57**(12): 2543-2543.

Miura, G., M. H. Wang, K. M. Ivers and L. J. Frishman (2009). "Retinal pathway origins of the pattern ERG of the mouse." Experimental eye research **89**(1): 49-62.

Morici, J. F., P. Bekinschtein and N. V. Weisstaub (2015). "Medial prefrontal cortex role in recognition memory in rodents." Behavioural brain research **292**: 241-251.

Mutlu, U., J. M. Colijn, S. Licher, F. J. Wolters, P. W. Bonnemaijer, C. C. Klaver, P. J. Koudstaal, M. A. Ikram and M. K. Ikram (2017). "RETINAL NEURODEGENERATION ON OPTICAL COHERENCE TOMOGRAPHY AND RISK OF DEMENTIA AND STROKE." Alzheimer's & Dementia: The Journal of the Alzheimer's Association **13**(7): P1014-P1015.

Nadel, L. and O. Hardt (2011). "Update on memory systems and processes." Neuropsychopharmacology **36**(1): 251.

Nesher, R. and G. L. Trick (1991). "The pattern electroretinogram in retinal and optic nerve disease." Documenta ophthalmologica **77**(3): 225-235.

Neves, A. C., S. Chiquita, R. Carecho, E. Campos, P. Moreira, F. Baptista and F. Ambrósio (2017). "Alzheimer's disease: can the retina be a window to the brain?" Acta Ophthalmologica **95**(S259).

Ning, A., J. Cui, E. To, K. H. Ashe and J. Matsubara (2008). "Amyloid-β deposits lead to retinal degeneration in a mouse model of Alzheimer disease." Investigative ophthalmology & visual science **49**(11): 5136.

Oddo, S., L. Billings, J. P. Kesslak, D. H. Cribbs and F. M. LaFerla (2004). "Aβ immunotherapy leads to clearance of early, but not late, hyperphosphorylated tau aggregates via the proteasome." Neuron **43**(3): 321-332.

Oddo, S., A. Caccamo, M. Kitazawa, B. P. Tseng and F. M. LaFerla (2003). "Amyloid deposition precedes tangle formation in a triple transgenic model of Alzheimer's disease." Neurobiology of aging **24**(8): 1063-1070.

Oddo, S., A. Caccamo, J. D. Shepherd, M. P. Murphy, T. E. Golde, R. Kayed, R. Metherate, M. P. Mattson, Y. Akbari and F. M. LaFerla (2003). "Triple-transgenic model of Alzheimer's disease with plaques and tangles: intracellular Aβ and synaptic dysfunction." Neuron **39**(3): 409-421.

Okello, A., P. Edison, H. Archer, F. Turkheimer, J. Kennedy, R. Bullock, Z. Walker, A. Kennedy, N. Fox and M. Rossor (2009). "Microglial activation and amyloid deposition in mild cognitive impairment A PET study." Neurology **72**(1): 56-62.

Oliveira, F. P., A. P. Moreira, A. de Mendonça, A. Verdelho, C. Xavier, D. Barroca, J. Rio, E. Cardoso, Â. Cruz and A. Abrunhosa (2018). "Can 11C-PiB-PET Relative Delivery R 1 or 11C-PiB-PET Perfusion Replace 18F-FDG-PET in the Assessment of Brain Neurodegeneration?" Journal of Alzheimer's Disease **65**(1): 89-97.

Onishi, T., H. Iwashita, Y. Uno, J. Kunitomo, M. Saitoh, E. Kimura, H. Fujita, N. Uchiyama, M. Kori and M. Takizawa (2011). "A novel glycogen synthase kinase-3 inhibitor 2-methyl-5-(3-{4-[(S)-methylsulfinyl] phenyl}-1-benzofuran-5-yl)-1, 3, 4-oxadiazole decreases tau phosphorylation and ameliorates cognitive deficits in a transgenic model of Alzheimer's disease." Journal of neurochemistry **119**(6): 1330-1340.

Onos, K. D., S. J. S. Rizzo, G. R. Howell and M. Sasner (2016). "Toward more predictive genetic mouse models of Alzheimer's disease." Brain research bulletin **122**: 1-11.

OPTIMALZ, E. S. G. (2015). "Optical imaging of ocular pathology in Alzheimer's disease." Retrieved 07-03-2018, from https://cordis.europa.eu/project/rcn/197083_en.html.

Organization, W. H. (2012). Dementia: a public health priority, World Health Organization.

Orta-Salazar, E., A. Feria-Velasco, G. Medina-Aguirre and S. Díaz-Cintra (2013). "Morphological analysis of the hippocampal region associated with an innate behaviour task in the transgenic mouse model (3xTg-AD) for Alzheimer disease." Neurología (English Edition) **28**(8): 497-502.

Paquet, C., M. Boissonnot, F. Roger, P. Dighiero, R. Gil and J. Hugon (2007). "Abnormal retinal thickness in patients with mild cognitive impairment and Alzheimer's disease." Neuroscience Letters **420**(2): 97-99.

Parisi, V. (2003). Correlation between morphological and functional retinal impairment in patients affected by ocular hypertension, glaucoma, demyelinating optic neuritis and Alzheimer's disease. Seminars in ophthalmology, Taylor & Francis.

Parisi, V., R. Restuccia, F. Fattapposta, C. Mina, M. G. Bucci and F. Pierelli (2001). "Morphological and functional retinal impairment in Alzheimer's disease patients." Clinical neurophysiology **112**(10): 1860-1867.

Parnell, M., L. Guo, M. Abdi and M. F. Cordeiro (2012). "Ocular manifestations of Alzheimer's disease in animal models." International Journal of Alzheimer's Disease **2012**.

Paxinos, G. and K. B. Franklin (2004). The mouse brain in stereotaxic coordinates, Gulf professional publishing.

Pennesi, M. E., S. S. Magee, A. K. Garg, D. C. Tu, Y. Wen and A. Maricle (2011). "Characterization Of Retinal Degeneration In rd1 And rd10 Mice Using Spectral Domain Oct." Investigative Ophthalmology & Visual Science **52**(14): 4348-4348.

Pennesi, M. E., K. V. Michaels, S. S. Magee, A. Maricle, S. P. Davin, A. K. Garg, M. J. Gale, D. C. Tu, Y. Wen and L. R. Erker (2012). "Long-term characterization of retinal degeneration in rd1 and rd10 mice using spectral domain optical coherence tomography." Investigative ophthalmology & visual science **53**(8): 4644-4656.

Perez, S. E., S. Lumayag, B. Kovacs, E. J. Mufson and S. Xu (2009). "β-amyloid deposition and functional impairment in the retina of the APPswe/PS1ΔE9 transgenic mouse model of Alzheimer's disease." Investigative ophthalmology & visual science **50**(2): 793-800.

Pernet, V. E., L. Rodriguez, B. Mdzomba, S. Joly, M. Boudreau-Laprise and E. Planel (2018). "Human Tau expression does not induce mouse retina neurodegeneration, suggesting differential toxicity of Tau in brain vs retinal neurons." Frontiers in molecular neuroscience **11**: 293.

Petrella, L. I., J. M. Castelhano, M. Ribeiro, J. V. Sereno, S. I. Gonçalves, M. N. Laço, M. R. Hayden, A. C. Rego and M. Castelo-Branco (2018). "A whole brain longitudinal study in the YAC128 mouse model of Huntington's disease shows distinct trajectories of neurochemical, structural connectivity and volumetric changes." Human molecular genetics **27**(12): 2125-2137.

Pietropaolo, S., J. Feldon and B. K. Yee (2008). "Age-dependent phenotypic characteristics of a triple transgenic mouse model of Alzheimer disease." Behavioral neuroscience **122**(4): 733.

Porciatti, V. (2007). "The mouse pattern electroretinogram." Documenta Ophthalmologica **115**(3): 145-153.

Porciatti, V., M. Saleh and M. Nagaraju (2007). "The pattern electroretinogram as a tool to monitor progressive retinal ganglion cell dysfunction in the DBA/2J mouse model of glaucoma." Investigative ophthalmology & visual science **48**(2): 745-751.

Power, D. A., J. Noel, R. Collins and D. O'Neill (2001). "Circulating leptin levels and weight loss in Alzheimer's disease patients." Dementia and geriatric cognitive disorders **12**(2): 167-170.

Pozueta, J., R. Lefort and M. Shelanski (2013). "Synaptic changes in Alzheimer's disease and its models." Neuroscience **251**: 51-65.

Prager, T. C., F. C. Schweitzer, L. W. Peacock and C. A. Garcia (1993). "The effect of optical defocus on the pattern electroretinogram in normal subjects and patients with Alzheimer's disease." American journal of ophthalmology **116**(3): 363-369.

Preston, A. R. and H. Eichenbaum (2013). "Interplay of hippocampus and prefrontal cortex in memory." Current Biology **23**(17): R764-R773.

Prince, M., A. Wimo, M. Guerchet, G. Ali, Y. Wu and M. Prina (2015). "World Alzheimer Report 2015—The Global Impact of Dementia: An analysis of prevalence, incidence, cost and trends." Alzheimer's Disease International (ADI), London.

Provencher, S. W. (1993). "Estimation of metabolite concentrations from localized in vivo proton NMR spectra." Magnetic resonance in medicine **30**(6): 672-679.

Purves, D., G. J. Augustine, D. Fitzpatrick, L. C. Katz, A.-S. LaMantia, J. O. McNamara and S. M. Williams (2001). Neuroscience. 2nd edition, Sunderland (MA): Sinauer Associates.

Puzzo, D., L. Lee, A. Palmeri, G. Calabrese and O. Arancio (2014). "Behavioral assays with mouse models of Alzheimer's disease: practical considerations and guidelines." Biochemical pharmacology **88**(4): 450-467.

Raftopoulos, R. and A. Trip (2012). "The Application of Optical Coherence Tomography (OCT) in Neurological Disease." ACNR **12**(2): 30-33.

Rajendran, L., M. Honsho, T. R. Zahn, P. Keller, K. D. Geiger, P. Verkade and K. Simons (2006). "Alzheimer's disease β-amyloid peptides are released in association with exosomes." Proceedings of the National Academy of Sciences **103**(30): 11172-11177.

Ramirez, A. I., R. de Hoz, E. Salobrar-Garcia, J. J. Salazar, B. Rojas, D. Ajoy, I. López-Cuenca, P. Rojas, A. Triviño and J. M. Ramírez (2017). "The role of microglia in retinal neurodegeneration: Alzheimer's disease, Parkinson, and glaucoma." Frontiers in aging neuroscience **9**: 214.

Ribeiro, M., J. Castelhano, L. I. Petrella, J. Sereno, T. Rodrigues, C. Neves, L. Letra, F. I. Baptista, R. Seiça and P. Matafome (2018). "High-fat diet induces a neurometabolic state characterized by changes in glutamate and N-acetylaspartate pools associated with early glucose intolerance: An in vivo multimodal MRI study." Journal of Magnetic Resonance Imaging.

Rodrigues, T., P. Matafome, J. Sereno, J. Almeida, J. Castelhano, L. Gamas, C. Neves, S. Gonçalves, C. Carvalho and A. Arslanagic (2017). "Methylglyoxal-induced glycation changes adipose tissue vascular architecture, flow and expansion, leading to insulin resistance." Scientific reports **7**(1): 1698.

Rodriguez, J., J. Witton, M. Olabarria, H. Noristani and A. Verkhratsky (2010). "Increase in the density of resting microglia precedes neuritic plaque formation and microglial activation in a transgenic model of Alzheimer's disease." Cell death & disease **1**(1): e1.

Romberg, C., M. P. Mattson, M. R. Mughal, T. J. Bussey and L. M. Saksida (2011). "Impaired Attention in the 3xTgAD Mouse Model of Alzheimer's Disease: Rescue by Donepezil (Aricept)." The Journal of Neuroscience **31**(9): 3500-3507.

Roska, B. and M. Meister (2014). The retina dissects the visual scene into distinct features. The new visual neurosciences, MIT Press, Cambridge**:** 163-182.

Ruggeri, M., H. Wehbe, S. Jiao, G. Gregori, M. E. Jockovich, A. Hackam, Y. Duan and C. A. Puliafito (2007). "In vivo three-dimensional high-resolution imaging of rodent retina with spectral-domain optical coherence tomography." Investigative ophthalmology & visual science **48**(4): 1808-1814.

Sadun, A. A. and C. J. Bassi (1990). "Optic nerve damage in Alzheimer's disease." Ophthalmology **97**(1): 9-17.

Sadun, A. A., M. Borchert, E. DeVita, D. R. Hinton and C. J. Bassi (1987). "Assessment of visual impairment in patients with Alzheimer's disease." American journal of ophthalmology **104**(2): 113-120.

Santana, I., F. Farinha, S. Freitas, V. Rodrigues and Á. Carvalho (2015). "Epidemiologia da Demência e da Doença de Alzheimer em Portugal: Estimativas da Prevalência e dos Encargos Financeiros com a Medicação." Acta Médica Portuguesa **28**(2): 182-188.

Sartucci, F., D. Borghetti, T. Bocci, L. Murri, P. Orsini, V. Porciatti, N. Origlia and L. Domenici (2010). "Dysfunction of the magnocellular stream in Alzheimer's disease evaluated by pattern electroretinograms and visual evoked potentials." Brain research bulletin **82**(3): 169-176.

Satue, M., J. Obis, M. J. Rodrigo, S. Otin, M. I. Fuertes, E. Vilades, H. Gracia, J. R. Ara, R. Alarcia and V. Polo (2016). "Optical coherence tomography as a biomarker for diagnosis, progression, and prognosis of neurodegenerative diseases." Journal of ophthalmology **2016**.

Sawiak, S. J., N. I. Wood, G. B. Williams, A. J. Morton and T. A. Carpenter (2013). "Voxel-based morphometry with templates and validation in a mouse model of Huntington's disease." Magnetic resonance imaging **31**(9): 1522-1531.

Schön, C., N. A. Hoffmann, S. M. Ochs, S. Burgold, S. Filser, S. Steinbach, M. W. Seeliger, T. Arzberger, M. Goedert and H. A. Kretzschmar (2012). "Long-term in vivo imaging of fibrillar tau in the retina of P301S transgenic mice." PloS one **7**(12).

Schuff, N., N. Woerner, L. Boreta, T. Kornfield, L. Shaw, J. Trojanowski, P. Thompson, C. Jack Jr, M. Weiner, Alzheimer's and D. N. Initiative (2009). "MRI of hippocampal volume loss in early Alzheimer's disease in relation to ApoE genotype and biomarkers." Brain **132**(4): 1067-1077.

Schuitemaker, A., M. A. Kropholler, R. Boellaard, W. M. van der Flier, R. W. Kloet, T. F. van der Doef, D. L. Knol, A. D. Windhorst, G. Luurtsema and F. Barkhof (2013). "Microglial activation in Alzheimer's disease: an (R)-[11 C] PK11195 positron emission tomography study." Neurobiology of aging **34**(1): 128-136.

Seger, C. A. and C. M. Cincotta (2005). "Dynamics of frontal, striatal, and hippocampal systems during rule learning." Cerebral cortex **16**(11): 1546-1555.

Selkoe, D. J. (2001). "Alzheimer's disease: genes, proteins, and therapy." Physiological reviews **81**(2): 741-766.

Selkoe, D. J. (2002). "Alzheimer's disease is a synaptic failure." Science **298**(5594): 789-791.

Shi, Z., Y. Zhu, M. Wang, Y. Wu, J. Cao, C. Li, Z. Xie and Y. Shen (2016). "The utilization of retinal nerve fiber layer thickness to predict cognitive deterioration." Journal of Alzheimer's Disease **49**(2): 399-405.

Shimazawa, M., Y. Inokuchi, T. Okuno, Y. Nakajima, G. Sakaguchi, A. Kato, H. Oku, T. Sugiyama, T. Kudo and T. Ikeda (2008). "Reduced retinal function in amyloid precursor protein-over-expressing transgenic mice via attenuating glutamate-N-methyl-d-aspartate receptor signaling." Journal of neurochemistry **107**(1): 279-290.

Sivak, J. M. (2013). "The Aging Eye: Common Degenerative Mechanisms Between the Alzheimer's Brain and Retinal DiseaseCommon Degenerative Mechanisms between Brain and Retina." Investigative ophthalmology & visual science **54**(1): 871-880.

Small, S. A. and K. Duff (2008). "Linking Aβ and tau in late-onset Alzheimer's disease: a dual pathway hypothesis." Neuron **60**(4): 534-542.

Snellman, A., F. R. López-Picón, J. Rokka, M. Salmona, G. Forloni, M. Scheinin, O. Solin, J. O. Rinne and M. Haaparanta-Solin (2013). "Longitudinal amyloid imaging in mouse brain with 11C-PIB: comparison of APP23, Tg2576, and APPswe-PS1dE9 mouse models of Alzheimer disease." J Nucl Med **54**(8): 1434-1441.

Snigdha, S., N. W. Milgram, S. L. Willis, M. Albert, S. Weintraub, N. J. Fortin and C. W. Cotman (2013). "A preclinical cognitive test battery to parallel the National Institute of Health Toolbox in humans: bridging the translational gap." Neurobiology of aging **34**(7): 1891-1901.

Sperling, R. A., P. S. Aisen, L. A. Beckett, D. A. Bennett, S. Craft, A. M. Fagan, T. Iwatsubo, C. R. Jack, J. Kaye and T. J. Montine (2011). "Toward defining the preclinical stages of Alzheimer's disease: Recommendations from the National Institute on Aging-Alzheimer's Association workgroups on diagnostic guidelines for Alzheimer's disease." Alzheimer's & dementia **7**(3): 280-292.

Spires-Jones, T. L. and B. T. Hyman (2014). "The intersection of amyloid beta and tau at synapses in Alzheimer's disease." Neuron **82**(4): 756-771.

Stelzmann, R. A., H. Norman Schnitzlein and F. Reed Murtagh (1995). "An English translation of Alzheimer's 1907 paper,"Über eine eigenartige Erkankung der Hirnrinde"." Clinical anatomy **8**(6): 429-431.

Stevens, L. M. and R. E. Brown (2015). "Reference and working memory deficits in the 3xTg-AD mouse between 2 and 15-months of age: A cross-sectional study." Behavioural brain research **278**: 496-505.

Stover, K. R., M. A. Campbell, C. M. Van Winssen and R. E. Brown (2015). "Early detection of cognitive deficits in the 3xTg-AD mouse model of Alzheimer's disease." Behavioural brain research **289**: 29-38.

Strenn, K., P. Dal-Bianco, H. Weghaupt, G. Koch, C. Vass and I. Gottlob (1991). Pattern electroretinogram and luminance electroretinogram in Alzheimer's disease. Age-associated Neurological Diseases, Springer**:** 73-80.

Su, J. H., G. Deng and C. W. Cotman (1997). "Transneuronal degeneration in the spread of Alzheimer's disease pathology: immunohistochemical evidence for the transmission of tau hyperphosphorylation." Neurobiology of disease **4**(5): 365-375.

Sutphen, C. L., A. M. Fagan and D. M. Holtzman (2014). "Progress update: fluid and imaging biomarkers in Alzheimer's disease." Biological psychiatry **75**(7): 520-526.

T Reed, B., F. Behar-Cohen and S. Krantic (2017). "Seeing Early Signs of Alzheimer's Disease Through the Lens of the Eye." Current Alzheimer Research **14**(1): 6-17.

Tanimoto, N., V. Sothilingam, M. Kondo, M. Biel, P. Humphries and M. W. Seeliger (2015). "Electroretinographic assessment of rod-and cone-mediated bipolar cell pathways using flicker stimuli in mice." Scientific reports **5**: 10731.

Thomson, K. L., J. M. Yeo, B. Waddell, J. R. Cameron and S. Pal (2015). "A systematic review and meta-analysis of retinal nerve fiber layer change in dementia, using optical coherence tomography." Alzheimer's & Dementia: Diagnosis, Assessment & Disease Monitoring **1**(2): 136-143.

Trick, G. L., M. C. Barris and M. Bickler-Bluth (1989). "Abnormal pattern electroretinograms in patients with senile dementia of the Alzheimer type." Annals of neurology **26**(2): 226-231.

Tzekov, R. and M. Mullan (2014). "Vision function abnormalities in Alzheimer disease." Survey of ophthalmology **59**(4): 414-433.

Van Dam, D., R. D'hooge, M. Staufenbiel, C. Van Ginneken, F. Van Meir and P. P. De Deyn (2003). "Age-dependent cognitive decline in the APP23 model precedes amyloid deposition." European Journal of Neuroscience **17**(2): 388-396.

von Reutern, B., B. Grünecker, B. H. Yousefi, G. Henriksen, M. Czisch and A. Drzezga (2013). "Voxel-based analysis of amyloid-burden measured with [11 C] PiB PET in a double transgenic mouse model of Alzheimer's disease." Molecular Imaging and Biology **15**(5): 576-584.

Wang, H., E. J. Golob and M. Y. Su (2006). "Vascular volume and blood-brain barrier permeability measured by dynamic contrast enhanced MRI in hippocampus and cerebellum of patients with MCI and normal controls." Journal of magnetic resonance imaging **24**(3): 695-700.

Wang, Y., V. Balaji, S. Kaniyappan, L. Krüger, S. Irsen, K. Tepper, R. Chandupatla, W. Maetzler, A. Schneider and E. Mandelkow (2017). "The release and trans-synaptic transmission of Tau via exosomes." Molecular neurodegeneration **12**(1): 5.

Warburton, E. and M. Brown (2015). "Neural circuitry for rat recognition memory." Behavioural brain research **285**: 131-139.

Wegiel, J., H. Imaki, K.-C. Wang, J. Wegiel, A. Wronska, M. Osuchowski and R. Rubenstein (2003). "Origin and turnover of microglial cells in fibrillar plaques of APPsw transgenic mice." Acta neuropathologica **105**(4): 393-402.

Weiner, M. W., P. S. Aisen, C. R. Jack, W. J. Jagust, J. Q. Trojanowski, L. Shaw, A. J. Saykin, J. C. Morris, N. Cairns and L. A. Beckett (2010). "The Alzheimer's disease neuroimaging initiative: progress report and future plans." Alzheimer's & Dementia **6**(3): 202-211. e207.

Weiner, M. W., D. P. Veitch, P. S. Aisen, L. A. Beckett, N. J. Cairns, J. Cedarbaum, R. C. Green, D. Harvey, C. R. Jack and W. Jagust (2015). "2014 Update of the Alzheimer's Disease Neuroimaging Initiative: A review of papers published since its inception." Alzheimer's & Dementia **11**(6): e1-e120.

White, H., C. Pieper and K. Schmader (1998). "The association of weight change in Alzheimer's disease with severity of disease and mortality: a longitudinal analysis." Journal of the American Geriatrics Society **46**(10): 1223-1227.

Williams, P. A., R. A. Thirgood, H. Oliphant, A. Frizzati, E. Littlewood, M. Votruba, M. A. Good, J. Williams and J. E. Morgan (2013). "Retinal ganglion cell dendritic degeneration in a mouse model of Alzheimer's disease." Neurobiology of aging **34**(7): 1799-1806.

Winters, B. D., S. E. Forwood, R. A. Cowell, L. M. Saksida and T. J. Bussey (2004). "Double dissociation between the effects of peri-postrhinal cortex and hippocampal lesions on tests of

object recognition and spatial memory: heterogeneity of function within the temporal lobe." Journal of Neuroscience **24**(26): 5901-5908.

Wong, P. C., H. Cai, D. R. Borchelt and D. L. Price (2002). "Genetically engineered mouse models of neurodegenerative diseases." Nature neuroscience **5**(7): 633.

Xiao, T., W. Zhang, B. Jiao, C.-Z. Pan, X. Liu and L. Shen (2017). "The role of exosomes in the pathogenesis of Alzheimer'disease." Translational neurodegeneration **6**(1): 3.

Ye, M., H.-S. Chung, Y. H. An, S.-j. Lim, W. Choi, A. R. Yu, J. S. Kim, M. Kang, S. Cho and I. Shim (2016). "Standardized herbal formula PM012 decreases cognitive impairment and promotes neurogenesis in the 3xTg AD mouse model of Alzheimer's disease." Molecular neurobiology **53**(8): 5401-5412.

Ye, M., H.-S. Chung, C. Lee, M. S. Yoon, A. R. Yu, J. S. Kim, D.-S. Hwang, I. Shim and H. Bae (2016). "Neuroprotective effects of bee venom phospholipase A2 in the 3xTg AD mouse model of Alzheimer's disease." Journal of neuroinflammation **13**(1): 10.

Zheng, H., M. Jiang, M. E. Trumbauer, D. J. Sirinathsinghji, R. Hopkins, D. W. Smith, R. P. Heavens, G. R. Dawson, S. Boyce and M. W. Conner (1995). "β-Amyloid precursor protein-deficient mice show reactive gliosis and decreased locomotor activity." Cell **81**(4): 525-531.